SRF

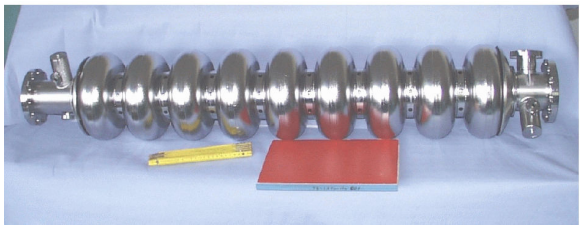

CARE/JRA1 Annual report 2006

Research and Development on Superconducting Radio-Frequency Technology for Accelerator Applications

Participating Laboratories and Institutes:

Institute (Participating number)	Acronym	Country	Coordinator	SRF Scientific Contact	Associated to
DESY (6)	DESY	D	D. Proch	D. Proch	
CEA/DSM/DAPNIA (1)	CEA	F	O. Napoly	O. Napoly	
CNRS-IN2P3-Orsay (3)	CNRS-Orsay	F	T.Garvey	T.Garvey	CNRS
INFN Legnaro (10)	INFN-LNL	I	S. Guiducci	E. Palmieri	INFN
INFN Milano (10)	INFN-Mi	I	S. Guiducci	P. Michelato	INFN
INFN Roma2 (10)	INFN-Ro2	I	S. Guiducci	S. Tazzari	INFN
INFN Frascati (10)	INFN-LNF	I	S. Guiducci	M. Castellano	INFN
Paul Scherer Institute (19)	PSI	CH	V. Schlott	V. Schlott	
Technical University of Lodz (12)	TUL	PL	A.Napieralski	M. Grecki	
Warsaw University of Technology (14)	WUT-ISE	PL	R.Romaniuk	R. Romaniuk	
IPJ Swierk (13)	IPJ	PL	M. Sadowski	M. Sadowski	

Industrial Involvement:

Company Name	Country	Contact Person
ACCEL Instruments GmbH	D	M. Peiniger
WSK Mess- und Datentechnik GmbH	D	F. Schölz
E. ZANON SPA	I	G. Corniani
Henkel Lohnpoliertechnik GmbH	D	B. Henkel

Work supported by the European Community-Research Infrastructure Activity under the FP6 "Structuring the European Research Area" programme (CARE, contract number RII3-CT 2003-506395).

Table of contents

1. Executive Summary

The aim of the JRA on Superconducting RF Technology is to improve the quality and performance of the superconducting test accelerator TTF (Tesla Test Facility), a unique test facility to explore the operating conditions of a high gradient superconducting accelerator, at DESY.
The ultimate objectives of this research activity are

- to increase the accelerating gradient from 25 to 35 MV/m and
- to increase the quality factor from 5×10^9 to 2×10^{10},
- to improve the reliability, operating performance and availability of the superconducting accelerating system,
- to achieve a cost reduction of the SRF cavities and their associated components.

Change of WP or Task leaders.

Dr. P. Strzyzewski from Soltan Institute replaces task leader Dr. J. Langner (WP4.1) who died after a shot but severe illness. We will keep him in our memory as a very competent, highly motivated and friendly colleague
Dr. A. Matheisen replaces WP leader L.Lilje who has to manage increasing work load for ILC.
Mr. N. Steinhau-Kühl replaces Dr. A. Matheisen as Task leader in WP5.2.
Mr. F. Eozénou replaced Dr. C. Antoine as task leader in WP5.1 because of her leave of absence to FNAL.
Ms. C. Simon replaced Mr. C. Magne as task leader in WP11.1.

Great progress has been made by the group of W. Singer (WP3.2) in fabrication of cavities from large grain and even single crystal Niobium sheets. Excellent results were reported in his highlight talk at the CARE06 annual meeting at CERN. Based on these results it can be expected to fabricate high gradient and high Q (low RF loss) cavities at reduced material and processing costs. The progress of this work follows the experience of intensive material studies for hydroforming of Niobium cavities. Because of the enormous impact of single grain cavity production a new subtask in WP3.2 about further work on single grain cavity production will be defined early 2007.

Use and Dissemination of knowledge.

Communication is an important aspect of the JRA-SRF, both between participating institutes as well as with external institutes who share our interest in high gradient, low loss superconducting cavities. Contributions from JRA-SRF members were given to several conferences and meetings, the major ones being as follows:

- The IEEE-SPIE ELHEP.ISE XVII SYMPOSIUM 2006 (Warsaw, PL)
- The IEEE-SPIE WILGA Conference of Electronics for HEP (Wilga, PL)
- The Int. Conf. on Metallurgical Coatings and Thin Films (San Diego, USA)

- The NSTI Nanotechnology Conference and Trade Show 2006 (Boston, USA)
- The European Particle Accelerator Conference 2006 (Edinburgh, GB)
- The Int. Conf. on Mixed Design of Integrated Circuits and Systems (Gdynia, PL)
- The Multiconference CryoPrague 2006 (Prague, Czech Rep.)
-The Int. Conf. on Charged and Neutral Particles Channeling Phenomena 2006 (Frascati, Italy)
- The 2006 Linear Accelerator Conference (Knoxville, USA)
- The 2nd Int. Con. on Radiation Physics and Modifications of Materials (Tomsk, Russia)
- The 22nd Int. Symp. on Discharges and Electrical Insulation in Vacuum (Matsue, Japan)
- The TESLA Technology Collaboration Meeting (KEK-Tsukuba, Japan)
- The Int. Workshop on Thin Film (Legnaro, Italy)
- Several GDE/ILC meetings

Papers and talks were also presented at TESLA Technology Collaboration meetings in this reporting year as well as at the annual CARE meeting held at Frascati in November

The impressive progress made in WP3 (Cavity production) and WP6 (Material Analysis) was presented as highlight talks at the CARE 06 annual meeting. The presentations can be found on the meeting WEB site.

Annual SRF Meeting

In addition to the above conferences and several telephone meetings, the SRF JRA held their dedicated annual meeting the day before and during the annual CARE06 meeting at Frascati. This meeting included an entire review of all work-packages and tasks therein. It was the opportunity for the external scientific advisory committee to review the program of work. Their findings can be found later within this report. What was clear from the Frascati meeting is that, despite some delay in certain milestones / deliverables, the project has made enormous progress in the last twelve months. The technical summaries to be found in later sections bears witness to this.

The strong connection between the R&D activities in JRA-SRF and the European X-FEL, the International Linear Collider activities and the TTC (TESLA technology Collaboration) community continues. It seems likely that many of the results of the work from SRF will have a major impact on these projects and collaboration.

2. Report of the International Advisory Committee

Annual Review by the International Advisory Committee
of the Activities performed by the
JRA1 Project
of the Coordinated Accelerator Research in Europe (CARE).

Frascati, Italy, November 14 and 15, 2006

Executive Summary

The International Advisory Committee (IAC) reviewed the progress achieved during the previous year by the Work Packages related to the JRA1 section of CARE.
The Committee acknowledges the continued progress in all areas and commends the Management for the efforts to coordinate and blend such diverse set of research activities performed by many different Institutions in several Countries. The Committee encourages the Management to continue the efforts to integrate and unify the various research areas and recommends that all participants in the research efforts comply with the requirements set by the funding Agency.
The overall progress and quality of the work is at the forefront of the technology and the results of the research carried out by the JRA1 Groups are looked after by the SRF Community and set a high standard to be met by other Laboratories around the World.
In general, the Work Packages have shown substantial progress, even though the overall work timeline is behind the original schedule, which may pose some funding profile conflicts. A small fraction of the activities have not shown substantial progress and in some cases some areas of work have been delayed by the slower pace of other interrelated activities. However, the overall momentum and the degree of coordination among laboratories and researchers are simply impressive and substantial progress has been made in addressing issues which are of the utmost importance for the advancement of the SRF field as a whole.

Detailed analysis and comments for the individual work packages follow:

General Comments

Due to travel issues, during the first review day Knobloch and Campisi alone represented from the IAC, whereas during the second day Weingarten and Campisi were present. The views reported here are those of this subset of the IAC.

The collaboration appears to be strong in most work packages, although in a few the interaction could be improved. A good example of collaboration in the spirit of CARE is the DC

emission scanning (WP 6.3), which is being used to evaluate samples produced by several groups, to identify appropriate cavity preparation techniques.

Towards the end of last year much of the preparatory work had been completed and the program was ready to enter the data taking/experimental phase. The progress here is somewhat varied with notable results being achieved in, for example, WP6.3 (DC scanning). Other work packages, however, appear to have stalled somewhat at this critical juncture with only few new results being presented. For example, no nine-cell cavity tests of hydroformed or spun cavities were available. WP4 (thin-film coated cavities) also cannot proceed because substrate cavities for coating have not been received.

Overall, it seems that attendance by members of the Collaboration was down compared to last year, with only few people involved in each work package being present. The annual meeting is the main opportunity for information exchange and should be taken advantage of. Rather than simply considering it a "status report" it should provide a forum for scientific discussion and information exchange. A single day to address the wide spectrum of scientific aspects of the collaboration appears not sufficient. Another option is to include a poster session to trigger discussion of more details than is possible during the presentations. For the final year this may be especially useful to tie together all the scientific results. It would also be useful for the IAC to receive at least partial status reports in advance and that the talks should contain a comparison of the status from the previous year.

WP1: Management and Communication

This JRA covers a rather wide spectrum of activities important for the progress of superconducting RF technology and therefore needs a large degree of coordination and communication. **The IAC is of the opinion that this goal was well achieved**, also proven by the relatively advanced reporting (with some exceptions), frequent participation at conferences and working meetings, and publishing in refereed journals.

WP2: Standard Cavity Fabrication

The work-package aims at understanding any lack of reproducibility, if observed, of the performance (accelerating gradient) for the vertical test of the cavity up till the horizontal tests of the full-size module. The analysis presented shows a correlation between the number of unforeseen events (leak, etc.) and the performance (cryomodule 1). However, in the absence of major problems, a degradation of the performance of the cavities when integrated into the cryo-module is not always obvious (cryomodule 5). A report on the reliability analysis has been published at EPAC06 and this activity has now been completed (2.1). However, no new results were presented at this JRA1-SRF meeting and the only critical item that was analyzed in detail as part of WP2.2 so far has been the vacuum gaskets. The direct collaborative flow between 2.1 and 2.2 thus appears to have been limited. Also, it was unclear what performance criterion was used to compare cavity test results. In particular, what defines the field limit of cavities when there is no thermal breakdown? If such a definition does not exist, one should be developed.
The IAC recommends making further use of a larger sample size based on a precise logging of unforeseen events and user-friendly access to the relevant data. Also, a better definition of the testing protocols and of the results should be given and more interaction between the people who analyze the data and those who originally took them is desirable.

The relevance of the various parameters for the EB welding process is not yet precisely known (e.g. vacuum conditions, oil-free motion units, welding from the inside), and is lacking data on EB welding machines in other European laboratories besides DESY. No new information regarding the E-beam welding was provided (2.3). It is not clear whether any progress has been made with respect to the 2005 annual meeting.
The flange and seal analysis has been completed and provides in depth information for future designs (2.2). Not only does it include a theoretical FE analysis of the system but measurements, including temperature cycles. A well documented understanding of the response of the gasket upon an external load was obtained by FEM computer simulations.

The change in compression force during thermal cycles was found to be only 10 kN, and is not affected by repeated cycles. This provides confidence for long term operation of accelerating modules. As far as the redesign of other cavity subsystems are concerned, little appears to have been done here. A simple change to improve the stiffness of the helium tank was identified, other specifics were not mentioned. There is a danger that the new cavity design will not be complete by mid 2007.

The IAC strongly encourages the continuation of this activity.

WP3: Seamless Cavity Production

The procedure for the production of seamless 9-cell cavities by hydroforming is solved and enters the industrialization phase. All technical issues producing seamless tubes appear to have been solved as well and the equipment is ready for cavity production (3.2). Three cell units have been produced and were been sent to industry for welding into nine-cell cavities. Since DESY has recently commissioned a high-vacuum beam welder, it is not clear why these cavities are not being welded at DESY.

A multicell seamless cavity has also been spun at INFN and is ready for testing (3.1). The cavity treatment, however, was different than the hydroformed ones. It is recommended that for future cavities, the treatment be identical for the two processes to be able to better compare results, or if different, a justification for the different treatment should be given which takes into account the different manufacturing steps and material properties.

The IAC acknowledges this excellent achievement and encourages the completion of the work.

WP4: Thin Film Cavity Production

The operation of both the linear cathode and planar arc systems with samples has been extensive with a number of analyses of their RF, morphological, chemical and crystalline properties complete. It appears that in many respects the samples exhibit near-bulk-Nb properties. The IAC eagerly awaits cavity results.

The development of the linear cathode arc coating apparatus is progressing nicely, and the design of the microdroplet filter has gone through several generations to optimize its performance. Nevertheless, a significant number of microdroplets are still created on the coating surface. Since it is not clear what level is acceptable, cavity tests should be performed as soon as possible. Unfortunately, suitable copper cavities have not yet been supplied. This should receive

a high priority to enable qualification of the existing system and to avoid putting the following multi-cell program in jeopardy. In the meantime, sample analyses can continue to improve the filter design and the operating parameters. Field emission measurements with these samples at Wuppertal should also be considered to characterize their performance.

The planar arc system is also presently being adapted to coat cavities. If possible, a coated cavity should be tested as well.

The management of the JRA1 is encouraged to find a solution to the lack of available substrate cavities.

The IAC has the impression that the droplets have of a loose contact with the surface, and recommends, therefore, to study mechanical methods of their removal (e.g. high pressure water rinsing).

The results stemming from this work package are well documented and correctly published.

WP5: Surface Preparation

Given the extensive delays for both the single-cell EP program (5.1), the automated EP (5.3) and the dry-ice cleaning (5.4) it has become apparent that the results achieved here can no longer flow into the optimization of EP for multicells at DESY (5.2). Modified objectives were presented which appear reasonable.

Full industrialization of the DESY EP system (5.2) has proven too ambitious and consequently has been scaled back. Recent results have shown that quality control of the acid as delivered and during the EP process is critical, and the new goal targets industrial quality control as a first step towards industrialization. Again, this appears reasonable.

Since there is no longer a direct link between 5.1, 5.2, 5.3 and 5.4, it becomes even more important that qualifying tests for 5.1, 5.3, and 5.4 take place in the DESY single-cell program (or elsewhere) as part of the modified implementation plan presented at the meeting. **Careful documentation and communication of these results is critical**, so that they may form the basis of optimization and industrialization that will follow in a subsequent program.

The IAC welcomes the fact, that the single-cell EP system (5.1) is now operational at Saclay. The results previously obtained with coupons should now be transferred to cavities as quickly as possible, especially for the most promising solutions. The IAC recommends that checks should be made to demonstrate that similar surface finishes are obtained with the cavities as with the coupons under the same conditions. Three cavities have already been polished, but not yet been tested. These tests should take place as soon as possible at DESY rather than wait for the test setup at Saclay to become operational again. Also comparisons of cavity tests to compare etching with the vertical and horizontal EP systems under the same polishing conditions should be performed for cross-reference.

The oxypolishing system is behind schedule (5.2). While this delay is being made up, samples can be treated reasonably easily for testing at Wuppertal to demonstrate whether there is truth to the anecdotal evidence that particle removal is improved for oxypolished surfaces.

A review of alternative electrolytes for EP was presented (5.3). It appears remarkable how many potential alternatives exist to the “traditional recipe”. Ionic liquids appear to be the new “buzz word”. A well structured report is needed to summarize these and to enable one to see the forest for the trees. A small subset should be chosen to explore further, to perhaps even point the

way for single-cell tests further in the future. A clear choice of method and a plan to apply it to real structures would be desirable.

Progress for the automated EP activities (5.3) since the last 2005 Annual Meeting was not apparent. Tests have been performed on Cu samples, but not yet with Nb. It should be transferred to Nb as soon as possible, with the goal to apply the automation to single cell cavities soon.

The dry ice cleaning system (5.4) is considerably delayed, in part because of safety regulations. These should be addressed as soon as possible to permit the resumption of tests, even if the new nozzle is not yet available. As stated in the report, single-cell dry-ice cleaning results are key to designing the multicell system. At present, there is a discrepancy between the single-cell results and field emission measurements made with dry-ice-cleaned samples (the former performing worse). A new nozzle is being designed to improve the cleaning procedure, but it has not yet been ruled out whether cavity assembly may be responsible. One may consider testing coupons in the Wuppertal FE scanning setup that were present during cavity cleaning and assembly to rule out this possibility. To optimize the heating system for 9-cells, 3-cell tests with the current setup may help point the way.
This work package underwent frequent changes of focus and responsibilities. The scope of the work was extended, for well justified reasons of safety and environmental protection, from the original electro-polishing (optimization of the parameters) and dry ice cleaning to alternatives: other methods of polishing, hot water rinsing, and oxipolishing. **The advisory group therefore recommends a re-focusing of the activities on less diversified goals.**

WP6: Material Analysis

As reported the previous year, the squid scanning setup is now operational and is being applied to a batch of 20 Nb sheets delivered by Fa. Plansee. Unfortunately, the production of sample defects has been delayed so that the last two steps in the implementation plan need to be reversed. In light of the potential delay that would otherwise be incurred, the change appears reasonable. It is encouraging to see that depth information on defects can now be obtained by observing the phase delay between the eddy current field and the excitation field, an issue that was mentioned in the committee's last report.

The field emission scanning results (6.3) from Wuppertal were one of the highlights of last year's activities. It is very encouraging to see the use of this tool to systematically investigate the techniques being developed by other laboratories, in particular the EP and dry-ice cleaning. This apparatus has proven very powerful and is being used effectively to identifying preparation techniques that are capable of producing field-emission-free cavities.

The coupon measurements have demonstrated that they can be transported cleanly since peak field levels of 120 MV/m without or little field emission were achieved. The measurements have shown that the efficiency of particle removal improves considerably from EP to HPR to dry-ice cleaning (DIC). DIC appears to impact the surface mechanically (particle removal), thermally (cracking of adhesives) and chemically (dissolution of hydrocarbons), which may explain its effectiveness. This underscores the importance of pursuing DIC with vigor in WP5. Very interesting was also the correlation between surface roughness and the number of observed emitters. Further investigations are needed here and can tie in with single crystal studies as well as the optimization of the EP process being performed at Saclay. Another key result is the correlation between FE onset and emitter size. Results suggest that for operation up to 40 MV/m

(E_{acc}) only particles greater than 2 μm must be eliminated, thus supplying, for the first time, a quality control criterion for FE-free surfaces. To underpin this statement, an effort should be made to increase the statistics.
The original eddy current method to examine the surface of niobium sheets was extended by other methods, all of them showing useful results: SQUID scanning, surface scanning for parasitic field emitters on Nb surfaces, or Giant Magneto Resistive (GMR) sensors. These scanning methods were applied for other related technological developments, such as the optimisation of the electro-polishing cathode. **The advisory group acknowledges the excellent progress made for this work package.**

WP7: Couplers

The two prototype coupler systems (TTF-V and TW60) have been delivered. Both appear to have problems that prevent high power testing at this time: the TTF-V coupler/connecting waveguide for processing is off resonance and the TW60 has mechanical issues. Workarounds for prototype testing appear possible and should be implemented as soon as possible. Parallel to this, the cause for the shift in resonance for the TTF-V coupler should be investigated. The use of "cold" models with adjustable dimensions is recommended

Multipacting simulations have been performed for the TTF-III and TTF-V coupler. So far there seems to be little correlation between electronic activity during conditioning and the predicted multipacting thresholds for the TTF-III coupler. Given the extensive data base for this coupler, this should be investigated further. The impact of antenna biasing can be included in the simulations for comparison with conditioning runs. Multipacting simulations for the TW60 coupler should also be performed for comparison with future conditioning studies and to identify strengths or weaknesses compared to the TTF-V coupler.

It is impressive how conditioning times were shortened significantly following the improved handling and storage in nitrogen cabinets towards the middle of 2005. A re-evaluation of the multipacting simulations with this new set of conditioning studies may lead to a clearer correlation.

Towards the beginning of JRA1-SRF, discussions also centered on the possible TiN coating of a full TTF-III coupler, and systematic conditioning studies including argon discharge cleaning. Given the delay of the TiN coating system, as well as the new prototype couplers, expansion of the studies of the TTF-III system should be considered.

Sample studies of TiN coated ceramics have been performed. At present the coatings have been very thick and chemical/stoichiometric analyses have been performed. Thinly coated samples should be studied as well and qualified by multipacting/secondary electron yield experiments.

The IAC endorses the ongoing efforts of identifying the cause of the problems related to coupler manufacturing and encourages continued and expanded interactions with the manufactures themselves to avoid similar problems in the future.

WP8: Tuners

The activities are centered on five different activities, IN2P3-Orsay (piezo-electric actuators) and CEA-Saclay in France (piezo-tuning system), Technical University of Lodz in Poland (magneto-strictive actuators and tuner prototype, control system), INFN-Milano in Italy (blade-piezo tuner) and DESY-Hamburg in Germany (control electronics). Other tuner developments are on schedule, or are waiting for the test with cavities. **In large parts the work is well advanced as demonstrated by the new cryomodule from industry (ACC6), which is equipped with the CEA tuner. The IAC encourages the efforts toward lowering the costs of each tuner design.**

WP9: Low level RF

All deliverables, as indicated in the proposal for the JRA, were addressed or provided. **Results of radiation damage to electronic hardware were not yet reported**. **Interaction with other laboratories using pulsed superconducting cavities is encouraged.**

WP10: Horizontal Cryostat Integration Tests

This facility (now being moved) allows, in a horizontal cryostat, integrated tests of cavities equipped with improved components resulting from developments in other work packages (tuners and couplers) as well as novel thermometric calibration techniques. **A big step towards these objectives was demonstrated by the validation of the complete CEA-Saclay piezo-tuning system.**

WP11: Beam Diagnostics

Beam position monitor: The reentrant cavity beam position monitor is operational and provides an RMS spatial resolution better than 40 μm in a dynamic range of ± 5 mm, and a time resolution of 40 ns. Provisions to further improve the resolution in space and time are being studied and shall be implemented in the next future (early 2007).
Emittance monitor: The commissioning of the Optical Diffraction Radiation (ODR) experiment at FLASH started and first results proved a qualitative agreement between measurements and simulations. A new is planned in the next future (January 2007).

3. List of Work packages, tasks and responsibilities

2 Improved Standard Cavity Fabrication (ISCF)	***P.Michelato***	INFN Mi
2.1 Reliability analysis	L. Lilje	DESY
2.2 Improved component design	P.Michelato	INFN Mi
2.3 EB welding	J. Tiessen	DESY
3 Seamless Cavity Production (SCP)	***W.-D. Moeller***	DESY
3.1 Seamless cavity production by spinning	E. Palmieri	INFN LNL
3.2 Seamless cavity production by hydroforming	W. Singer	DESY
4 Thin Film Cavity Production (TFCP)	***M. Sadowski***	IPJ
4.1 Linear arc cathode	P. Strzyzewski	IPJ
4.2 Planar arc cathode	S. Tazzari	INFN Ro2
5 Surface Preparation (SP)	***A. Matheisen***	DESY
5.1 EP on single cells	F. Eozénou	CEA
5.2 EP on multicells	N. Steinhau-Kühl	DESY
5.3 Automated EP	E. Palmieri	INFN LNL
5.4 Dry ice cleaning	D. Reschke	DESY
6 Material Analysis (MA)	***E. Palmieri***	INFN LNL
6.1 Squid scanning	W. Singer	DESY
6.2 Flux gate magnetometry	M. Valentino	INFN LNL
6.3 DC field emission studies of Nb samples	X. Singer	DESY
7 Couplers (COUP)	***A. Variola***	CNRS-Orsay
7.1 New proto-types	L. Grandsire	CNRS-Orsay
7.2 Titanium-nitride coating system	L. Grandsire	CNRS-Orsay
7.3 Conditioning studies	P. Lepercq	CNRS-Orsay
8 Tuners (TUN)	***P. Sekalski***	TUL
8.1 UMI Tuner	A. Bosotti	INFN-Milano
8.2 Magnetostrictive Tuner	A. Grecki	TUL
8.3 CEA Tuner	P. Bosland	CEA
8.4 IN2P3 activities	M. Fouaidy	CNRS-Orsay
9 Low Level RF (LLRF)	***S. Simrock***	DESY
9.1 Operability and Technical performance	S. Simrock	DESY
9.2 Cost and reliabilty	M. Grecki	TUL
9.3 Hardware technolgy	R. Romaniuk	WUT-ISE
9.4 Software technology	T. Jezynski	WUT-ISE
10 Cryostat Integration Tests	***B. Visentin***	CEA
11 Beam Diagnostics (BD)	***M. Castellano***	INFN-LNF
11.1 Beam position monitor	C. Simon	CEA
11.2 Emittance monitor	M. Castellano	INFN-LNF
11.3 HOM BPM monitor	O. Napoly	CEA

4. Deliverables of the reporting period

	Task	**Deliverables**	Title	planned end	expected end	Reference	task leader	contractor
1	**2.1.7**	**Final Report (D)**	**Final Report on reliability issue**	**30/12/05**	**29/09/06**	**CARE-Report-06-029-SRF**	L..Lilje	DESY
2	**3.1.3.5**	**Final Report (D)**	**Spinning parameters defined**	**18/05/06**	**31/12/06**	**CARE-Report-07-012-SRF**	E.Palmieri	INFN-Lnl
3	**3.1.4.3**	**Final Report (D)**	**1-cell spinning parameters defined**	**07/12/06**	**31/12/06**	delayed	E.Palmieri	INFN-Lnl
4	**5.1.1.4**	**Final Report (D)**	**Best EP parameters**	**15/01/06**	**15/01/06**	**CARE-Report-06-010-SRF**	C.Antoine	CEA
5	**5.2.1.3.5**	**Final Report (D)**	**Process parameters fixed**	**31/03/06**	**31/10/06**	**CARE-Report-07-013-SRF**	A.Matheisen	DESY
6	**5.3.3.5**	**Final Report (D)**	**Automated EP is defined**	**13/02/06**	**31/12/06**	**CARE-Report-07-010-SRF**	E.Palmieri	INFN-Lnl
7	**5.4.2.4**	**Final Report (D)**	**Cleaning parameters fixed**	**30/06/06**	**30/11/06**	**CARE-Report-07-011-SRF**	D.Reschke	DESY
8	**8.4.8**	**Final Report (D)**	**Report on IN2P3 tuner activities**	**07/08/06**	**31/12/06**	In preparation	M.Fouaidy	CNRS
9	**9.3.3.8**	**Final Report (D)**	**Report on new LLRF hardware comp**	**01/03/06**	**30/11/06**	**CARE-Report-06-013-SRF**	R.Romaniuk	WUT-ISE
10	**9.4.2.5**	**Final Report (D)**	**Report on RF gun control tests**	**06/10/06**	**30/11/06**	**CARE-Report-07-009-SRF**	T.Jezynski	WUT-ISE
11	**11.1.10**	**BPM Protot.(D)**	**New BPM ready for Installation**	**01/01/06**	**finished**	**CARE-Report-06-030-SRF**	C.Simon	CEA
12	**11.3**	**Final Report (D)**	**Evaluation of HOM-BPM operation**	**30/12/06**	**finished**	**CARE-Report-06-034-SRF**	O. Napoly	CEA

5. List of major meetings organized under JRA1

Date	Title/Subject	Location	Number of attendees	Web-site address
20-21 Jan 2006	IEEE-SPIE ELHEP‐ISE XVII SYMPOSIUM 2006	Warsaw, Poland	40	http://wilga.ise.pw.edu.pl/20061/downloads/program/program.htm
March 28-31, 2006	CARE-JRA1-WP4 (Thin film production) Collaboration Meeting	INFN, Tor Vergata University, Rome	8	None
May 12, 21006	WP 6.3: DC field emission scanning	University of Wuppertal	4	None
May 11, 2006	Parameters of electropolishing / coordination of work task 5.1/5.2	DESY	4	None
May 12, 2006	WP6.3: DC field emission scanning	University of Wuppertal	4	None
May 22-24, 2006	MIXDES 2006, special CARE session	Gdynia, Poland	300	www.mixdes.org
May 22-28, 2006	IEEE-SPIE WILGA Conference of Electronics for HEP	WILGA, Poland	200	http://wilga.ise.pw.edu.pl
June	EPAC	Edinburgh		http://epac06.org/
July 2, 2006	Status of the Project and Future Steps	Frascati	6	
August	LINAC	Knoxville		http://www.sns.gov/linac06/
Sept 5, 2006	Evaluation of Previous Shift Results	Desy	5	
Sept 7-8, 2006	CARE-JRA1-WP4 (Thin film production) Collaboration Meeting	IJP Swierk, Poland	5	None
Oct 9-12, 2006	Int. Workshop on thin films and pushing the limits od RF superconductivity	Padua/Legnaro	64	http://www.lnl.infn.it/~master/thinfilms
Oct 10, 2006	WP 6.3: DC field emission scanning	DESY	4	None
Nov 14-15, 2006	JRA-SRF annual meeting 2006	Rome/Frascati	45	https://indico.desy.de/conferenceDisplay.py?confId=141
Nov 14-15, 2006	The third annual CARE Meeting	Rome/Frascati	200	http://www.lnf.infn.it/conference/care06/index.htm

6. List of talks from JRA1 members

Subject	Speaker/Lab	Event	Date	Web site
Development of adaptive feed forward algorithm for Lorentz force compensation for VUV-FEL ACC1 cav5 purpose	P. Sekalski, DMCS-TUL	IEEE-SPIE Symposium	20. Jan 06	
Low temperature electromechanical and dynamic properties of piezostacks for superconducting RF cavities fast tuners	M. Fouaidy, IPN Orsay	CRYOPRAGUE 2006	17-21 July, 2006	
High power couplers for linear accelerators	A. Variola	LINAC 06	Aug 28, 2006	http://www.sns.gov/linac06
Electromechanical System For Lorentz Force Compensation	A. Napieralski, DMCS-TUL	NSTI-Nanotech 2006	May10, 2006	http://www.nsti.org/ Nanotech2006/
Low temperature electromechanical and dynamic properties of piezostacks for superconducting RF cavities fast tuners	M. Fouaidy, IPN Orsay	CRYOPRAGUE2006	July 17-21, 2006	
Status of the Electron Beam Transverse Diagnostics with Optical Diffraction Radiation at FLASH	E. Chiadroni	Channelling 2006 Conference - Frascati	July 2, 2006	http://www.lnf.infn.it/conference/channeling2006/
Status and First Results of Optical Diffraction Radiation Experiment at FLASH	E. Chiadroni	FLASH Seminar - Desy	Sept 5, 2006	http://flash.desy.de/meetings/index_eng.html
Single bunch induced transient detection, Poland	P. Pawlik	2006 Wilga Symposium	29.05-04.06.2006	wilga.ise.pw.edu.pl
SEU Tolerance in Microsystems by Application of Hardware and Software Redundancy	Adam Piotrowski	2006 Wilga Symposium	29.05-04.06.2006	wilga.ise.pw.edu.pl
Application of RadFET for ionizing radiation dosimetry	D.Makowski	2006 Wilga Symposium	29.05-04.06.2006	wilga.ise.pw.edu.pl
Fault-Tolerant VHDL Descriptions: A case-study for SEU-tolerant digital library	M. Tomczak	2006 Wilga Symposium	29.05-04.06.2006	wilga.ise.pw.edu.pl
Control system modeling for superconducting accelerator	T.Czarski	2006 Wilga Symposium	29.05-04.06.2006	wilga.ise.pw.edu.pl

Adaptive Control of a SC Cavity based on the Physical Parameters Identification	T.Czarski	Linac 2006 Conference, Knoxville	21.08-25.08.2006	http://www.sns.gov/linac06/
UHV Arc for High Quality Film Deposition	R. Russo INFN-Na, Naple, Italy	ICMCTF-06, San Diego, USA	May 5, 2006	http://www.sns.gov/linac06
Status of Research on Deposition of Thin Superconducting Films for RF Accelerating Cavities	S. Tazzari Tor Vergata Uni –INFN Roma-2, Rome, Italy	2nd Intern. Congress on Radiation Physics, High-Current Electronics and Modifications of Materials, Tomsk, Russia	Sept. 12, 2006	http://www.congress-2006.hcei.tsc.ru
Progress in Use of Ultra-High Vaccum Cathodic Arcs for Deposition of Thin SuperconductingLayers	M.J. Sadowski IPJ, Swierk, Poland	22nd ISDEIV, Matsue, Japan	Sept. 15, 2006	http://isdeiv.eee.u-ryukyu.ac.jp
Progress in Research on Deposition of Thin Superconducting Films by Means of Ultra-High Vacuum Arc Discharges	M.J. Sadowski IPJ, Swierk, Poland	Intern. Workshop on Thin Films, Padua-Legnaro, Italy	Oct. 12, 2006	http://master.lnl.infn.it/thinfilms
The UHV Cathodic Arc; The Results on Samples and the Plasma Transport for Cavity Coating	R. Russo INFN-Na, Naple, Italy	Intern. Workshop on Thin Films, Padua-Legnaro, Italy	Oct. 12, 2006	http://master.lnl.infn.it/thinfilms
Deposition of Pure Lead Photo-Cathodes by Means of UHV Cathodic Arc	P. Strzyzewski IPJ, Swierk, Poland	Intern. Workshop on Thin Films, Padua-Legnaro, Italy	Oct. 12, 2006	http://master.lnl.infn.it/thinfilms
WP4 - Thin film cavity production	M.J. Sadowski IPJ, Swierk, Poland	JRA1 Annual Meeting, IFNF-Frascati, Italy	Nov 14, 2006	http://care.lal.in2p3.fr
Advances in investigation of clean Nb surfaces	G. Müller, Uni. Wuppertal	Annual CARE06, Frascati	Nov 15, 2006	http://care.lal.in2p3.fr
Smart Materials as Sensors and Actuators for Lorentz Force Tuning System	P.Sekalski	Open Seminar, DMCS-TUL	Sept 5, 2006	
Nb SRF	B. Visentin / CEA	ILC Meeting, Lyon, France	Jan 12th, 2006	http://lappagenda.in2p3.fr/cdsagenda/fullAgenda.php?ida=a05157
Laboratory Report	B. Visentin / CEA	TTC Meeting, KEK - Japan	Sept 25th 2006	https://indico.desy.de/conferenceDisplay.py?confId=92

Q-Drop	B. Visentin / CEA	Thin Film Workshop, Legnaro - Italy	Oct 10th 2006	http://master.lnl.infn.it/thinfilms/index.php?cont=main
Report on single cell results	D. Reschke / DESY	1st TTC Video Meeting	July 28, 2006	https://indico.desy.de/conferenceDisplay.py?confId=106
Latest 9-cell cavity measurement at DESY	D. Reschke / DESY	3rd TTC Video Meeting	Aug 30, 2006	https://indico.desy.de/conferenceDisplay.py?confId=118
Planning on new cavity tuning machines for XFEL	D. Proch / DESY	3rd TTC Video Meeting	Aug 30, 2006	https://indico.desy.de/conferenceDisplay.py?confId=118
Summary Report	B. Visentin / CEA	5th TTC Video Meeting	Oct 18th 2006	https://indico.desy.de/conferenceDisplay.py?confId=143
Update on large grain 9-cell cavities	W. Singer / DESY	6th TTC Video Meeting	Nov 22,2006	https://indico.desy.de/conferenceDisplay.py?confId=175
Advance in investigation of clean Niobium surfaces	G. Müller / Uni Wuppertal	6th TTC Video Meeting	Nov 22,2006	https://indico.desy.de/conferenceDisplay.py?confId=175
Advance in investigation of single crystal cavities	W. Singer / DESY	7th TTC Video Meeting	Dec 13 2006	https://indico.desy.de/conferenceDisplay.py?confId=187
Update new tuning machine	J. Iversen / DESY	7th TTC Video Meeting	Dec 13 2006	https://indico.desy.de/conferenceDisplay.py?confId=187

7. Publications

CARE- Pub	Title	Authors	Journal/Conf.
	Magnetic Filters in UHV Arc-Discharges: Constructions, Field Modelling and Tests of Efficiency	P. Strzyżewski, J. Langner, R. Mirowski, M.J. Sadowski, S. Tazzari and J. Witkowski	Physica Scripta T123 (2006) 135-139
	Behaviour Of Gas Conditions During Vacuum Arc Discharges Used For Deposition Of Thin Films	P. Strzyzewski, L. Catani, A. Cianchi, J. Langner, J. Lorkiewicz, R. Mirowski, R. Russo, M. Sadowski, S. Tazzari and J. Witkowski	AIP CP 812 (2006) 485-488

	RRR of copper coating and low temperature electrical resistivity of materials for TTF couplers	M. Fouaidy, N. Hammoudi, IPNOrsay, France	PHYSICA C
	Cathodic Arc Grown Niobium Films for RF Superconducting Cavity Applications	L.Catani, A. Cianchi, J.Lorkiewicz, S.Tazzari, J.Langner, P.Strzyzewski, M.Sadowski, A.Andreone, G.Cifariello, E.Di Gennari, G.Lamura and R.Russo	Physica **C441** (2006) 130-133
	Progress in Use of Ultra-High Vacuum Cathodic Arcs for Deposition of Thin Superconducting Layers	J.Langner, M.J. Sadowski, P.Strzyzewski, J.Witkowski, S.Tazzari, L.Catani, A.Cianchi, J.Lorkiewicz, R.Russo , J.Sekutowicz, T.Paryjczak and J. Rogowski	IEEE Trans. Plasma Sci. (2006) – in print.
	Seamless/Bonded Niobium Cavities	W. Singer	Physica C 441 (2006) 89-94
	Deposition of Superconducting Niobium Films for RF Cavities by Means of UHV Cathodic Arc	J. Langner, R. Mirowski, M.J.Sadowski,P.Strzyżewski, J. J. Witkowski, S.Tazzari, L. L.Catani, A.Cianchi, J.Lorkiewicz and R. Russo	Vacuum **80** (2006) 1288-1293.
	DC field emission scanning measure-ments on electropolished Nb sampels	A.Dangwal, D. Reschke, G.Müller	Physica C 441 (2006) p. 83-88
	A distributed system for radiation monitoring at linear accelerators	D. Makowski, M. Grecki, A. Napieralski, S. Simrock, and B. Mukherjee	IEEE Transactions on Nuclear Science (TNS), Vol. 53, Issue 4, Part 1, pp. 2008â€„2015, 2006, ISSN: 0018-9499
	The Application of SRAM Chip as a Novel Neutron Detector	D. Makowski, M. Grecki, B. Mukherjee, S. Simrock, B. Swiercz and A. Napieralski	Journal of Experimental Nanoscience, vol. 1, no. 2, pp. 1-8, May 2005
	TESLA cavity modeling and digital implementation in FPGA technology for control system development	Tomasz Czarski, Krzysztof T. Pozniak, Ryszard S. Romaniuk and Stefan Simrock	Nuclear Instruments and Methods in Physics Research Section A , Volume 556, Issue 2, 15 January 2006, Pages 565-576
	Superconducting cavity driving with FPGA controller	Tomasz Czarski, Waldemar Koprek, Krzysztof T. Poźniak, Ryszard S. Romaniuk, Stefan Simrock, Alexander Brandt, Brian Chase, Ruben Carcagno, Gustavo Cancelo and Timothy W. Koeth	Nuclear Instruments and Methods in Physics Research Section A, Volume 568, Issue 2, 1 December 2006, Pages 854-862

CARE-Conf			
1	Electromechanical characterization of piezoelectric actuators subjected to a variable preloading force at cryogenic temperature	M. Fouaidy, M. Saki, N. Hammoudi, L. Simonet, IPN Orsay, France	EPAC2006
2	Low temperature properties of piezoelectric actuators used in SRF cavities cold tuning systems	G. Martinet, M. Fouaidy, N. Hammoudi, A. Olivier, F. Chatelet, S. Blivet, H. Saugnac IPNOrsay, France	EPAC 2006
3	Low temperature electromechanical and dynamic properties of piezostacks for superconducting RF cavities fast tuners	Fouaidy M., Martinet G., Hammoudi N., IPNOrsay, France	CRYOPRAGUE 2006
4	Status of the XFEL testcavity program	D. Reschke, A. Brinkmann, W. Singer, X. Singer, J. Ziegler	LINAC 06
5	Dry-ice cleaning on SRF cavities	A. Brinkmann,J. Iversen, D. Reschke, J. Ziegler	EPAC 2006, Edinburgh, UK
6	Electromechanical System for Lorentz Force Compensation	P. Sekalski, A.Napieralski, S. Simrock	NSTI Nanotech 2006, Vol. 3 pp.393-396
7	Automatic, resonant excitation based, system for Lorentz Force compensation for VUV-FEL	P. Sekalski, A.Napieralski, S. Simrock	EPAC 2006 Edinburgh UK
8	Smart materials based system operated at 2K used at superconducting cavity tuner for VUV-FEL purpose	P. Sekalski, A. Napieralski, S. Simrock, C. Albrecht, L. Lilje, P. Bosland, M. Fouaidy, N. Hammoudi, A. Bosotti, R. Paparella	Int. Conf. On New ACTUATORS, Bremen, June 14-16, 2006
9	Metal Film Photo-Cathodes For High Brightness Electron Injectors	L.Cultrera, G.Gatti, F.Tazzioli, C. Vicario, A. Perrone, C. Ristoscu, J. Langner, M. Sadowski, P. Strzyzewski, S.Orlanducci and A.Fiori	Proc. EPAC2006, Edinburg, UK, Paper MOPCH02.
10	Deposition of Lead Thin Films Used as Photo-cathodes by Means of Cathodic Arc under UHV Conditions	P.Strzyzewski, J.Langner, M.J.Sadowski, J.Witkowski, S.Tazzari, R.Russo, J.Sekutowicz, J. Smedley J.Sekutowicz, J. Smedley	Proc. EPAC2006, Edinburgh, UK, Paper THPCH176.
11	Novel Development on Superconducting Niobium Film Deposition for RF Applications	A. Cianchi, L. Catani, D.DiGiovenale, J.Lorkiewicz B. Ruggiero, R. Russo, J. Langner, M. Sadowski, P.Strzyzewski, V. Merlo, M.Salvato and S.Tazzari	Proc. EPAC2006, Edinburgh, UK, Paper MOPCH168
12	Progress in Use of Ultra-High Vacuum Cathodic Arcs for Deposition of Thin Superconducting Layers	J. Langner, M.J. Sadowski, P. Strzyzewski, R. Mirowski, J. Witkowski, S. Tazzari, L. Catani, A. Cianchi, J. Lorkiewicz, R. Russo, T. Paryjczak, J. Rogowski and J. Sekutowicz	Proc. 22nd ISDEIV, Matsue, Japan, 2006 – to be published.
13	Compensation of Lorentz Force Detuning of a TTF 9-cell Cavity with a New Integrated Piezo Tuner	G. Devanz, P. Bosland, M. Desmons , E. Jacques, M. Luong, B. Visentin	EPAC 2006, **CARE-Conf-06-016-SRF**

14	Active compensation of Lorentz force detuning of a TTF 9-cell cavity in CRYHOLAB	G. Devanz, P. Bosland, M. Desmons , E. Jacques, M. Luong, B. Visentin, CEA-Saclay, France, M. Fouaidy, IPN-Orsay, France	LINAC2006
15	Status of the Electron Beam Transverse Diagnostics with Optical Diffraction Radiation at FLASH	E Chiadroni et al.	Channelling 2006
16	High Speed Synchronization Module Implemented in ALTERA Stratix II FPGA	M. Grecki, K. Przygoda	13th Mixed Design of Integrated Circuits and Systems, MIXDES, 2006
17	TIMING BASED PROCESS EXECUTION IN LINUX ENVIRONMENT	M. Borzecki, B. Swiercz, A. Napieralski	13th Mixed Design of Integrated Circuits and Systems, MIXDES, 2006
18	Novel Approach for Operating Systems Protection Against Single Event Upset	B. Swiercz, D. Makowski, A. Napieralski	13th Mixed Design of Integrated Circuits and Systems, MIXDES, 2006
19	The Radiation Tolerant Readout System for SRAM-based Neutron Detector	D. Makowski, M. Grecki, B.Mukherjee, B. Swiercz, S. Simrock, A. Napieralski	13th Mixed Design of Integrated Circuits and Systems, MIXDES, 2006
20	Research of Fault-Tolerant Computing Using COTS Elements	B. Swiercz, D. Makowski, A. Napieralski	NSTI Nanotechnology Conference and Trade Show Nanotech 2006 May 2006
21	NEW METHOD FOR RF FIELD AMPLITUDE AND PHASE CALIBRATION IN FLASH ACCELERATOR	P. PAWLIK, M. GRECKI, S. SIMROCK	13th Int. Conf. MIXDES 2006, Gdynia, Poland
22	FPGA-based Neutron Radiation Tolerant Microcontroller	D. Makowski, G. JabĹ‚oĹ„ski, J. Mielczarek, A. Napieralski, and M. Grecki	NSTI Nanotechnology Conference and Trade Show Nanotech 2006 May 2006
23	Ultra High Vacuum Cathodic Arc for Deposition of Superconducting Pb Photocathodes	P. Strzyzewski, J. Langner, R. Mirowski, M.J. Sadowski, J. Witkowski	Proc. 11th Int. Conf. PP&CF, Alushta, Ukraine, 2006 – to be published.
24	Status of Research on Deposition of Thin Superconducting Films for RF Accelerating Cavities	J. Langner, R. Mirowski, M.J.Sadowski,P.Strzyzewski, J. Witkowski, S. Tazzari, L. Catani, A. Cianchi, J. Lorkiewicz and R. Russo	Proc. 2nd Intern. Congress, Tomsk, Russia, 2006 – to be published
25	UHV Arc for High Quality Film Deposition	R. Russo, A. Cianchi, Y.H.Akhmadeev, L. Catani, J. Langner, J. Lorkiewicz, R. Polini, B. Ruggiero, M.J.Sadowski, S.Tazzari and N.N. Koval	Proc. ICMCTF06, San Diego, USA, Session B2-1-8, P.132.

26	SRAM-based Passive Dosimeter for High-Energy Accelerator Environments	D. Makowski, M. Grecki, B. ´Swiercz, A. Napieralski, DMCS, Lodz, Poland; B. Mukherjee, S. Simrock, DESY, Hamburg, Germany	7th European Workshop on Diagnostics and Instrumentation for Particle ACcelerators, DIPAC2005, June 2005
27	External radiation shielding for the protection of electronic devices operating in the FLASH facility tunnel at DESY	B.Murkherjee, D.Makowski, D.Rybka; O.Kroeplin, S.Simrock, H.J.Eckoldt	13th Mixed Design of Integrated Circuits and Systems, MIXDES 2006,pp. 65-68
28	IMPROVEMENTS OF EXPERT SYSTEM FOR RF-POWER STATIONS	B.P. KOS DA, W. CICHALEWSKI	MIXDES 2006
29	High resolution BPM for linear colliders	C. Simon, S. Chel, M. Luong, O. Napoly, J. Novo, D. Roudier, CEA-Saclay, Gif sur Yvette, France; N. Rouvière, CNRS-IN2P3-IPN, Orsay, France	BIW 06, Batavia, EPAC 06, **CARE-Conf-06-013-SRF**
30	High resolution BP for linear colliders	C. Simon, S. Chel, M. Luong, O. Napoly, J. Novo, D. Roudier, CEA-Saclay, Gif sur Yvette, France; N. Rouvière, CNRS-IN2P3-IPN, Orsay, France	BIW 06, Batavia, EPAC 06, **CARE-Conf-06-015-SRF**
31	Developments in conditioning procedures for the TTF-III power couplers	H. Jenhani, T. Garvey, P. Lepercq, M. Omeich, C. Prevost, A. Variola	EPAC 06, Edinburgh (UK), **CARE-Conf-06-017-SRF**
32	Performance limitations of TESLA cavities in the flash accelerator and their relation to the assembly process	L. Lilje	EPAC'06, Edinburgh (UK), **CARE-Conf-06-047-SRF**
33	USING HIGHER ORDER MODES IN SUPERCONDUCTING ACCELERATING CAVITIES FOR BEAM MONITORING	S. Molloy, N. Baboi, N. Eddy, J. Frisch, L. Hendrickson, O. Hensler, D. McCormick, J. May, S. Nagaitsev, O. Napoly, R.C. Paparella, L. Petrosyan, L. Piccolli,R. Rechenmacher, M. Ross, C. Simon, T. Smit1, K. Watanabe and M. Wendt	**CARE-Conf-06-052-SRF**
34	Experimental and theoretical analysis of the TESLA-like SRF cavity flanges	L. Monaco, P. Michelato, C. Pagani, N. Panzeri	EPAC'06
35	ILC Coaxial Blade Tuner (MOPCH171)	C. Pagani, A. Bosotti, P. Michelato, N. Panzeri, R. Paparella, P. Pierini	EPAC'06, 10th European Particle Accelerator Conference Edinburgh, UK 26-30 June 2006
36	High Power Couplers for linear accelerators	A.Variola	LINAC06 Knoxville, USA, 2006

37	Readout system for cost-effective neutron fluence monitoring system	D. Makowski, G. Jabłoński, M. Grecki, J. Mielczarek, A. Napieralski	RADiation and its Effects on Component and Systems RADECS, September 2005
38	Metal-Based Photo-cathodes for High-Brightness RF Photoinjectors	L. Cultrera, G. Gatti, F. Tazzioli, A. Perrone, P. Miglietta, C. Ristoscu, S. Orlanducci, A. Fiori, J. Langner and P. Strzyzewski	Proc. Linear Accelerator Conf. LINAC06, Knoxville, TN, USA, Aug. 2006.
39	Progress in Research on Deposition of ThinSuperconducting Films by Means of Ultra-High Vacuum Arc Discharges	M.J. Sadowski, J. Langner, P.Strzyzewski, R. Mirowski, J. Witkowski, S. Tazzari, L. Catani, A. Cianchi, J. Lorkiewicz and R. Russo	Proc. Intern. Workshop on Thin Films, Padua-Legnaro, Italy, Oct. 2006. P. 51.
40	The UHV Cathodic Arc; The Results on Samples and the Plasma Transport for Cavity Coating	L. Catani, A. Cianchi, J. Lorkiewicz, S. Tazzari, J. Langner, R. Mirowski, M.J.Sadowski, P.Strzyzewski, J. Witkowski, B. Ruggiero and R. Russo	Proc. Intern. Workshop on Thin Films, Padua-Legnaro, Italy, Oct. 2006, P. 52.
41	Deposition of Pure Lead Photo-Cathodes by Means of UHV Cathodic Arc	P. Strzyzewski, J. Langner, R. Mirowski, M.J. Sadowski, J. Witkowski, J. Sekutowicz, T. Rao, J. Smedley, P. Kneisel, J. Smedley, P. Kneisel, L. Cultrera, G. Gatti and F. Tazzioli	Proc. Intern. Workshop on Thin Films, Padua-Legnaro, Italy, Oct. 2006, P. 52.
42	CARE-JRA1-SRF WP4 –Thin Film Cavity Production	M.J.Sadowski, J.Langner, P.Strzyzewski and S.Tazzari	Proc. CARE-JRA1 Working Meeting, INFN-Frascati, Italy, Nov. 2006
43	Analysis of Microphonic Disturbances and Simulation for Feedback Compensation	M. Luong *et al.*	EPAC 2006

CARE-Note			
	Reports about new design for components: Cold Flanges	P. Michelato, L. Monaco, N. Panzeri	CARE-Note-2006-002-SRF
	Integration of piezoelectric actuators in the piezotuner developed at Saclay	M. Fouaidy, N. Hammoudi, G. Martinet, IPNOrsay, France, G. Devanz, P. Bosland, E. Jacques, Sylvie Regnaud, CEA Saclay, France	CARE-Note-2006-006-SRF
	Electromechanical characterization of piezoelectric actuators subjected to a variable preloading force at cryogenic temperature	M. Fouaidy, M. Saki, N. Hammoudi, L. Simonet.	CARE-Note-2006-007-SRF

8. Overview of status of JRA1 SRF

N°	Task Name	Ende
2	**WP 2 IMPROVED STANDARD CAVITY FABRICATION**	**Mi 17.12.08**
2.1	**Reliability Analysis**	**Fr 29.09.06**
2.1.1	Review of data bank: cavity fabrication	Fr 13.02.04
2.1.2	Review of data bank :cavity treatment	Di 30.03.04
2.1.3	Review of data bank: cavity VT performance	Do 13.05.04
2.1.4	Review of data bank: string assembly	Do 05.08.04
2.1.5	Review of data bank: string performance	Do 28.10.04
2.1.6	Establish correlations	Do 10.02.05
2.1.7	**Final report on reliability issue**	Fr 29.09.06
2.2	**Improved component design**	**Mi 17.12.08**
2.2.1	**Documentation retrieving**	**Mo 31.07.06**
2.2.1.1	Start up meetings	Mo 09.02.04
2.2.1.2	Access and study of Jlab, DESY, LLAN, KEK experience	Mi 13.10.04
2.2.1.3	**Summary report on the status of the art on ancillaries**	Mi 13.10.04
2.2.1.4	Sealing material and shape design	Fr 29.07.05
2.2.1.5	Flange preliminary design	Fr 24.06.05
2.2.1.6	Material and geometric compatibility	Fr 02.09.05
2.2.1.7	Final assembly design	Fr 09.09.05
2.2.1.8	End plate preliminary design	Fr 09.09.05
2.2.1.9	**Report about new design for components**	Fr 16.09.05
2.2.1.10	Stiffness optimization	Fr 10.02.06
2.2.1.11	Manufacturing procedure analysis	Fr 22.07.05
2.2.1.12	Final assembly design	Fr 17.02.06
2.2.1.13	Other ancillaries design	Fr 24.02.06
2.2.1.14	**Final Report for new components**	Mo 31.07.06
2.2.2	**Review of criticality in welding procedures**	**Fr 29.12.06**
2.2.2.1	Review of available parameters on vendor welding machine	Fr 21.10.05
2.2.2.2	Definition of prototype requirements for tests	Mo 11.07.05
2.2.2.3	Welding test on specimens	Fr 24.02.06
2.2.2.4	Analysis of the results	Fr 11.08.06
2.2.2.5	**Report about welding parameters**	Fr 29.12.06
2.2.3	**Finalize new component design**	**Di 18.12.07**
2.2.3.1	Do drawings	Di 18.12.07
2.2.3.2	**New components design finished**	Di 18.12.07
2.2.4	**Finalize new cavity design**	**Do 01.11.07**
2.2.4.1	Make drawings	Do 01.11.07
2.2.4.2	**New cavity design finished**	Do 01.11.07
2.2.5	**Fabrication of new cavity**	**Mi 17.12.08**
2.2.5.1	Fabrication	Mi 17.12.08
2.2.5.2	New cavity finished	Do 11.09.08

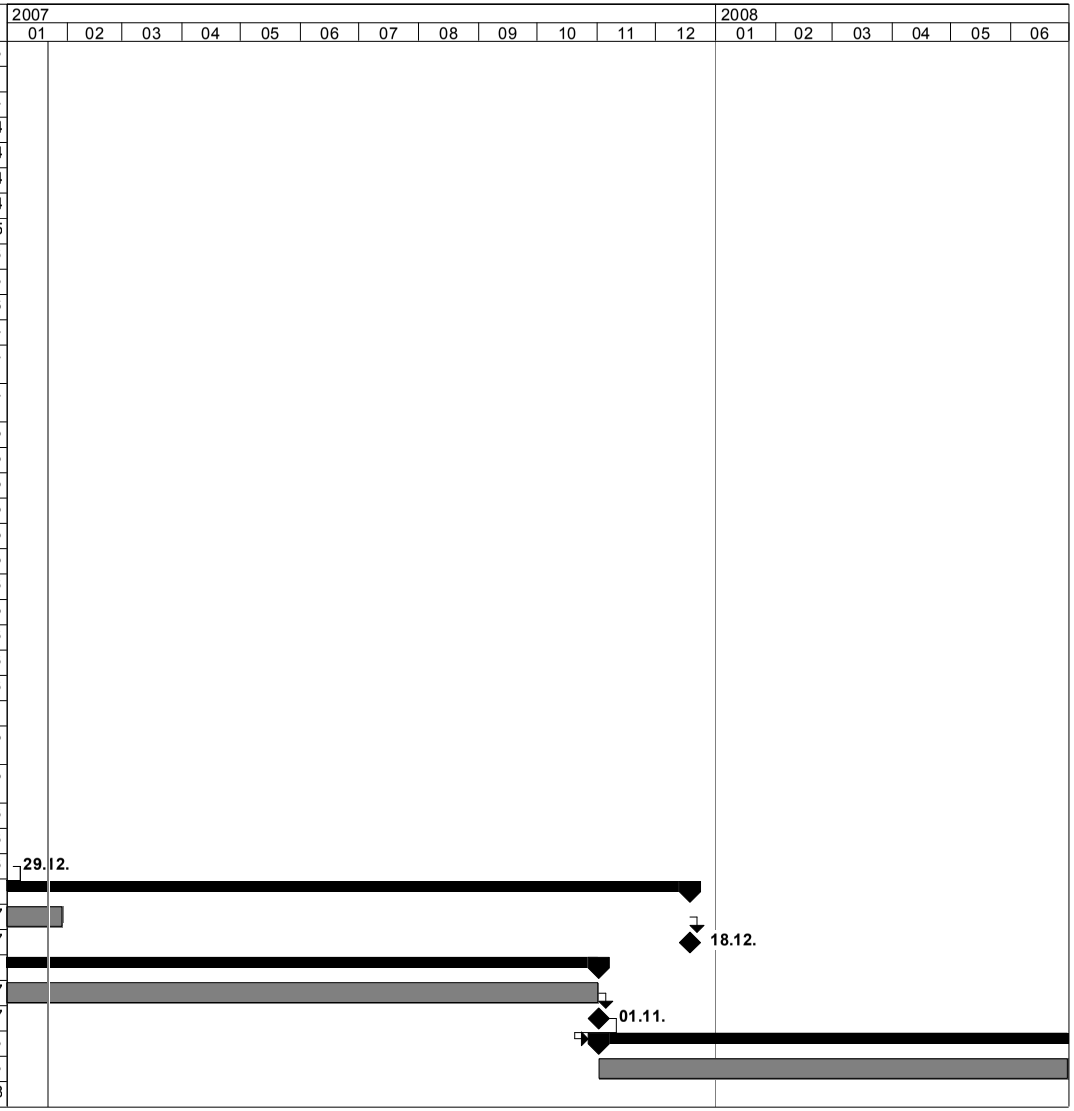

N°	Task Name	Ende
2.3	**EB welding**	**Fr 04.01.08**
2.3.1	**Design tooling**	**Mi 15.12.04**
2.3.1.1	Tools for flange welding	Fr 20.02.04
2.3.1.2	Tools for pipe welding	Di 13.04.04
2.3.1.3	Tools for stiffening rings	Do 03.06.04
2.3.1.4	Tools for single cell welding	Mo 23.08.04
2.3.1.5	Tools for 9-cells	Mi 15.12.04
2.3.1.6	**Tools design finished**	Mi 15.12.04
2.3.2	**Tools production**	**Fr 11.03.05**
2.3.2.1	Tools for flange welding	Di 30.03.04
2.3.2.2	Tools for pipe welding	Do 13.05.04
2.3.2.3	Tools for stiffening rings	Do 15.07.04
2.3.2.4	Tools for single cell welding	Mi 27.10.04
2.3.2.5	Tools for 9-cells	Fr 11.03.05
2.3.2.6	**Tools fabrication finished**	Fr 11.03.05
2.3.3	**Welding**	**Fr 04.01.08**
2.3.3.1	Commissioning welding machine	Fr 16.04.04
2.3.3.2	Test welding	Fr 03.09.04
2.3.3.3	**Start production welding of components**	Fr 11.03.05
2.3.3.4	Single cell welding	Fr 24.11.06
2.3.3.5	Multicell welding	Fr 04.01.08
2.3.3.6	**Welding of prototypes of components finished**	Fr 04.01.08

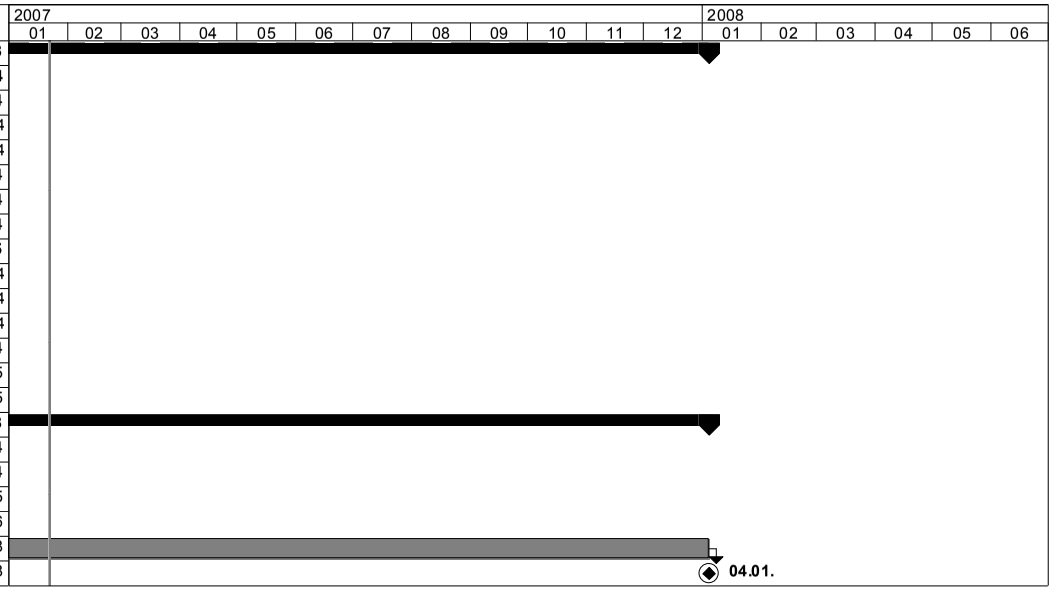

N°	Task Name	Ende
3	**WP3 SEAMLESS CAVITY PRODUCTION**	**Fr 04.01.08**
3.1	**Seamless by spinning**	**Fr 04.01.08**
3.1.1	**Design spinning machine**	**Fr 17.09.04**
3.1.1.1	Drawings of the matrices	Fr 16.04.04
3.1.1.2	Drawings of the support system	Fr 17.09.04
3.1.1.3	**Drawings of spinning machine finished**	Fr 17.09.04
3.1.2	**Fabrication of spinning machine**	**Do 10.11.05**
3.1.2.1	Fabrication of machine parts	Fr 29.04.05
3.1.2.2	Softw are for the machine	Do 31.03.05
3.1.2.3	Assembly of machine	Fr 29.07.05
3.1.2.4	Commissioning of the machine	Do 10.11.05
3.1.2.5	**Spinning machine ready**	Do 10.11.05
3.1.3	**Evaluation of spinning parameters**	**Do 18.05.06**
3.1.3.1	Drawings of the support system and turning mechanism	Do 26.01.06
3.1.3.2	Drawings of the necking mechanism	Fr 26.08.05
3.1.3.3	Fabrication of the tube necking machine	Do 23.03.06
3.1.3.4	Commissioning of the machine	Do 18.05.06
3.1.3.5	**Spinning parameters defined**	Do 18.05.06
3.1.4	**Spinning of 1-celll cavities**	**Do 07.12.06**
3.1.4.1	Material and fabrication of bulk Nb test tubes	Do 07.09.06
3.1.4.2	Material and fabrication of bimetallic NbCu test tubes	Do 07.12.06
3.1.4.3	**1-cell spinning parameters defined**	Do 07.12.06
3.1.5	**Extension of spinning apparatus to multicells**	**Do 11.01.07**
3.1.5.1	Computer simulation of the necking	Do 11.01.07
3.1.5.2	**Start of Multi-cell spinning**	Do 11.01.07
3.1.6	**Spinning of multi-cell cavities cavities**	**Do 02.08.07**
3.1.6.1	Computer simulation of the spinning	Do 02.08.07
3.1.6.2	Spinning of bulk Nb 9-cell cavities	Do 12.07.07
3.1.6.3	**Parameters of multi-cell spinning defined**	Do 12.07.07
3.1.7	**Series production of multi-cell cavities**	**Fr 04.01.08**
3.1.7.1	Spinning	Fr 04.01.08
3.1.7.2	**Multi-cell cavities finished**	Fr 04.01.08

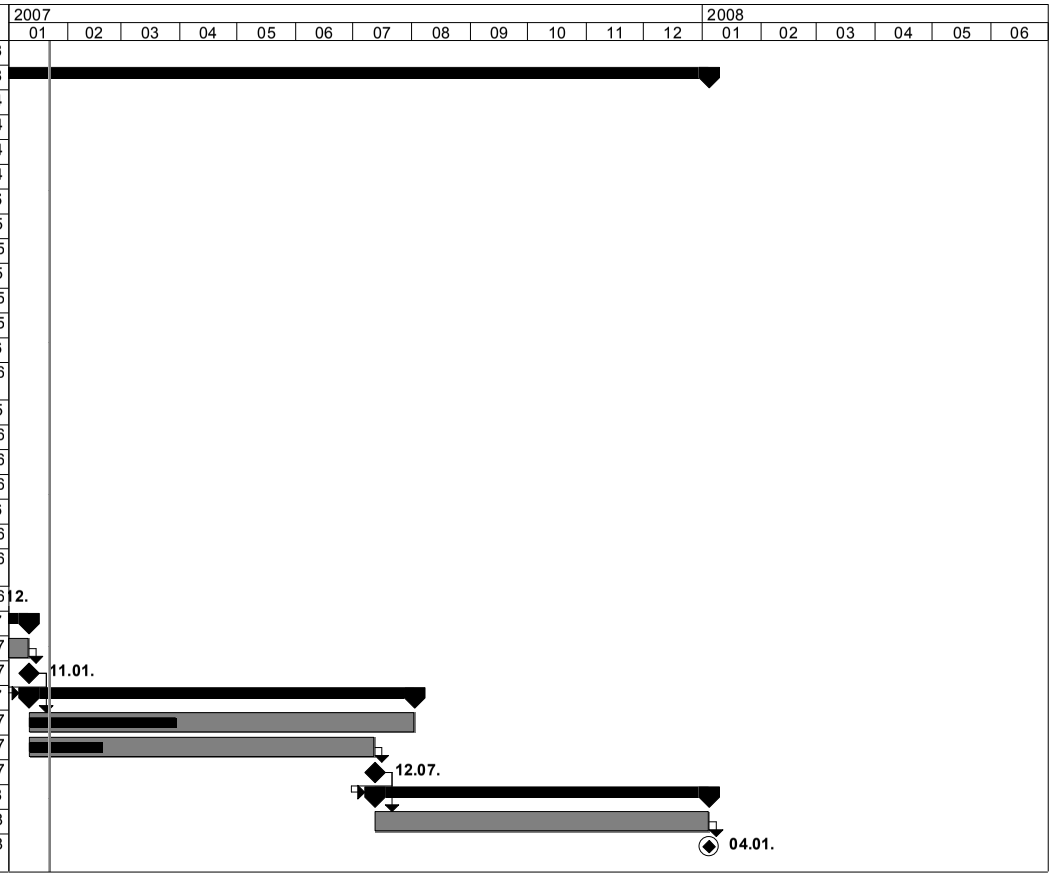

N°	Task Name	Ende
3.2	**Seamless by hydroforming**	**Fr 16.11.07**
3.2.1	**Design hydro forming machine**	**Fr 17.09.04**
3.2.1.1	Drawings of the matrices	Fr 17.09.04
3.2.1.2	Drawings of the support system	Fr 17.09.04
3.2.1.3	**Drawings matrix & support finished**	Fr 17.09.04
3.2.2	**Construction of hydro forming machine**	**Fr 01.07.05**
3.2.2.1	Hydraulic for machine	Mi 14.07.04
3.2.2.2	Software for the machine	Fr 17.09.04
3.2.2.3	Machine fabrication	Mo 21.03.05
3.2.2.4	Commissioning of the machine	Fr 01.07.05
3.2.2.5	**Hydro forming machine ready**	Fr 01.07.05
3.2.3	**Construction of tube necking machine**	**Do 24.02.05**
3.2.3.1	Drawings of the support system and turning mechanism	Fr 27.08.04
3.2.3.2	Drawings of the necking mechanism	Fr 27.08.04
3.2.3.3	Fabrication of the tube necking machine	Do 24.02.05
3.2.3.4	Software for the tube necking machine	Do 30.12.04
3.2.3.5	**Construction tube necking machine finished**	Do 24.02.05
3.2.4	**Development of seamless tubes for 9-cell cavities**	**Fr 01.07.05**
3.2.4.1	Material and fabrication of bulk Nb test tubes	Fr 01.07.05
3.2.4.2	Material and fabrication of bimetallic NbCu test tubes	Fr 01.07.05
3.2.4.3	**Seamless tubes ready**	Fr 01.07.05
3.2.5	**Development of tube necking**	**Fr 15.12.06**
3.2.5.1	Computer simulation of the necking	Fr 30.06.06
3.2.5.2	Experiments on tube necking at iris	Fr 15.12.06
3.2.5.3	**Tube necking machine operational**	Fr 15.12.06
3.2.6	**Hydro forming of seamless cavities**	**Fr 16.11.07**
3.2.6.1	Computer simulation of the hydro forming	Fr 24.11.06
3.2.6.2	Hydro forming of bulk Nb 9-cell cavities	Fr 16.11.07
3.2.6.3	**Hydro formed 9-cell cavities ready**	Fr 16.11.07

N°	Task Name	Ende
4	**WP4 THIN FILM CAVITY PRODUCTION**	**Fr 28.12.07**
4.1	**Linear-arc cathode coating**	**Fr 28.12.07**
4.1.1	**Installation & commissioning of coating apparatus**	**Fr 29.06.07**
4.1.1.1	Modification of a prototype facility for single cells	Di 14.09.04
4.1.1.2	Optimization of a triggering system	Mo 11.10.04
4.1.1.3	**Prototype facility ready**	Mo 11.10.04
4.1.1.4	Study of arc current reduction and stabilization	Mo 07.02.05
4.1.1.5	Optimization of powering system	Mo 14.03.05
4.1.1.6	**Coating apparatus operational**	Mo 14.03.05
4.1.1.7	**Coating single cells**	**Fr 29.06.07**
4.1.1.7.1	Coating of single cells without micro droplet filtering	Fr 29.06.07
4.1.1.7.2	Design and construction of a micro droplet filter sys	Fr 30.06.06
4.1.1.7.3	**Droplet filter ready**	Fr 30.06.06
4.1.1.7.4	Coating of single cell with micro droplet filtering	Fr 29.06.07
4.1.2	**Coating multi-cell**	**Fr 28.12.07**
4.1.2.1	Design and commissioning	Fr 28.12.07
4.1.2.2	First multicell coating	Fr 26.10.07
4.2	**Planar-arc cathode coating**	**Sa 30.06.07**
4.2.1	**Modification of a planar-arc & trigger system**	**Fr 27.05.05**
4.2.1.1	Modification	Fr 16.04.04
4.2.1.2	Optimization of the laser triggering system	Fr 03.09.04
4.2.1.3	**Planar arc system fully tested**	Fr 27.05.05
4.2.2	**Routine Operation of planar arc system**	**Fr 30.06.06**
4.2.2.1	Characterization of samples coated at different conditions	Fr 30.06.06
4.2.2.2	Characterization of Nb-coated sapphire samples	Fr 30.06.06
4.2.2.3	Characterization of Nb-coated copper samples	Fr 30.06.06
4.2.2.4	**Summary report on quality of planar arc coating**	Fr 27.05.05
4.2.3	**Studies of other HTC superconducting coating**	**Sa 30.06.07**
4.2.3.1	Study of superconducting properties	Sa 30.06.07
4.2.3.2	**Report on quality of superconducting properties**	Sa 30.06.07

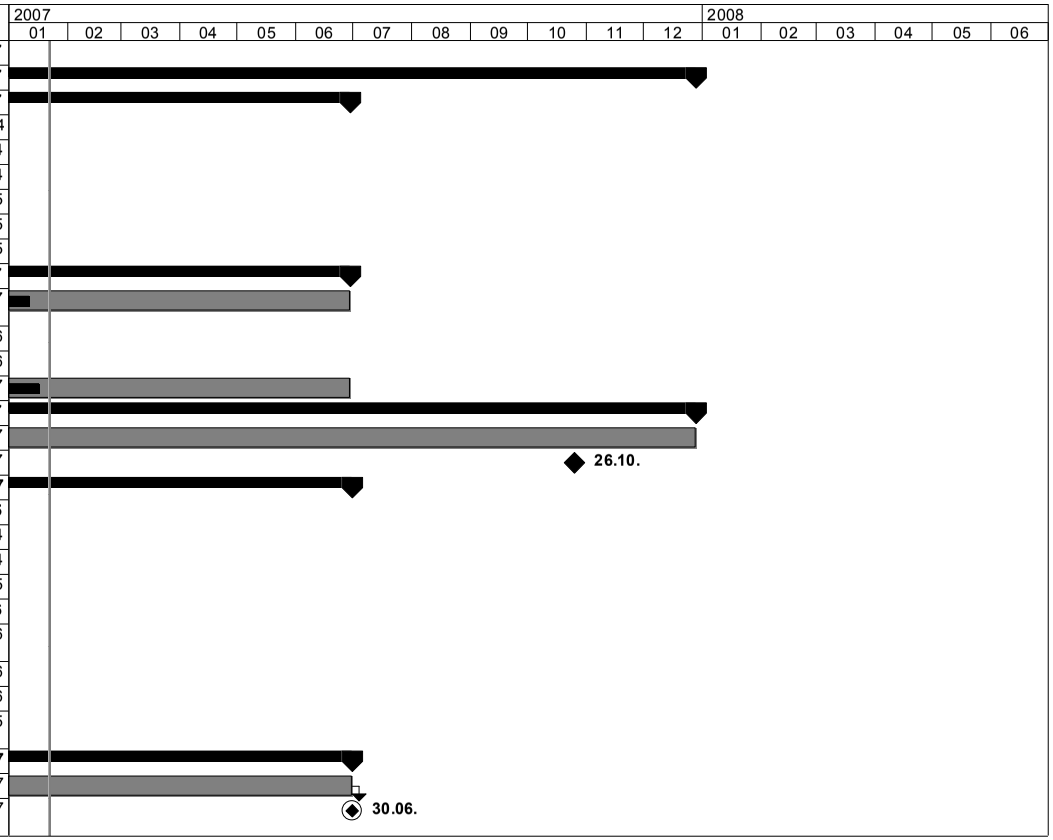

N°	Task Name	Ende
5	**WP5 SURFACE PREPARATION**	**Mi 30.12.09**
5.1	**EP on single cells**	**Fr 29.08.08**
5.1.1	**EP on samples**	**So 15.01.06**
5.1.1.1	Establishing method of surface characterization	Fr 28.05.04
5.1.1.2	**Surface characterization fixed**	Fr 28.05.04
5.1.1.3	Series of EP with samples for surface investigations	Do 31.03.05
5.1.1.4	**Best EP parameters**	So 15.01.06
5.1.2	**Single cell cavities**	**Do 31.03.05**
5.1.2.1	Order Nb and fabricate 3 cavities	Do 31.03.05
5.1.2.2	**3 cavities fabricated**	Do 31.03.05
5.1.3	**Build EP chemistry for single cells**	**Sa 31.12.05**
5.1.3.1	Design of EP set-up	Fr 27.02.04
5.1.3.2	Fabrication of EP set-up	Mo 28.02.05
5.1.3.3	Commissioning of EP set-up	Sa 31.12.05
5.1.3.4	**First operation of EP set-up**	Sa 31.12.05
5.1.4	**Operation of single cell EP**	**Fr 09.06.06**
5.1.4.1	Continous single cell operation	Fr 09.06.06
5.1.4.2	**Define working parameters for single cells**	Fr 09.06.06
5.1.5	**Continuous operation, search for best parameters**	**Fr 29.08.08**
5.1.5.1	Parametrising EP procedure	Fr 29.08.08
5.1.5.2	**EP parameters fixed**	Fr 29.08.08
5.2	**EP on multi-cells**	**Fr 19.09.08**
5.2.1	**Transfer of parameters from 1 cell to multi cell equipment**	**Do 30.11.06**
5.2.2	**Laser roughness**	**Fr 20.01.06**
5.2.2.1	Evaluate existing systems	Do 05.05.05
5.2.2.2	Specify laser system	Do 08.09.05
5.2.2.3	Built laser system	Fr 20.01.06
5.2.2.4	**Roughness measurement finished**	Fr 20.01.06
5.2.3	**Oxipolishing as final chemical cleaning**	**Di 01.04.08**
5.2.3.1	Laboratory studies	Fr 22.04.05
5.2.3.2	Design of OP system	Mi 18.05.05
5.2.3.3	Setup one-cell system	Mi 31.01.07
5.2.3.4	**Proof-of-Principle experiment Oxipolishing**	Mi 31.01.07
5.2.3.5	Design OP for nine-cells	Di 29.05.07
5.2.3.6	Build OP for 9-cells	Di 25.09.07
5.2.3.7	**OP for 9-cells ready**	Di 25.09.07
5.2.3.8	Study op with 9-cell cavities	Di 01.04.08
5.2.3.9	Evaluate experiments	Di 01.04.08
5.2.4	**Transfer Electropolishing technology to industry**	**Fr 19.09.08**
5.2.4.1	Qualify industry with one-cells	Fr 02.06.06
5.2.4.2	Industrial design study on setup for multi-cells	Di 26.12.06
5.2.4.3	**Report on industrial design**	Di 26.12.06
5.2.4.4	Fabricate EP multi-cell industrial prototype	Mo 07.05.07
5.2.4.5	Commission EP multi-cell industrial prototype	Mo 27.08.07
5.2.4.6	**EP multi-cell industrial prototype ready**	Mo 27.08.07
5.2.4.7	Operate EP multi-cell industrial prototype	Fr 19.09.08
5.2.4.8	**Final report on industrial EP**	Fr 19.09.08

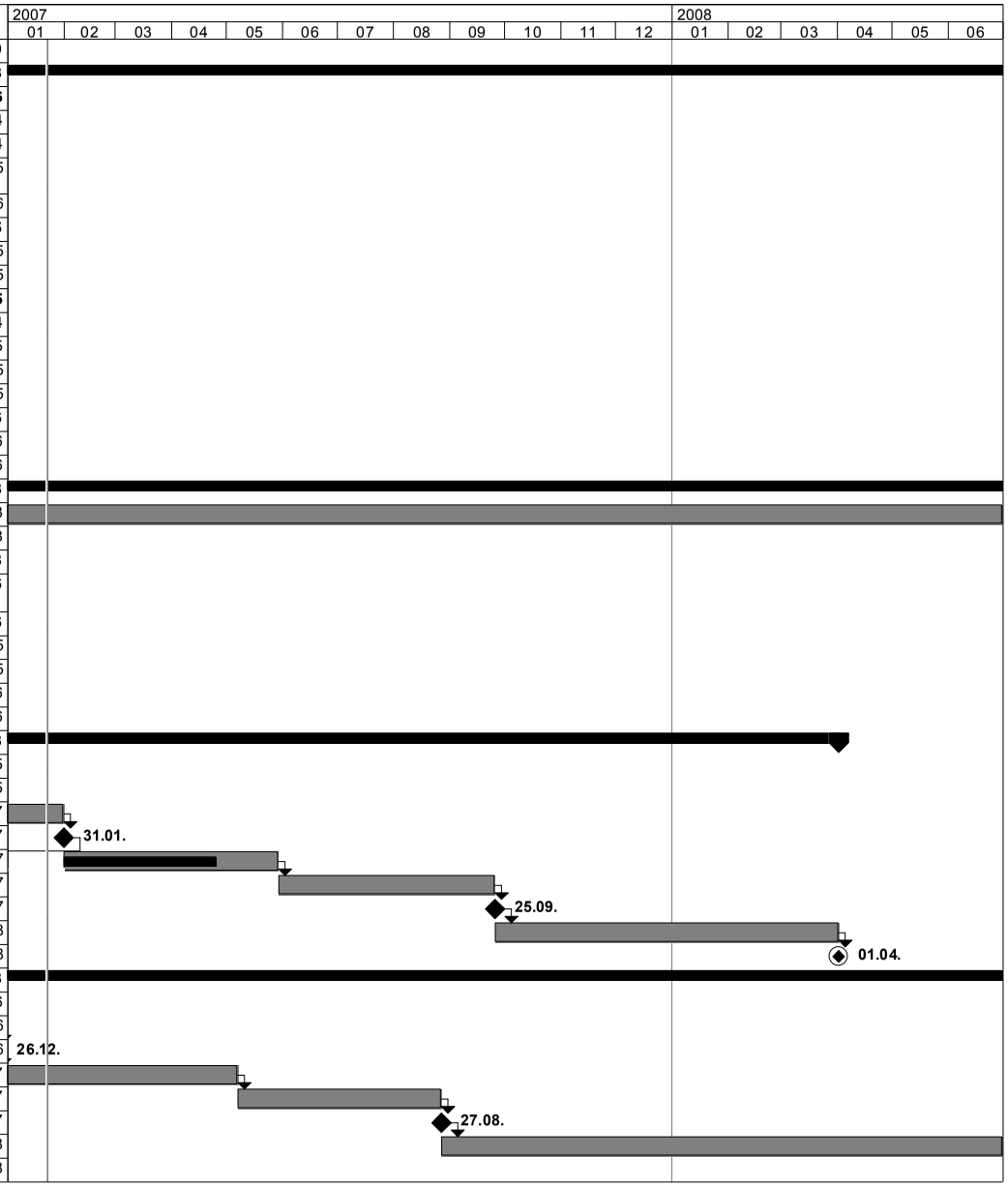

N°	Task Name	Ende
5.3	**Automated EP (AEP)**	**Do 03.01.08**
5.3.1	**Prototype EP installation**	**Di 08.02.05**
5.3.1.1	Design installation	Fr 05.03.04
5.3.1.2	Fabricate/ order components	Fr 02.07.04
5.3.1.3	Assemble EP installation	Di 08.02.05
5.3.1.4	**First operation of automated EP**	Di 08.02.05
5.3.2	**EP computer control**	**Mo 21.02.05**
5.3.2.1	Design control architecture	Di 27.04.04
5.3.2.2	Developed software	Di 10.08.04
5.3.2.3	Test of software	Mo 21.02.05
5.3.2.4	**Software ready**	Mo 21.02.05
5.3.3	**Operation of AEP prototype**	**Mo 13.02.06**
5.3.3.1	Correlate surface finish/ conductance	Mo 13.06.05
5.3.3.2	Determine optimum conductance	Mi 14.09.05
5.3.3.3	Optimize automated operation	Fr 02.12.05
5.3.3.4	Design report on AEP	Mo 13.02.06
5.3.3.5	**Automated EP is defined**	Mo 13.02.06
5.3.4	**Alternative electrolytes**	**Mo 30.10.06**
5.3.4.1	Review of EP chemistry	Di 24.05.05
5.3.4.2	**Proposal for alternative electrolytes**	Di 24.05.05
5.3.4.3	Experiments with alternative electrolytes	Mo 30.10.06
5.3.4.4	**Conclude experimental results**	Mo 30.10.06
5.3.5	**Define best AEP**	**Do 03.01.08**
5.3.5.1	Compare standard/new electrolyte method	Fr 05.01.07
5.3.5.2	Modify AEP installation for best electrolyte	Fr 06.04.07
5.3.5.3	Operate modified AEP	Do 25.10.07
5.3.5.4	Design report on best AEP	Do 03.01.08
5.3.5.5	**Conclude on best electrolyte**	Do 03.01.08
5.4	**Dry ice cleaning**	**Mi 30.12.09**
5.4.1	**Installation of full system for 1-3 cell cavities**	**Mo 11.04.05**
5.4.1.1	Installation of CO2 piping	Mi 31.03.04
5.4.1.2	Installation of motion system	Mi 30.06.04
5.4.1.3	Installation of control system	Di 08.02.05
5.4.1.4	Commissioning	Mo 11.04.05
5.4.1.5	**Installation finished**	Mo 11.04.05
5.4.2	**Optimization of cleaning parameters**	**Fr 14.07.06**
5.4.2.1	Sample cleaning	Fr 09.09.05
5.4.2.2	1-cell cavity cleaning	Mi 08.02.06
5.4.2.3	Fix best cleaning parameters	Fr 14.07.06
5.4.2.4	**Cleaning parameters fixed**	Fr 14.07.06
5.4.3	**VT 9-cell cleaning apparatus**	**Fr 30.11.07**
5.4.3.1	Design 9-cell apparatus VT	Do 28.12.06
5.4.3.2	Fabricated 9-cell apparatus	Do 29.03.07
5.4.3.3	Installation of 9-cell apparatus	Fr 29.06.07
5.4.3.4	Commissioning of 9-cell apparatus	Fr 30.11.07
5.4.3.5	**VT Cleaning Installation finished**	Fr 30.11.07
5.4.4	**VT Cleaning of 9-cell cavities**	**Mi 30.12.09**
5.4.4.1	Continuous cleaning	Mi 30.12.09
5.4.4.2	**Evaluation of experimental results**	Mi 30.12.09
5.4.5	**Design & construction of H 9-cell cleaning apparatus**	**Fr 03.04.09**
5.4.5.1	Design 9-cell apparatus VT	Mi 02.04.08
5.4.5.2	Fabricated 9-cell apparatus	Mo 04.08.08
5.4.5.3	Installation of 9-cell apparatus	Mo 03.11.08
5.4.5.4	Commissioning of 9-cell apparatus	Fr 03.04.09
5.4.5.5	**Start H 9-cell cleaning**	Fr 03.04.09
5.4.6	**Cleaning of horizontal nine-cell cavity**	**Mi 30.12.09**
5.4.6.1	Continuous cleaning	Mi 30.12.09
5.4.6.2	**Evaluation of experimental results**	Mi 30.12.09

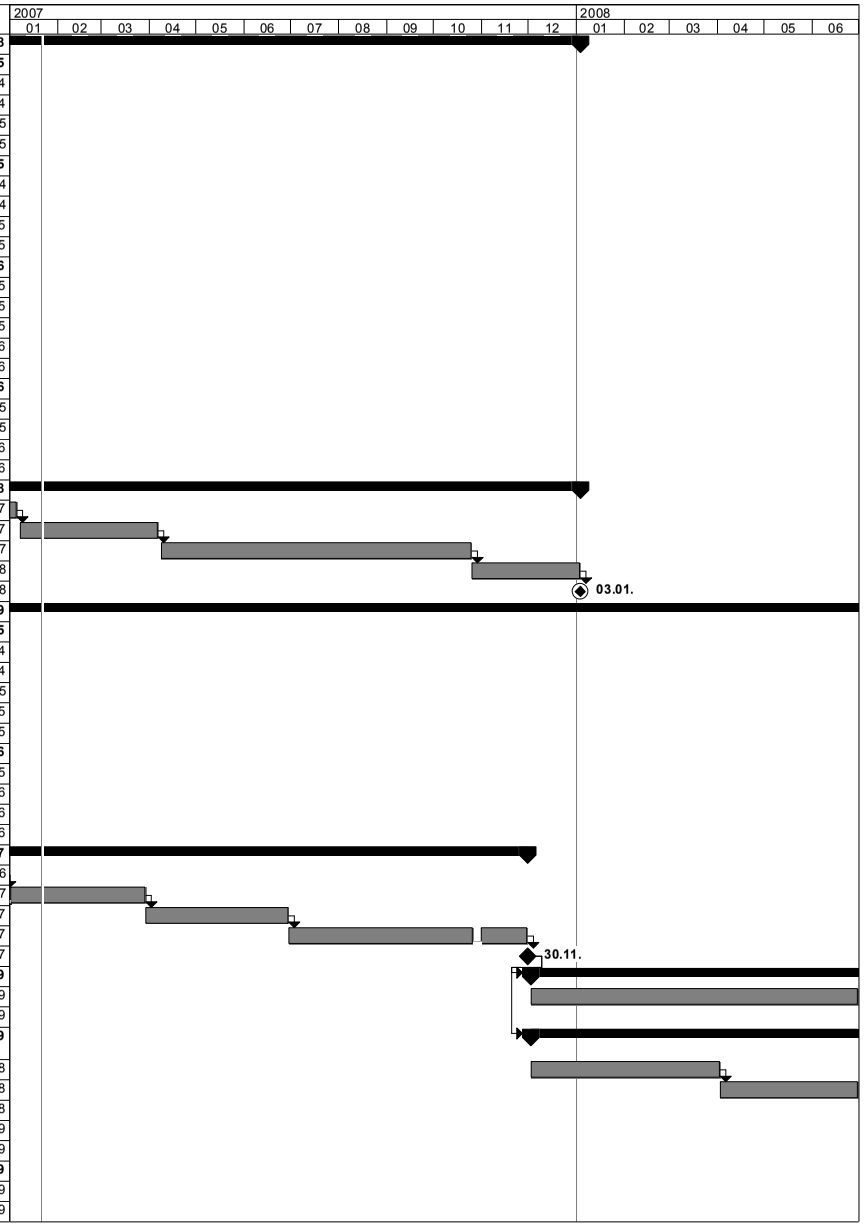

N°	Task Name	Ende
6.1	**SQUID scanning**	**Mo 31.12.07**
6.1.1	**Produce calibration defects**	**Do 12.08.04**
6.1.1.1	Production of surface defects	Fr 18.06.04
6.1.1.2	Production of bulk defects	Do 12.08.04
6.1.1.3	**Calibration defects finished**	Do 12.08.04
6.1.2	**Design components of Squid scanner**	**Di 30.11.04**
6.1.2.1	Design of the scanning table and support	Mi 30.06.04
6.1.2.2	Design of the SQUID cooling system	Di 30.11.04
6.1.2.3	**Design Scanner finished**	Di 30.11.04
6.1.3	**Construction of scanning apparatus**	**Fr 16.12.05**
6.1.3.1	Fabrication of the SQUID	Mi 30.03.05
6.1.3.2	Fabrication and purchase of components for SQUID apparatus	Do 30.06.05
6.1.3.3	Software for the SQUID scanner	Do 30.06.05
6.1.3.4	Commissioning and calibration of scanning apparatus	Fr 16.12.05
6.1.3.5	**Scanning apparatus operational**	Fr 16.12.05
6.1.4	**Scanning of sheets with artificial defects**	**Do 08.02.07**
6.1.4.1	Scanning of sheets with artificial surface defects	Do 01.06.06
6.1.4.2	Scanning of sheets with artificial bulk defects	Do 16.11.06
6.1.4.3	Development of algorithm for material defects classification	Do 08.02.07
6.1.4.4	**Classification of defects finished**	Do 08.02.07
6.1.5	**Scanning of production sheets**	**Mo 31.12.07**
6.1.5.1	Scanning of sheets of different producers	Do 20.09.07
6.1.5.2	Identification of defects by (EDX, SURFA etc.)	Fr 28.09.07
6.1.5.3	Conclusive comparison with eddy current data	Mo 31.12.07
6.1.5.4	**Final report on SQUID scanning**	Mo 31.12.07
6.2	**Flux gate magnetometry**	**Mi 11.06.08**
6.2.1	**Produce calibration defects**	**Sa 01.01.05**
6.2.1.1	Production of surface defects	Fr 07.05.04
6.2.1.2	Production of bulk defects	Do 01.07.04
6.2.1.3	**Calibration defects finished**	Sa 01.01.05
6.2.2	**Design components of flux gate head**	**Mo 20.12.04**
6.2.2.1	Design electronics	Fr 16.04.04
6.2.2.2	Design of flux gate head	Fr 17.12.04
6.2.2.3	Design of operations software	Fr 04.06.04
6.2.2.4	**Design flux gate head finished**	Mo 20.12.04
6.2.3	**Fabrication of flux gate detector**	**Mo 19.12.05**
6.2.3.1	Fabrication of flux gate head	Fr 29.04.05
6.2.3.2	Fabrication of mechanics	Di 12.07.05
6.2.3.3	Implementation of software	Mo 19.09.05
6.2.3.4	Commissioning of flux gate detector	Mo 21.11.05
6.2.3.5	Calibration of flux gate detector	Mo 19.12.05
6.2.3.6	**Flux gate detector operational**	Mo 19.12.05
6.2.4	**Commissioning of flux gate detector**	**Do 04.01.07**
6.2.4.1	Operational tets tests	Fr 21.07.06
6.2.4.2	Evaluation of test results	Do 04.01.07
6.2.4.3	**Flux gate scanner commissioned**	Do 04.01.07
6.2.5	**Operation of flux gate detector**	**Mo 17.09.07**
6.2.5.1	Regular operation	Mi 06.06.07
6.2.5.2	Report of operation	Mo 17.09.07
6.2.5.3	**Conclusion of flux gate scanning operation**	Mo 17.09.07
6.2.6	**Comparison with SQUID scanner**	**Mi 11.06.08**
6.2.6.1	Compare measurements	Mi 11.06.08
6.2.6.2	**Conclude SQUID scanner vs. flux gate detector**	Mi 11.06.08

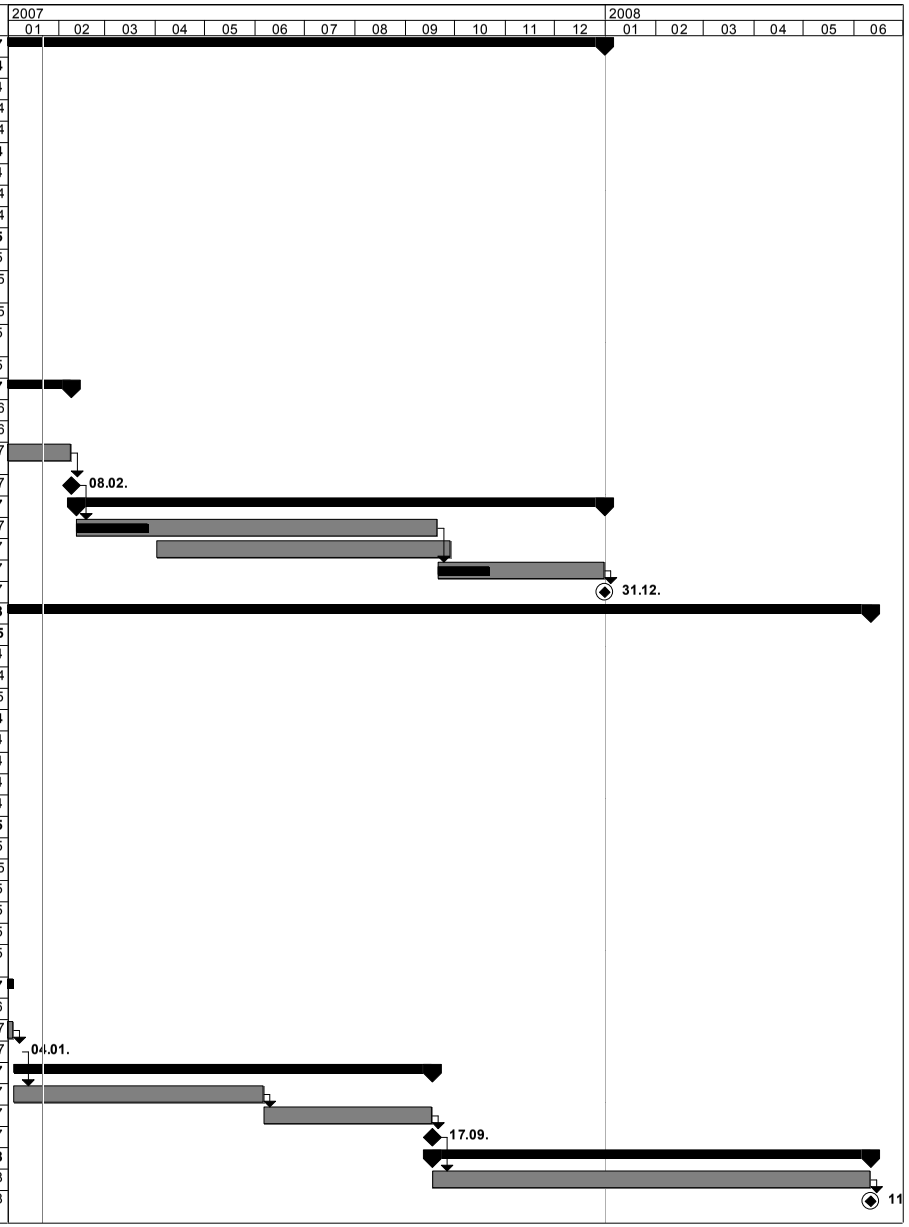

N°	Task Name	Ende
6.3	**DC field emission studies of Nb samples**	**Mi 26.12.07**
6.3.1	**Quality control scans**	**Mi 26.12.07**
6.3.1.1	Modification of Scanning apparatus	Fr 02.04.04
6.3.1.2	Calibration of Scanning apparatus	Fr 04.06.04
6.3.1.3	**Start scanning activity**	Fr 04.06.04
6.3.1.4	BCP and HPR samples	Do 26.05.05
6.3.1.5	EP and HPR samples	Mi 03.08.05
6.3.1.6	BCP/EP and DIC samples	Fr 10.06.05
6.3.1.7	**First report on BCP/EP and DIC surface**	Fr 10.06.05
6.3.1.8	Continue QA scanning	Mi 26.12.07
6.3.1.9	**Evaluation of scanning results**	Mi 26.12.07
6.3.2	**Detailed measurements on strong emitters**	**Mi 26.12.07**
6.3.2.1	Calibrate apparatus for high current	Mi 30.11.05
6.3.2.2	**Start strong emitter evaluation**	Mi 30.11.05
6.3.2.3	I/V curves and current limits	Mi 26.12.07
6.3.2.4	SEM and AES	Mi 26.12.07
6.3.2.5	Influence of heat treatment and ion impact	Mi 26.12.07
6.3.2.6	**Evaluate strong emitter investigations**	Mi 26.12.07

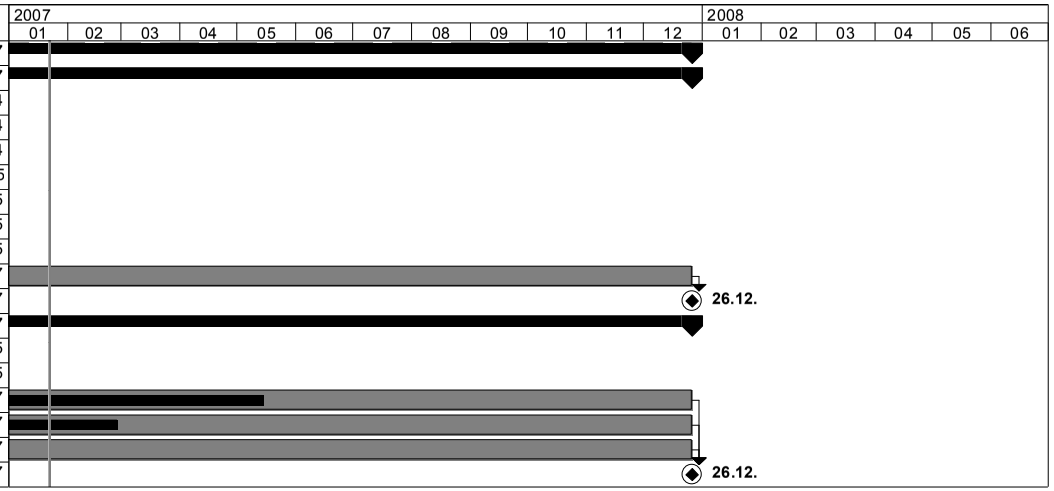

N°	Task Name	Ende
7.1	**New Prototype Coupler**	**Sa 15.07.06**
7.1.1	RF Simulations of Coupler	Mi 30.06.04
7.1.2	Report on Simulation	Mi 30.06.04
7.1.3	Detailed Engineering Drawings	Fr 31.12.04
7.1.4	Engineering complete	Fr 31.12.04
7.1.5	Call for tenders	Fr 01.04.05
7.1.6	Prototype Fabrication in Industry	Mi 31.05.06
7.1.7	Low Power tests	Fr 30.06.06
7.1.8	**Ready for High Power Tests**	Sa 15.07.06
7.2	**Fabrication of TiN Coating System**	**Fr 01.12.06**
7.2.1	Mechanical design of vacuum chamber	Fr 29.04.05
7.2.2	Fabrication drawings	Di 30.08.05
7.2.3	Construction of vacuum chamber	Fr 01.09.06
7.2.4	Define vacuum needs	Fr 30.06.06
7.2.5	Appropriation of vacuum equipment	Sa 30.09.06
7.2.6	Design of electronic circuitry	Do 30.03.06
7.2.7	Fabrication of electronics in industry	Fr 29.09.06
7.2.8	Installation and Test at Orsay	Do 30.11.06
7.2.9	**First Window Coating**	Fr 01.12.06
7.3	**Conditioning Studies of Proto-type Couplers**	**Fr 30.11.07**
7.3.1	Conditioning of couplers	Fr 30.11.07
7.3.2	Evaluate conditioning results	Fr 30.11.07
7.3.3	**Final report on conditioning**	**Fr 30.11.07**

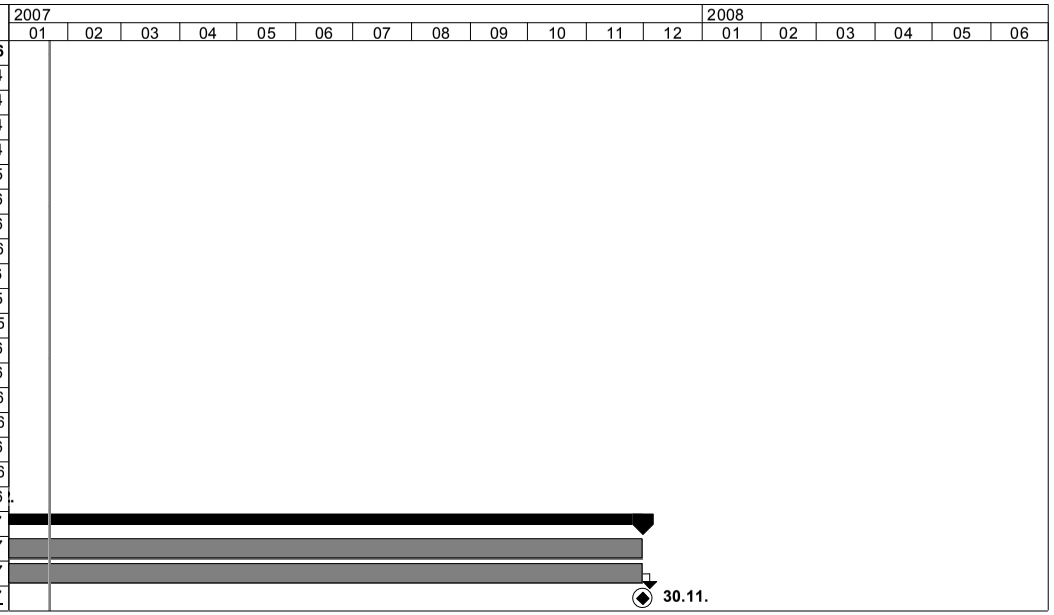

N°	Task Name	Ende
8.1	**UMI TUNER**	**Mo 31.12.07**
8.1.1	Control electronics	Fr 02.07.04
8.1.2	Mechanical tuner design, leverage system/motor	Do 29.09.05
8.1.3	Integration piezo design	Mo 09.05.05
8.1.4	Choice of transducer/actuator	Mi 10.08.05
8.1.5	**Report UMI tuner**	Mi 10.08.05
8.1.6	Tuner fabrication	Di 07.02.06
8.1.7	Piezo fabrication and bench tests	Di 06.02.07
8.1.8	Cavity-tuner-coupler integration	Sa 30.06.07
8.1.9	Pulsed RF tests	Mo 31.12.07
8.1.10	**Evaluation of tuner operation**	Mo 31.12.07
8.2	**Magneto-strictive Tuner**	**Di 31.01.06**
8.2.1	Complete specification	Fr 30.01.04
8.2.2	Conceptual design	Mi 31.03.04
8.2.3	Prototype and performance evaluation	Fr 04.02.05
8.2.4	Finalize tuner and drive electronics design	Do 14.04.05
8.2.5	Test of tuner	Di 31.01.06
8.2.6	**Report on magneto-strictive Tuner**	Di 31.01.06
8.3	**CEA Tuner**	**Mi 01.06.05**
8.3.1	Design Piezo + Tuning System	Fr 18.06.04
8.3.2	Fabrication	Do 31.03.05
8.3.3	Installation RF	Mi 01.06.05
8.3.4	**Start of Integrated Experitments**	Mi 01.06.05
8.4	**IN2P3 Activity**	**Mo 07.08.06**
8.4.1	Characterize actuators/piezo-sensors at low temperature	Mo 21.03.05
8.4.2	Report on actuator/piezo sensor	Mo 21.03.05
8.4.3	Test radiation hardness of piezo tuners	Mo 15.08.05
8.4.4	Report on radiation hardness tests	Mo 15.08.05
8.4.5	Integration of pieco and cold tuner	Mi 12.04.06
8.4.6	Cryostat tests	Fr 21.04.06
8.4.7	Tests with pulsed RF	Mo 07.08.06
8.4.8	**Report on IN2P3 tuner activities**	Mo 07.08.06

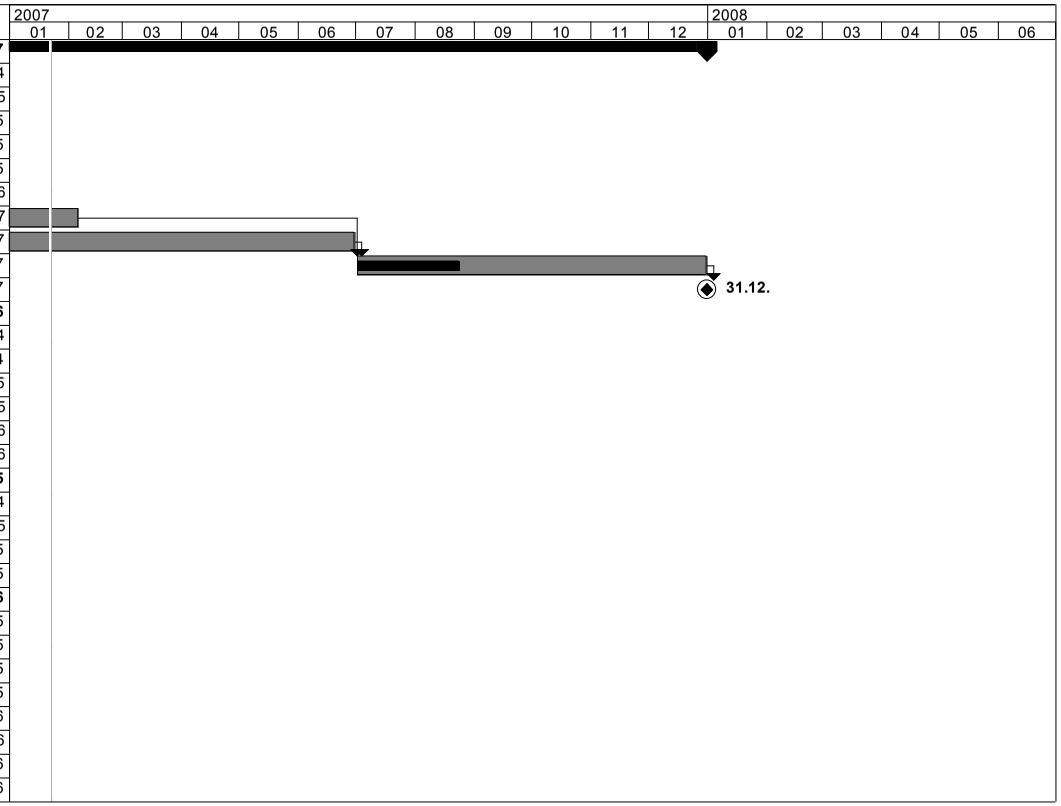

N°	Task Name	Ende	2007												2008					
			01	02	03	04	05	06	07	08	09	10	11	12	01	02	03	04	05	06
9.1	**Operability and technical performance**	**Fr 08.12.06**																		
9.1.1	**Transient detector**	**Fr 08.12.06**																		
9.1.1.1	Define requirements	Fr 30.01.04																		
9.1.1.2	Electronics design	Fr 27.02.04																		
9.1.1.3	Build prototype and evaluate	Fr 30.07.04																		
9.1.1.4	Final design of detector	Fr 01.10.04																		
9.1.1.5	Installation and commissioning	Mi 09.02.05																		
9.1.1.6	Test with beam	Fr 08.12.06																		
9.1.1.7	**Report on transient detector test**	Fr 08.12.06	**2.**																	
9.1.2	**LLRF Automation**	**Fr 23.06.06**																		
9.1.2.1	Dialogue with industrial experts	Fr 27.02.04																		
9.1.2.2	Develop full specification	Fr 26.03.04																		
9.1.2.3	Implement FMS for subsystems	Fr 29.10.04																		
9.1.2.4	Test and evaluation	Mi 23.02.05																		
9.1.2.5	Implement improvements	Di 26.04.05																		
9.1.2.6	Evaluation and acceptance by operators	Fr 23.06.06																		
9.1.2.7	**Report on LLRF atomization design**	Fr 23.06.06																		
9.1.3	**Control optimization**	**Fr 13.10.06**																		
9.1.3.1	Specification of system	Fr 02.04.04																		
9.1.3.2	Conceptual design of controller	Fr 30.04.04																		
9.1.3.3	Performance simulation	Fr 27.08.04																		
9.1.3.4	Implementation in DSP hardware	Mi 02.02.05																		
9.1.3.5	Implementation and tests on TTF	Fr 13.10.06																		
9.1.3.6	**Evaluation of test results**	Fr 13.10.06																		
9.1.4	**Exceptional handling routines**	**Fr 02.12.05**																		
9.1.4.1	Specification	Fr 23.01.04																		
9.1.4.2	Design of exceptional handler	Fr 30.04.04																		
9.1.4.3	Implementation and test on TTF	Fr 02.12.05																		
9.1.4.4	**Report on exceptional handler operation**	Fr 02.12.05																		
9.2	**LLRF cost and reliability study**	**Fr 27.10.06**																		
9.2.1	**Cost and reliability study**	**Fr 29.09.06**																		
9.2.1.1	Identify cost drivers of present LLRF	Fr 27.02.04																		
9.2.1.2	Develop cost reduction ideas	Fr 02.04.04																		
9.2.1.3	Build prototypes and evaluate	Fr 21.01.05																		
9.2.1.4	Final design of LLRF system	Fr 29.09.06																		
9.2.1.5	**Complete design of LLRF system for reduced cost**	Fr 29.09.06																		
9.2.2	**Radiation damage study**	**Fr 27.10.06**																		
9.2.2.1	Identify critical electronics issues	Fr 27.02.04																		
9.2.2.2	Evaluate TESLA radiation	Fr 02.04.04																		
9.2.2.3	Develop tests for components	Fr 28.05.04																		
9.2.2.4	Procure and assembles test set up	Fr 23.07.04																		
9.2.2.5	Data acquisition from radiation tests	Fr 29.10.04																		
9.2.2.6	Analyze results and develop countermeasures	Mi 09.02.05																		
9.2.2.7	Implement countermeasures and verify	Fr 27.10.06																		
9.2.2.8	**Report on radiation damage studies**	Fr 27.10.06																		

N°	Task Name	Ende	2007												2008					
			01	02	03	04	05	06	07	08	09	10	11	12	01	02	03	04	05	06
9.3	**Hardware**	**Mi 01.03.06**																		
9.3.1	**Multichannel downconvertor**	**Mi 26.01.05**																		
9.3.1.1	Study and compare technologies	Fr 27.02.04																		
9.3.1.2	Select optimum PCB design	Fr 23.04.04																		
9.3.1.3	Build prototype and evaluate	Fr 02.07.04																		
9.3.1.4	Finalize multichannel dow nconverter	Fr 03.09.04																		
9.3.1.5	Determine characteristics	Mi 26.01.05																		
9.3.2	**Third generation RF control**	**Mo 11.04.05**																		
9.3.2.1	Integrate system generator w ith VHDL	Fr 30.01.04																		
9.3.2.2	Complete specification	Fr 02.04.04																		
9.3.2.3	Demonstrate simulator	Fr 04.06.04																		
9.3.2.4	Final design of RF electronic board	Fr 28.01.05																		
9.3.2.5	Evaluate performance	Mo 11.04.05																		
9.3.3	**Stable frequency distribution**	**Mi 01.03.06**																		
9.3.3.1	Complete specification	Mi 04.02.04																		
9.3.3.2	Concept ional design of frequency	Fr 05.03.04																		
9.3.3.3	Build prototype and evaluate	Fr 06.08.04																		
9.3.3.4	Final design	Fr 22.10.04																		
9.3.3.5	Procurement and assembly of subsystems	Fr 28.01.05																		
9.3.3.6	Installation and commissioning	Fr 18.03.05																		
9.3.3.7	Performance test w ith beam	Mi 01.03.06																		
9.3.3.8	**Report on new LLRF hardware components**	Mi 01.03.06																		
9.4	**Softw are**	**Fr 06.10.06**																		
9.4.1	**Data management development**	**Mi 14.09.05**																		
9.4.1.1	Specification	Fr 30.04.04																		
9.4.1.2	Conceptional design w ith DOOCS	Fr 09.07.04																		
9.4.1.3	Prototype	Fr 10.09.04																		
9.4.1.4	User evaluation	Fr 05.11.04																		
9.4.1.5	Finalize design	Fr 31.12.04																		
9.4.1.6	Implementation in TTF	Mi 14.09.05																		
9.4.1.7	**Report on data management developments**	Mi 14.09.05																		
9.4.2	**RF gun control**	**Fr 06.10.06**																		
9.4.2.1	Write specification	Fr 30.01.04																		
9.4.2.2	Design of controller	Fr 23.04.04																		
9.4.2.3	Procurement and assembly	Fr 27.08.04																		
9.4.2.4	Installation and test	Fr 06.10.06																		
9.4.2.5	**Report on RF gun control tests**	Fr 06.10.06																		

Nr.	PSP-Code	Nom de la tâche	Ende
1	**10**	**WP10 CRYOSTAT INTEGRATION TESTS**	**Mi 18.07.07**
2	**10-1**	**Installation Moving**	**Fr 26.01.07**
3	10-1.2	Vertical cryostats moving	Mo 26.06.06
4	10-1.1	CRYHOLAB - Liquefier - Klystron moving, commissioning	Fr 26.01.07
5	**10-2**	**CRYHOLAB Adaptation to 9 cell**	**Fr 09.09.05**
6	10-2.1	Mechanical adaptations (design-manufacturing-mounting)	Fr 29.10.04
7	10-2.2	Low performance cavity and coupler transfert from DESY & LAL	Di 30.11.04
8	10-2.3	Assembly in Cryholab and Cryogenic test	Fr 28.01.05
9	10-2.4	High performance coupler - High Power Pulsed Test	Fr 02.09.05
10	10-2.5	Magnetic shielding with cryoperm	Fr 09.09.05
11	**10-3**	**Integration tests in cryostat (1st test)**	**Mo 17.04.06**
12	10-3.1	CEA Cold Tunning System + Piezo (Assembly & warm tests)	Fr 07.10.05
13	10-3.4	Installation of 9-cell & coupler - Cooldown	Di 15.11.05
14	10-3.3	Cold test (CTS + NOLIAC) in CryHoLab	Mo 03.04.06
15	10-3.2	Evaluate experimental results	Mo 17.04.06
16	**10-5**	**Integration tests in cryostat (2sd test)**	**Mo 05.06.06**
17	10-5.7	Installation of CTS + Piezo PICMA	Mo 17.04.06
18	10-5.5	Cold test (CTS + PICMA) in CryHoLab	Mo 22.05.06
19	10-5.6	Evaluate experimental results	Mo 05.06.06
20	**10-4**	**Integration tests in cryostat (3rd test)**	**Di 01.05.07**
21	10-4.4	Mechanical adaptation	Fr 26.05.06
22	10-4.3	Installation of CTS + MSM Energen	Fr 09.02.07
23	10-4.1	Cold test (CTS + ENERGEN) in CryHoLab	Di 17.04.07
24	10-4.2	Evaluate experimental results	Di 01.05.07
25	**10-6**	**Integration tests in cryostat (4th test)**	**Mi 18.07.07**
26	10-6.1	New Coupler TTF V from LAL	Mi 04.07.07
27	10-6.2	Evaluate experimental results	Mi 18.07.07

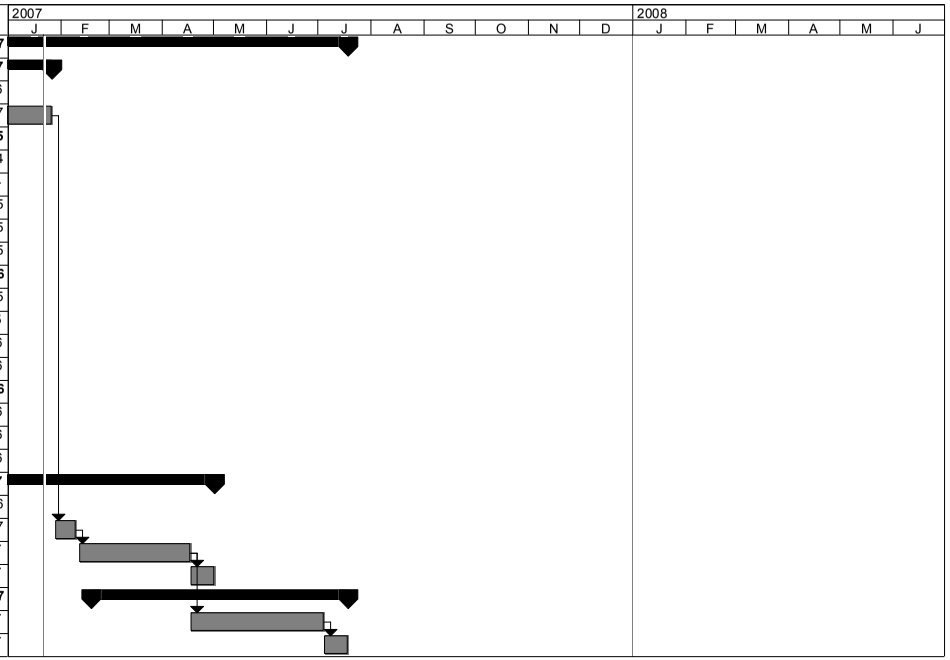

N°	Task Name	Ende
11.1	**Beam position monitor**	**Mi 12.12.07**
11.1.1	**Present BPM installed in TTF module**	Mi 30.06.04
11.1.2	Cryogenic measurements on BPM	Fr 06.08.04
11.1.3	Beam tests of BPM on TTF	Mo 03.10.05
11.1.4	Design of BPM Cavity	Fr 25.03.05
11.1.5	Design of BPM cavity ready	Fr 25.03.05
11.1.6	Fabrication of BPM Cavity	Fr 23.12.05
11.1.7	BMP cavity ready	Fr 23.12.05
11.1.8	Development of new hybrid coupler and electronics	Mo 05.09.05
11.1.9	Design of Digital Signal Processing	Mi 17.08.05
11.1.10	**New BPM ready for Installation**	So 01.01.06
11.1.11	Beam Tests with new BPM	Mi 12.12.07
11.1.12	**Evaluation of BPM operation**	Mi 12.12.07
11.2	**Beam Emittance Monitor**	**Mi 28.05.08**
11.2.1	Slit width simulations	Fr 02.04.04
11.2.2	Slit design	Fr 02.07.04
11.2.3	Optics simulations	Fr 02.07.04
11.2.4	Optics appropriations	Mo 15.08.05
11.2.5	System assembly and tests	Fr 30.09.05
11.2.6	Mechanical assembly at TTF	Mi 02.11.05
11.2.7	Optical assembly at TTF	Do 01.12.05
11.2.8	Integration of controls into TTF	Sa 31.12.05
11.2.9	**Ready for beam test in TTF**	Sa 31.12.05
11.2.10	Beam tests at TTF	Fr 02.06.06
11.2.11	Evaluate first beam test result	Fr 02.06.06
11.2.12	Successive measurements	Mi 28.05.08
11.2.13	**Final evaluation**	Mi 28.05.08
11.3	**HOM BMP Monitor**	**Fr 28.12.07**

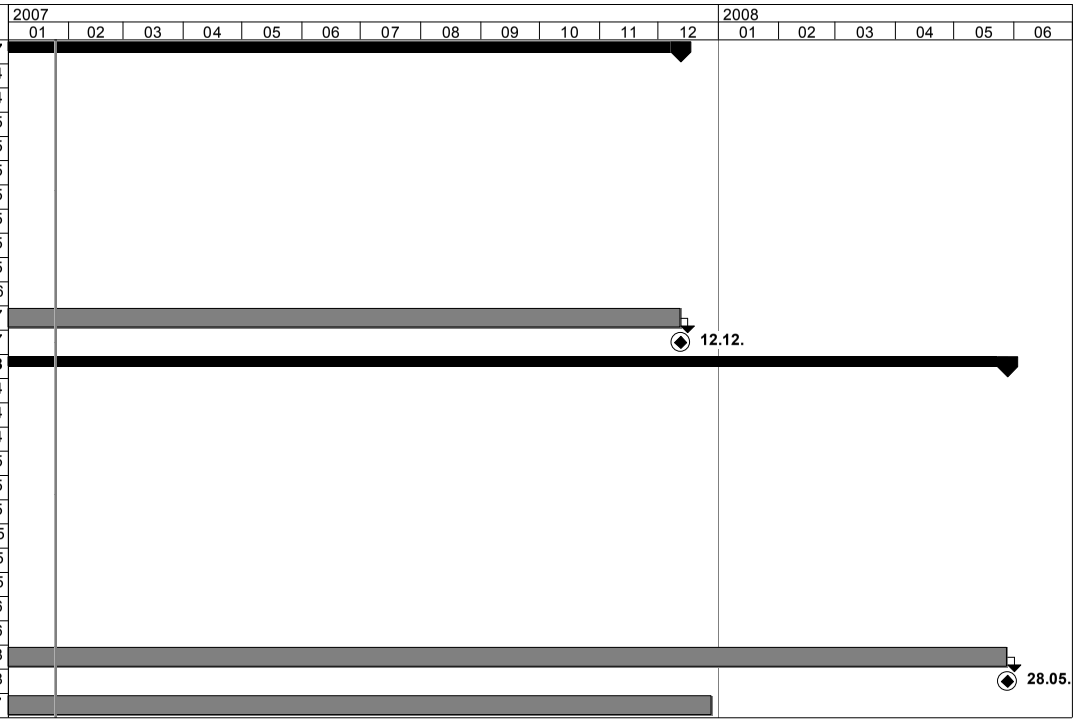

9. Status of activities
Work Package 2: Improved Standard Cavity Fabrication

Task 2.1 Reliability analysis

The activities relative to the reliability analysis have been summarized in a dedicated paper and poster presentation at the 2006 European Particle Accelerator Conference. The paper is entitled: “Performance Limitations of TTF Cavities in Accelerator Operation and their Relation to the Assembly Process” [1].

Task 2.2 Improved Component Design

During this period, the activity has been focused on three different items;

- experimental tests and analysis of cold flanges
- stiffening studies (end-dish shape etc.)
- e-beam welding.

Cold flanges: Experimental tests and analysis

The work relative to the cold connection flanges has been completed. We have performed new experimental tests (at room temperature and at liquid nitrogen temperature) and compared our FE model results with experimental measurements performed on the TESLA-like beam-line connections [2].
The whole activity has been dedicated to an in-depth study of the sealing mechanism, measuring the flattening of several gaskets as a function of the applied load. With these new data we have obtained information relative to the pressure needed to obtain tight seals for both of the gasket families we have studied (Al5754 and Al6060 alloys).
Cryogenic temperature tests have been performed in order to study the seal behavior after being subjected to several thermal cycles, and to identify possible long term and fatigue problems. The typical procedure consisted of 20 thermal cycles between room and LN_2 temperature, applied to a joint closed with a tightening torque of 25 Nm. It was directly immersed in liquid nitrogen and left to cool for 10 minutes. The joint was leak checked every cycle, both at cryogenic and at room temperature. The connection performed well and the measured leak rate was always less than $1 \cdot 10^{-10}$ mbar·l/s. In order to evaluate the criticality of the tightening procedure, a test was performed also on a joint closed with a lower torque, near to the required value for leak-tight seal generation. In this case the joint, tightened to 12 Nm, (about one half of the typical value used for the TTF beam-line flanges), also remained leak tight after one thermal cycle in LN_2, thus demonstrating the reliability of this joint.
As presented in the CARE-Note-2006-002-SRF an FE model for the analysis of beam-line connection flanges has been developed and its results were compared with the experimental data obtained. The availability of the mechanical characteristics of the Al5754 and Al6060 alloys (experimentally measured on specimens machined from the same alloy batch used for the gasket, Fig. 2.2.1) allowed us to successfully complete the comparison between the FE model results and the experimental measurements performed at room temperature (Fig. 2.2.2).

Fig. 2.2.1: Experimental tensile tests on an Al specimen alloy.

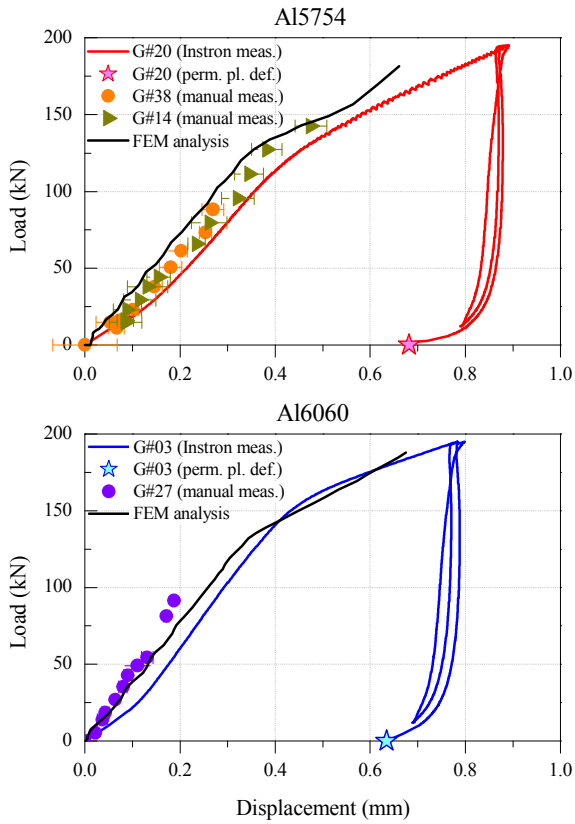

Fig. 2.2.2: Flange compression curves for the two Al alloys compared with the FEM analysis: the good agreement of the model with the measurements is clearly visible.

Stiffening studies (end dish shape etc.)

Minimal modifications have been realized on the existing cavity for the blade-tuner tests.
The coaxial tuner that will be used to meet the requirements for the ILC cavity, together with the reduction of the overall cavity length and the cost reduction request for mass production, has forced a review of the layout of the He-tank structure and the end dishes.
The adopted strategy is based on the analysis of different solutions developed for SC cavities in several laboratories. In particular, we are critically analyzing the TESLA, SNS, KEK and TRASCO-ADS solutions. For each solution, we have evaluated performance, weaknesses, construction problems and costs.
As an example, Fig. 2.2.3 and Fig. 2.2.4 show the FE analysis of the end dish configuration used for the blade-tuner test.
In order to achieve better results a different geometry has to be adopted. The solutions that we are investigating are similar to the ones we have chosen for the 700 MHz proton cavities, (see Fig. 2.2.5). This choice allows one to obtain a higher stiffness while saving the possibility to accommodate the helium tank length with the total length of the cavity during the final assembly.

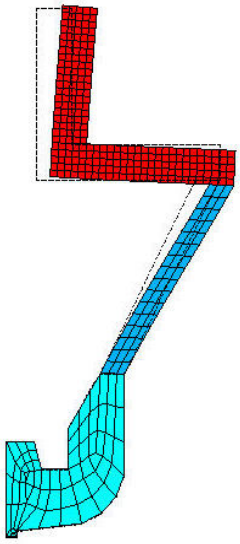

Fig. 2.2.3: deformed mesh of the end dish -tuner side.

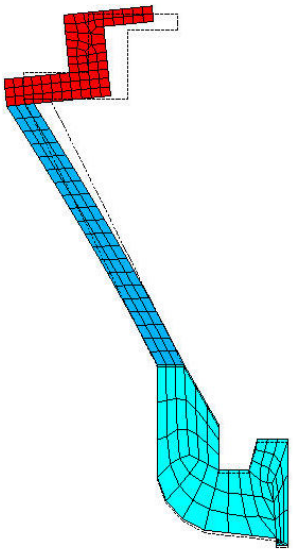

Fig. 2.2.4: deformed mesh of the end dish - coupler side.

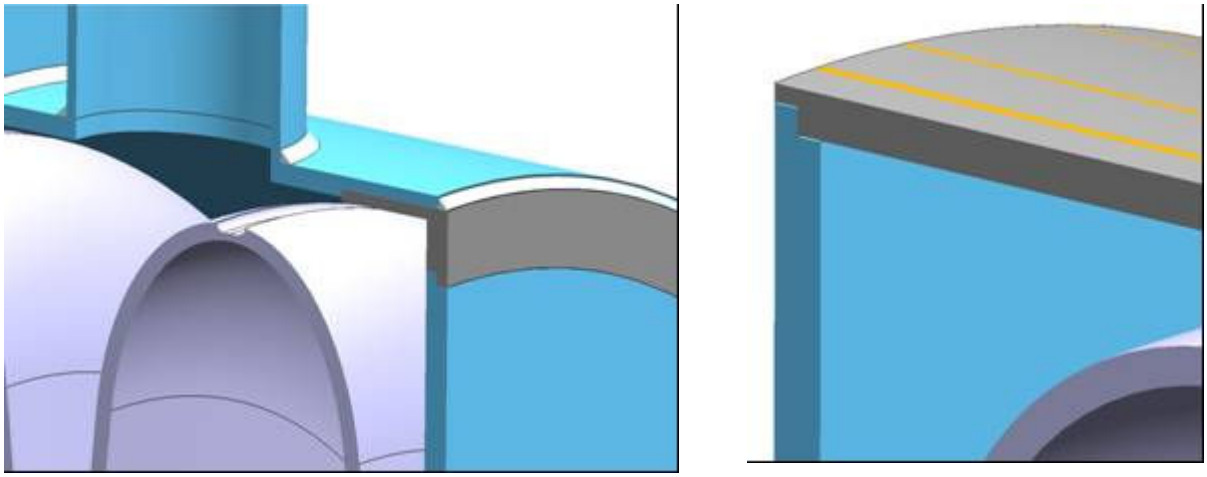

Fig. 2.2.5: Schematic of proposed helium tank – end dish stiffer connections

e-beam welding

A listing of the main parameters relative to the welding machine is in progress. Papers relative to the welding mechanism, on topics such as energy dissipation, electron scattering, etc., have been collected.
Moreover, we have analyzed the possibility to join dissimilar materials such as niobium and stainless steel [3,4] through a thin Vanadium interlayer: this might allow a significant cost reduction in the production of SC cavities. In Fig. 2.2.6 the phase diagram of some Vanadium alloys (Nb-V, Fe-V) is shown together with the Nb-Ti phase diagram.

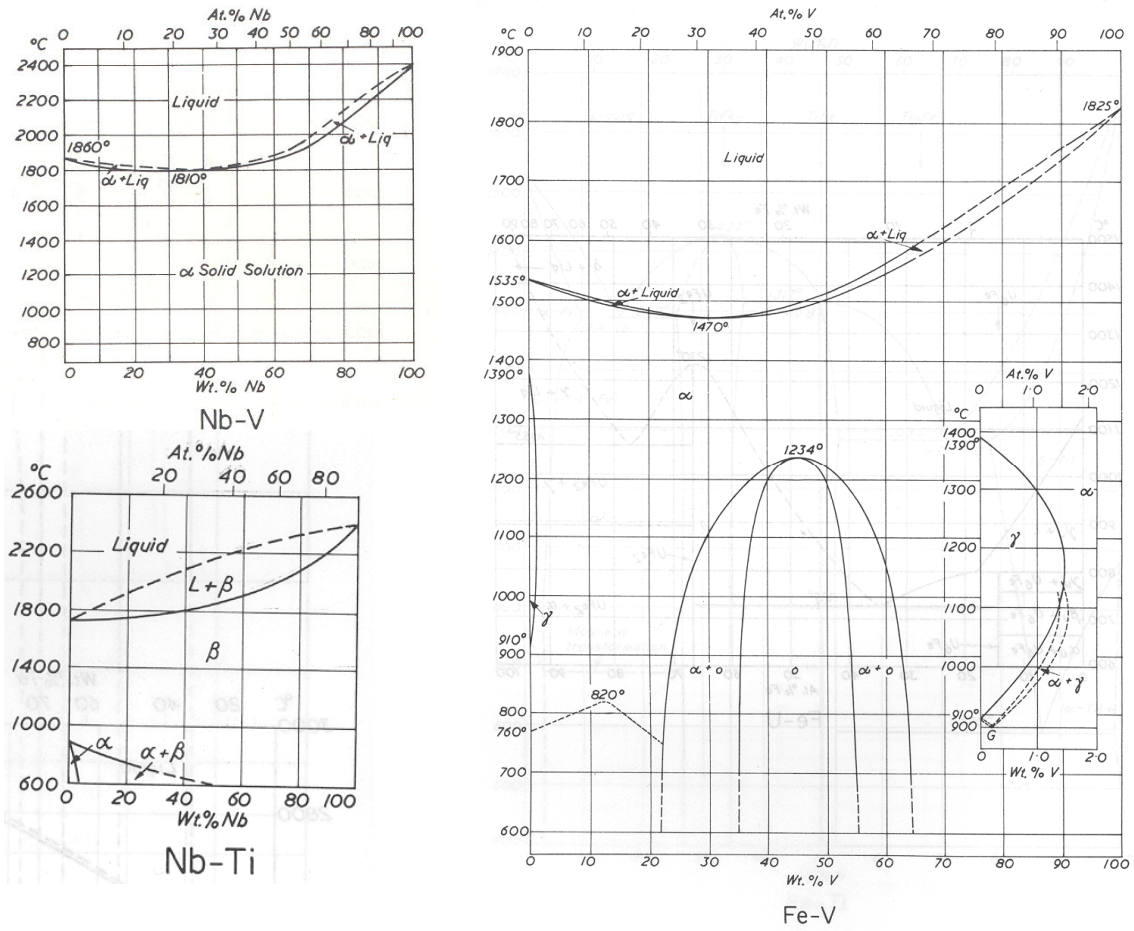

Fig. 2.2.6: Phase diagrams of some vanadium alloys and Nb-Ti.

References

[1] L. Lilje, "Performance limitations of TESLA cavities in the FLASH accelerator and their relation to the assembly process", proceeding EPAC'06, Edinburgh, UK.

[2] L. Monaco, P. Michelato, C. Pagani, N. Panzeri, "Experimental and theoretical analysis of the TESLA-like SRF cavity flanges", proceeding EPAC'06, Edinburgh, UK.

[3] N. P. Krutogolov, V. V. Diachenko, et al. "Defocused electron beam welding of Nb alloys and Stainless Steel", Industrial Welding, 4, 1980, p. 14.

[4] V. A. Veinik, V. V. Diachenko, et al. "Electron beam welding of Nb alloys and Stainless Steel through a Vanadium layer", Industrial Welding, 5, 1973, p. 16.

- **Task 2.3 EB welding**

During a three week shut down of the electro beam-welding machine, we dismounted the old mechanical rotation drive and installed the new stage and box for the UHV-motor.

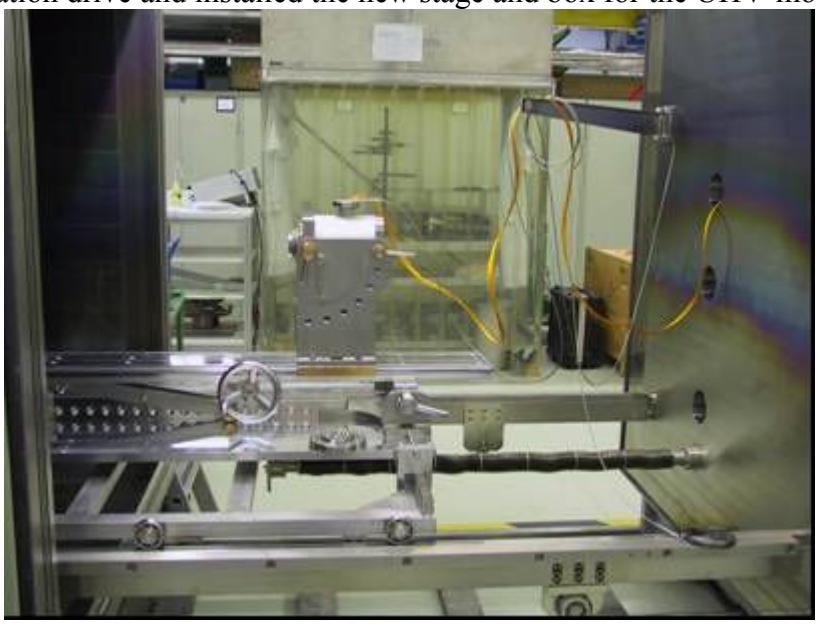

Figure 2.3.1: Motor box and current supply with Kapton© isolation

With the new support and rotation drive it is possible to change the working angle of the motor or the stage.

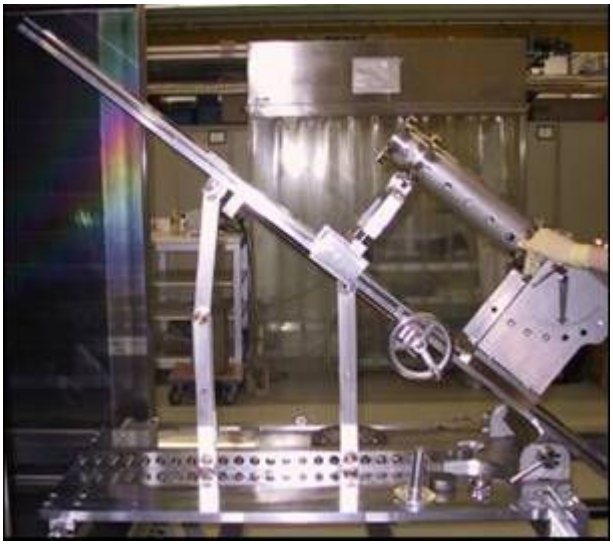

Figure 2.3.2: Stage at a 38° angle

The installation of the motion-drive for the y-axis has been prepared. It will be completed next month.
In order to manage new welding jobs, such as the neck of the nine-cell-cavity, we built a new universal support with wide rollers. A mandrel adjusts the axis-centre-distance of the rollers. Therefore, we can weld work pieces with different diameters without constructing a new welding fixation.

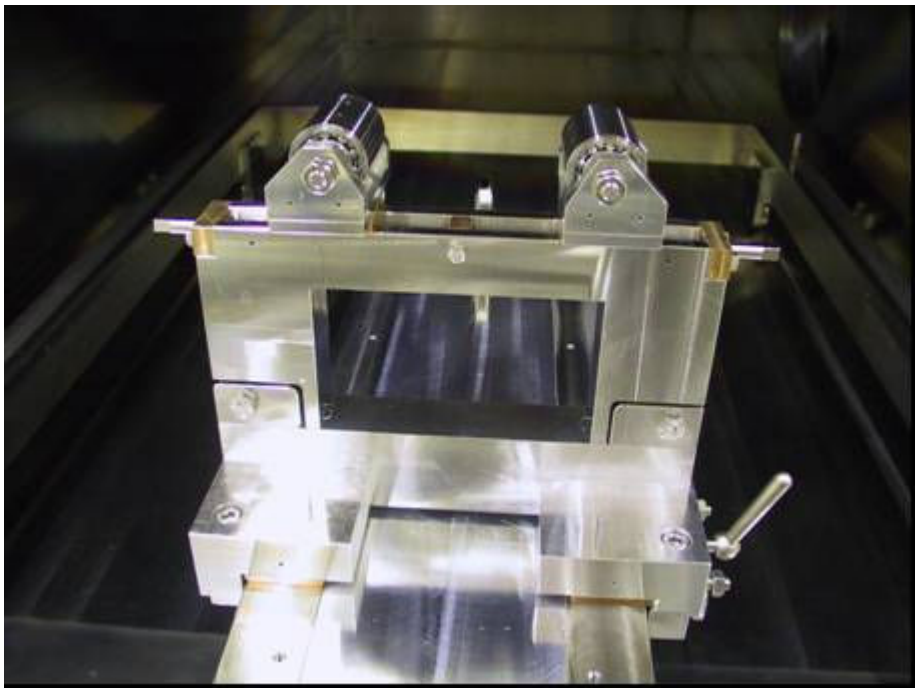

Figure 2.3.3: Front side of the new universal welding support

Work Package 3: Seamless Cavity Production

Task 3.1 Seamless cavity production by spinning

Spinning is a low-cost production method of forming axially symmetrical hollow parts of almost any shape. It is a point deformation process by which a metal disk, or a cylindrical pre-formed hollow component is plastically deformed by the axial or radial motions of a tool or rollers acting on a work piece clamped against a rotating chuck. A characteristic of this process is that the movement of tools onto a rotating piece acts upon a very localized area where plastic flow takes place. Spinning belongs to the tension-compression forming process since tangential compressive and radial tensile stresses are generated in the deformation zone just as in deep drawing. At LNL spinning has been applied for the construction of seamless TESLA-shape cavity prototypes. The technique primarily consists of a rotary-point method of extruding metal, pressing it against a mandrel rotated by the headstock of a lathe. A metal disk is first spun into a truncated-conical shape onto a pre-form. Subsequently the final shape is obtained by spinning the material from the external side, onto a mandrel that exactly reproduces the shape of the cavity interior. Hence the truncated cone piece is spun against the mandrel. The cut-off and the half-shell being closer to the truncated cone basis are the first to be obtained. Subsequently the manufactured piece is spun at the level of the equator looking for the closest fit of the metal to the mandrel. The material after the equator that has still to be spun has a conical shape. By the same method the material of such a region is made to flow under the external roller creating the second half shell and the second cut-off. The mandrel is made collapsible so it can be extracted from the cavity after forming. By this process the metal is made to flow under plastic deformation in a bi-dimensional space. In this way, a rather high percentage reduction can be achieved without any buckling or cracking. This method found for the forming of mono-cells has been successfully applied in an iterative way for the construction of seamless multi-cells. No matter the number of cells, no intermediate annealing is needed.

Spinning a multi-cell cavity directly from a 3 mm thick 1 meter diameter niobium blank is certainly impressive but is, however, impractical for industrial production. Hence the procedure has been engineered by first producing seamless tubes then by subsequently spinning the cavity. When spinning a multi-cell from a tube, the spinning procedure is the same for every cell. Moreover spinning from a tube, rather than directly from a blank, ensures a much better wall thickness uniformity for the spun cavity. Niobium seamless tubes are however not commercial, so we have been simultaneously developing three different methods: forward flow turning and deep-drawing, both direct and reversal.

Fabrication of the spinning machine

Fig. 3.1.1 shows the spinning lathe used before starting the CARE project. The lathe turret supporting the rollers moved along an axis of about 45 degrees with respect to the spinning axis. Since the shear force was applied onto the spun piece by the roller only when this moves forward, the necking process worked only for a half cell.

Fig. 3.1.1: The spinning lathe used for the fabrication of seamless cavity prototypes. The lathe had only one turret which held the rollers.

In other words, the main problem is the following: the revolving turret supporting rollers can move back and forward along a direction that is approximately 45 degrees from the cavity axis. It moves forward in order to have rollers applying a radial force to the tube that must be plastically deformed. It moves backward in order to retract the roller after the deformation in order to shift to another point. During this latter operation, the pressure is released and there is not any possibility to apply a plastic deformation. Due to the peculiar shape of the cavity in each dumb-bell, the actual machine can spin only the half cell that is encountered along the roller's rectilinear path. In order to spin the other half-cell, the cavity must be dismounted from the lathe together with the internal mandrel. The whole thing is turned through 180 degrees, the half-cell that was previously untouched by the roller becomes the part that must be plastically deformed. This operation is at the moment iterated several times up to the moment when the full dumb-bell is finished. This operation is rather laborious, time consuming, and is rather risky. Not only for the piece, which can be damaged during the operations of dismounting from lathe headstock, turning and remounting, but also because the collapsible mandrel can move from the correct position. Further, the lathe is not long enough for the nine-cell spinning and the pressure between headstock and tailstock is insufficient. Due to this limit, which is normally found on all spinning lathes that we know of, the cavity needs to be dismounted from the lathe headstock, tilted and remounted several times for each necking operation. This means wasting time, not only because of the time lost for dismounting the cavity and turning it on the lathe, but mainly because each time the cavity is dismounted and mounted from the lathe headstock, the cavity rotation axis must be aligned each time from the beginning.

The fabrication time will be strongly reduced by adding a second turret working in the opposite direction to the standard one. As shown in Fig. 3.1.2, the turret has been designed, fabricated and added to the lathe. In this configuration the cavity remains mounted onto the lathe during the whole spinning operation (apart from when the internal collapsible die is dismounted), while the operator moves around the lathe depending on the half cell he has to

spin. This makes the spinning procedure shorter in time, less expensive and therefore easier to industrialize.

The spinning machine for producing seamless multi-cell resonators starting from a tube has been finished and it is currently working. The research activity on spinning is executed in an external firm that already owns a lathe currently used for spinning resonators.

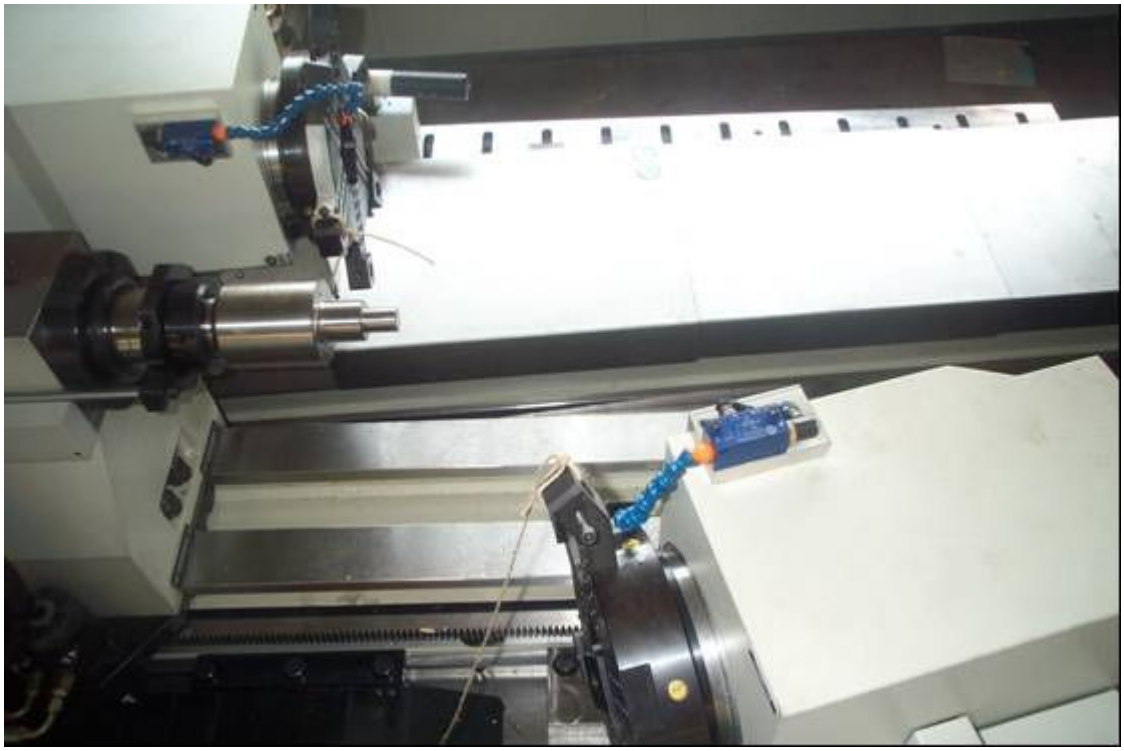

Fig. 3.1.2: The new spinning lathe with two turrets which hold the rollers. In this configuration, the rollers can work in opposite direction.

The previous machine however was also not powerful enough for the spinning operation. Therefore we adapted the already existing machine, designing some modified parts to add to it. All the work done is reported below and fully respected the milestone deadline:

- The new turret has been added and it works in the opposite direction and on the other side of the already existing one.
- The hydraulic plant was implemented and valves were added, for achieving a pressure of 120 bar.
- Since the increase in pressure was too large for the existing headstock configuration, and since the maximum rotation speed was 2000 rpm, the bearings supporting the headstock were changed adopting forced lubrication bearings with the related pump and ancillaries.
- The headstock was consequently lengthed by 100 mm and was designed for more robust construction.
- The lathe base and carriage appears more solid in the new design. The lathe-basement was lengthened by 200 mm.
- The lathe tailstock was also enforced in order to support the higher pressure applied between headstock and tailstock when spinning the part.
- A new motor of 18 KW power, an output speed of 8000/min and a speed reducer of 1:4 was also mounted.

Evaluation of spinning parameters

In standard operation the material wall thickness at the iris, at the end of the necking operation, could be lower than the initial tube thickness. This is actually possible in the double turret configuration, but it requires careful control of the roller working pressures, of the spinning angular velocity, of the roller feed speed and finally of the pressure between headstock and tailstock.

Fig. 3.1.3: Phase of the double turret necking process during the spinning parameter definition action.

The definition of spinning parameters must be twofold: first the piece must not crack or wrinkle, then the material must be spun in order to get a uniform wall thickness. Basically the tendency to wrinkle is dependent on the relationship between metal thickness and the area of the blank which, to be formed, is not clamped. Also material strength has a direct effect on the limits to tangential loading: a thin, large diameter blank will certainly require more intermediate steps than a smaller diameter, thick blank. The critical parameter is however the ratio **(v/ω)** between the feed speed **v** and the angular speed of the rotating part **ω**. Increasing **v** or decreasing **ω** will favour wrinkles appearing. For a given material and assigned cinematic conditions, lowering the angle between the lathe axis and the mandrel surface or increasing the roller nose radius will also provide a higher wrinkle probability. Subsequently radial cracks can form in the outermost portion of the work-piece at the end of the process when wrinkles are removed by continued spinning

The work of settling the parameters has just started on copper tubes to end on niobium tubes due to an obvious problem of the material cost. Many process variables have to be considered when spinning, in order to achieve the required shape, dimensional accuracy, surface finish and wall thickness profile and tolerances. On the basis of our experience, the parameters recognized to govern the final result can be seen in the work-piece parameters, material parameters, tooling parameters, machine parameters and process parameters. In particular for the work-piece parameters it is mainly important to control the blank diameter and thickness and the shape and size of the final piece to spin. For the material parameters it is important to control the material flow curve; the anisotropy; the compressive modulus and the compressive yield strength. For the tooling parameters it is important to control the shape, size and finishing of the mandrel, diameter, nose radius and shoulder radius of the roller, type and quantity of lubricant. More than the final mandrel, however, the series of the pre-mandrels needed for keeping a uniform wall thickness are important. For the machine

parameter it is important to control the positional accuracy; machine rigidity, operational distance between headstock and tailstock and the maximum radius of acceptable blank. For the process parameters the number of rollers, the roller feed speed, the angular speed of the rotation chuck, the forming force (tangential, axial and radial components) and the blank support force are important.

Task 3.2: Seamless cavity production by hydro-forming

Numerical simulation of the necking process

The numerical simulation was done using the finite element code ANSYS. The real geometry of the tubes after end reduction was taken into account.
A comparison of the measured and simulated wall thickness after the necking process is shown in Fig. 3.2.1. The comparison was made for Cu tubes with markers Rohr8 - Rohr13. For the comparison the tube thicknesses were normalized to 4mm.

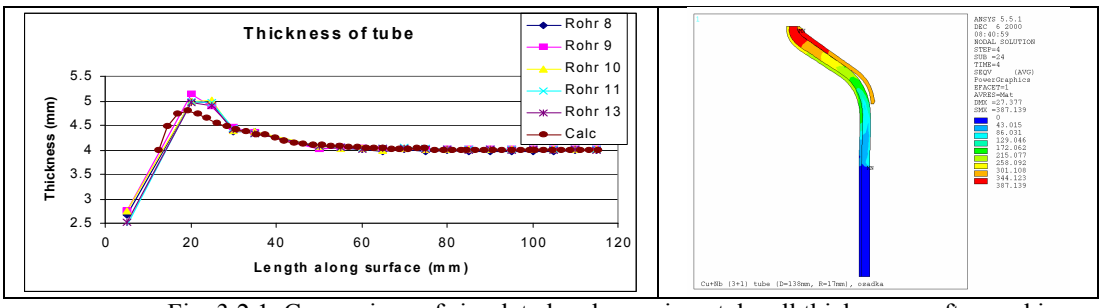

Fig. 3.2.1. Comparison of simulated and experimental wall thicknesses after necking.

The thickness of wall, obtained from simulation agrees with the experiment. The thickening of the tube region between the iris and the equator is in accordance with the measured dimensions of tubes with reduced ends.

Numerical simulation of hydroforming process

During the simulation of the hydro-forming process, the tube form and stress distribution after necking were taken into account. Applied loads (pressure and displacement) from real experiments on Rohr13 where used. The results are compared in Fig. 3.2.2. The agreement with experimental data seems acceptable.

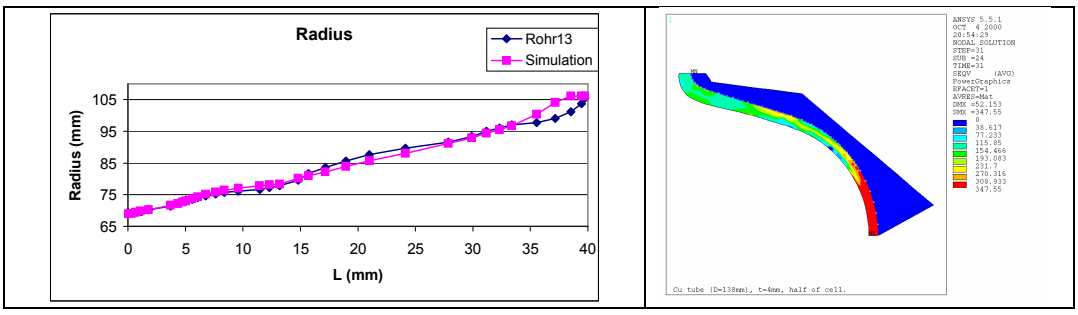

Fig. 3.2.2. Simulation of radius growth during hydro-forming in comparison with experiment

Experiments on tube necking at the iris

The necking experiments were performed on copper as well as on niobium tubes in order to optimize the necking parameters. The machine can be seen in Figure 3.2.3.

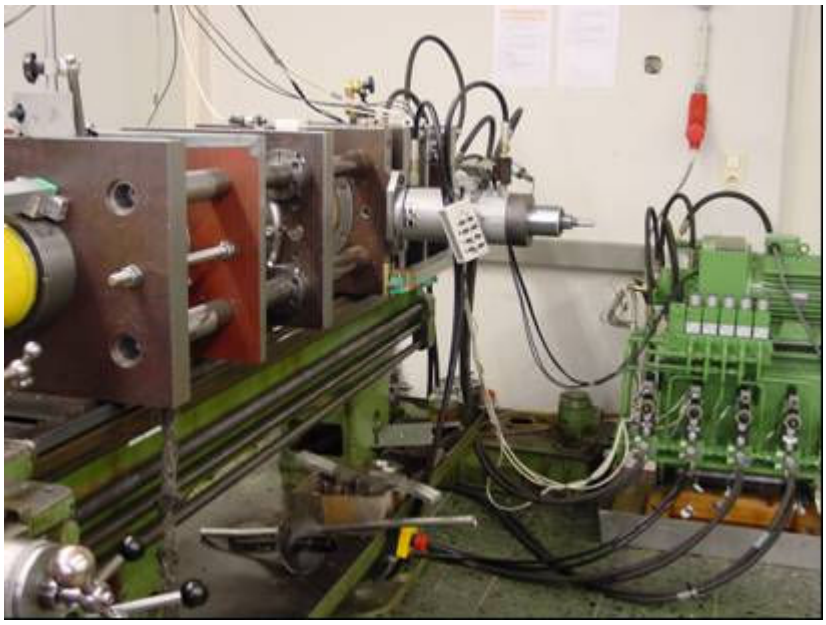

Fig. 3.2.3: View of the tube necking machine

A combination of radial and axial movements allows one to improve the uniformity of the circumferential wall thickness at the iris area without a noticeable reduction of the wall thickness. One example of the necking can be seen in Fig. 3.2.4.

Fig. 3.2.4: Example necking of the niobium three cell unit.

Hydro-forming of three cell units and fabrication of a seamless cavity

After successfully necking six 3-cell cell units for two 9-cell cavities, cavities have been fabricated by hydro-forming from earlier produced seamless tubes of dimensions: internal diameter of 150 mm, wall thickness 3 mm of bulk niobium (Fig. 3.2.5). The expansion of the tube diameter at the equator area (hydro-forming) is done by simultaneous application of internal pressure and of axial displacement. A definite relation between the applied internal pressure against axial displacement (path of the expansion) is fulfilled. The rough value of the pressure was derived from numerical simulations and further corrected on the basis of hydro-forming experiments. The hydroforming is done on the hydroforming machine (Fig.3.2.6) in

two stages in order to achieve the correct shape, rather uniform wall thickness of the complete cavity and to suppress instabilities during the tube expansion.

Fig. 3.2.5: Hydro-formed three cell units

Fig. 3.2.6: View of the hydroforming machine

An order for fabrication of a 1.3 GHz nine-cell seamless resonator (without equator welds) has been placed with industry.
Fabrication includes the following steps:

- Fabrication of the long and short end groups connected with the three cell units
- Machining, preparation and welding of the three units together to form a 9 cell cavity (two iris welds are done from outside)
- Machining, preparation and welding on of the stiffening rings

Delivery of the seamless resonator is expected for the beginning of 2007.

Work package 4: Thin Film Cavity Production

Task 4.1 – Linear cathode coating

Status of activities

The task 4.1 has been focused on the development of a UHV arc system with the linear (cylindrical) cathode configuration. A general view of the UHV linear-arc system, which has been slightly modified during operational tests, is presented in Fig. 4.1.1.

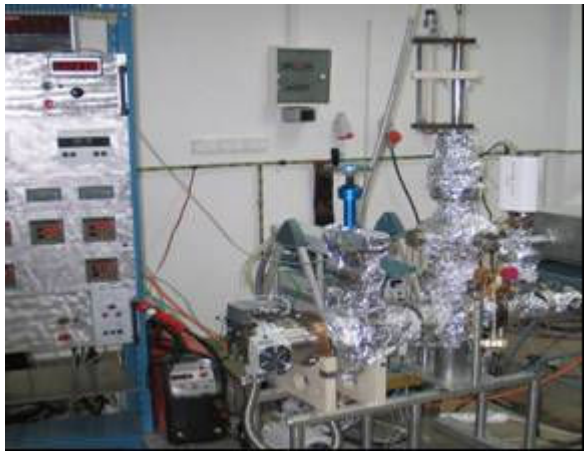

Fig. 4.1.1. UHV linear-arc facility operated at the IPJ in Swierk, Poland.

Modifications of the UHV linear-arc facility

During 2006, studies of the arc-current reduction and stabilization were continued with the use of a stainless-steel chamber of shape and dimensions similar to the single TESLA RF-cell. This chamber was equipped with two flanges, used as connections with the UHV pumping stand (at the bottom) and a magnet driving system (at the top), and four radial diagnostic ports in the central symmetry plane of the cell.

The prototype version of the pure-Nb cylindrical cathode was 32 mm in diameter. Taking into account the micro-droplet filter, that cathode could not be used within the original TESLA cavity. Therefore, two new pure-Nb tubes of 24 mm in diameter (with walls of 3 mm in thickness) were ordered. The first tube of about 50 cm in length was designed for coating a single RF cavity, while the second one of about 120 cm in length was designed for future experiments with a multi-cell structure. The first modified cylindrical cathode (described in the WP4 Quarter Report 1-2006) has already been exploited.

In order to facilitate biasing of samples, a so-called keying module was designed and constructed at IPJ, as described in the WP4 Quarter Report 1-2006. It can transform a DC input signal into pulsed output signals of amplitude variable from -800 V to 0, with a frequency setting within the range of 0-100 kHz. The module has already been delivered to the Tor Vergata laboratory in order to perform tests within a UHV planar-arc facility. An identical module will be constructed for the UHV linear-arc facility, if results of the current tests are positive.

Coating of single cells

Tests on the coating of single cells within the UHV linear-arc facility have been postponed because the collaborating laboratories (INFN-Legnaro and DESY) were unable to deliver the TESLA-type copper cavities in 2006. According to information announced during the CARE Annual Meeting 2006, the original TESLA-type copper cavities should be delivered in the first quarter of 2007. Therefore, it has been proposed to delay the coating of a single-cell without a micro-droplet filter until March 31, 2007 at the earliest, while the realization of the whole task (4.1.1.7) should be prolonged to at least June 30, 2007.

Taking into account the positive results of the previous tests on the coating of model TESLA–type copper cavities (described in WP4 Annual Report 2005) and the modifications of the UHV linear-arc facility it is estimated that 80% of the whole task has already been achieved, but its complete realization depends also on other sub-tasks, and particularly on the design and application of a micro-droplet filter (see below).

Design and construction of a micro-droplet filter

A micro-droplet filter is needed in order to eliminate micro-droplets emitted from the cathode surface. Such a filter must of course be adapted to the cylindrical configuration. A prototype of the cylindrical micro-droplet filter was constructed in 2005. After tests, it was decided to design and manufacture two versions of the modified filter. The first version consisted of a concentric set-up of thin Cu-tubes carrying magnetizing currents and a flow of cooling-water. Computations of the magnetic field distribution were performed in order to optimize the filter configuration and thermal loads (due to the magnetizing current and arc-plasma) were estimated in order to determine the appropriate construction, as shown in Fig.4.1.2.

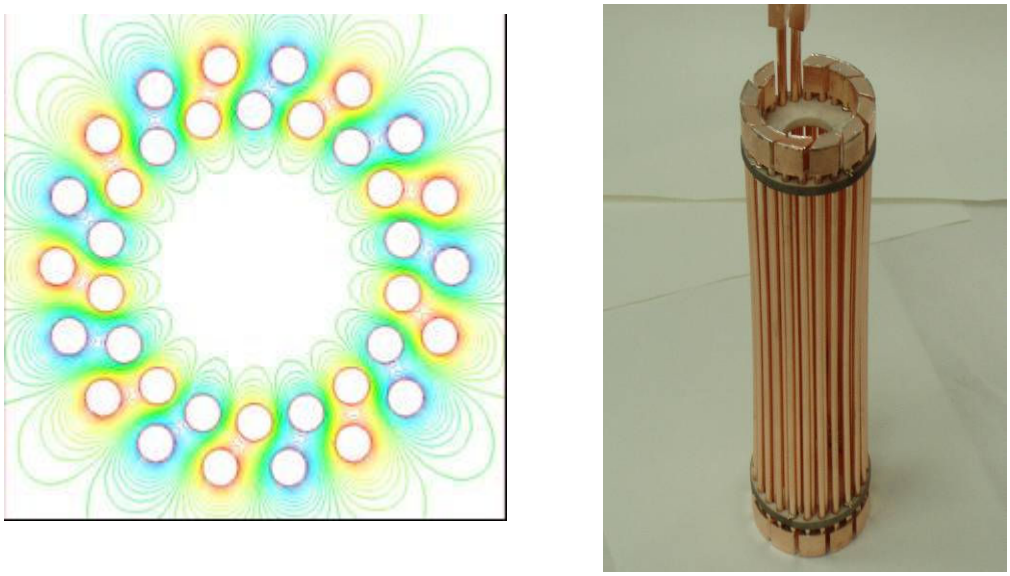

Fig.4.1.2. Distribution of magnetic field lines in the cross-section of the considered micro-droplet filter, and a general view of that filter prepared for the installation.

A second version of the micro-droplet filter was also designed. It consists of a cylindrical Venetian-blind system without any magnetizing current. It was equipped with a solid copper flange with connections for the water cooling, as shown in Fig.4.1.3

Fig.4.1.3. View of the cylindrical Venetian-type micro-droplet filter.

Both filters were manufactured (see Figs 4.1.2 and 4.1.3) according to the up-dated time-schedule of the project. They were installed within the model TESLA-type cavity and tested during typical UHV arc discharges in two successive experiments. At arc currents of about 60 A they could withstand 2-minute operation cycles, as reported at an International Congress in Tomsk (Sept.2006) and the International Workshop in Legnaro (Oct. 2006). Hence, the milestone "Micro-droplet filter ready" (task 4.1.1.7.3) was achieved according to the time-schedule.

Studies of samples coated within experimental chambers of the TESLA-type

In order to investigate characteristics of thin Nb-films deposited by means of the UHV linear-arc facility, use was made of several sapphire samples, which were placed in the diagnostic port of this facility. The deposition processes were performed under very clear and controlled vacuum conditions, but without any micro-droplet filter. Since the samples were mounted on the grounded support, no additional bias was applied. The Nb-coated sapphire samples were investigated in other laboratories in order to get SEM images, micro-droplet populations, RRR values and SIMS profiles.

The SEM pictures of the Nb layers deposited without any micro-droplet filter showed a relatively large population of micro-droplets, as shown in Fig.4.1.4.

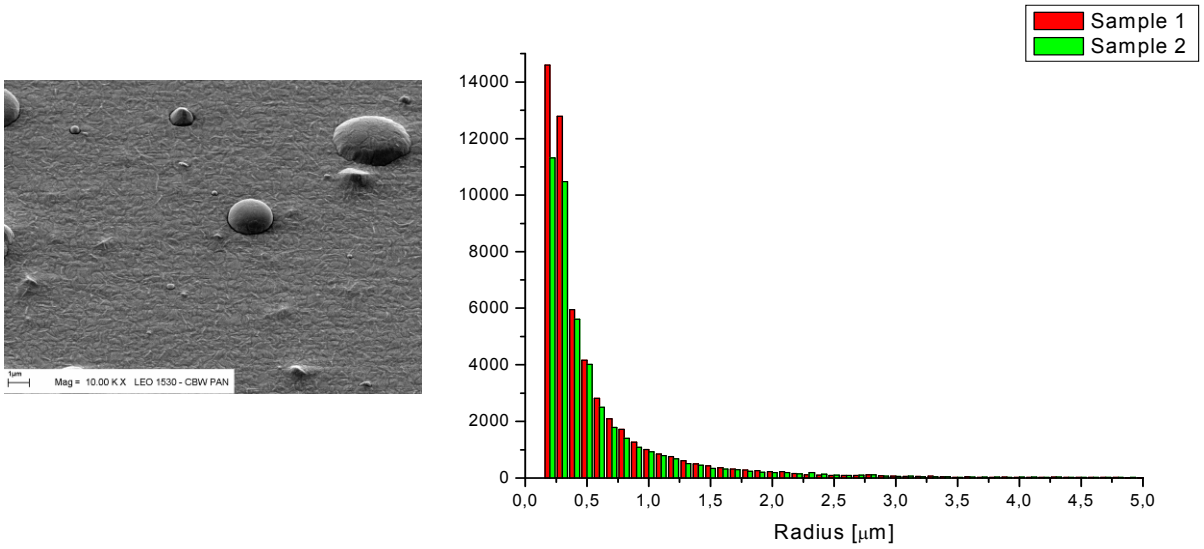

Fig.4.1.4. SEM picture of an unfiltered sample and the population of the deposited microdroplets.

Measurements performed at the Tor Vergata laboratory showed that the unfiltered Nb layers have low RRR values (from 5 to 25), which is explained by the influence of numerous micro-droplets. Better results (RRR up to 48) were obtained for the biased (-70 V) samples, but this procedure cannot be used when entire TESLA cavities are coated. Therefore, the application of a cylindrical micro-droplet filter seems to be necessary.

To study the chemical composition of the deposited layers, use was made of the SIMS technique. Preliminary measurements were performed with an O_2+ ion-gun and time-of-flight (ToF) mass analyzer, but the O_2+ ions caused the formation of an additional NbO mixture, as shown in Fig.4.1.5A. Therefore, the next SIMS measurements were carried out with non-reactive gas (Ar) ions. As a result, the oxygen contamination was considerably reduced, as shown in Fig.4.1.5B.

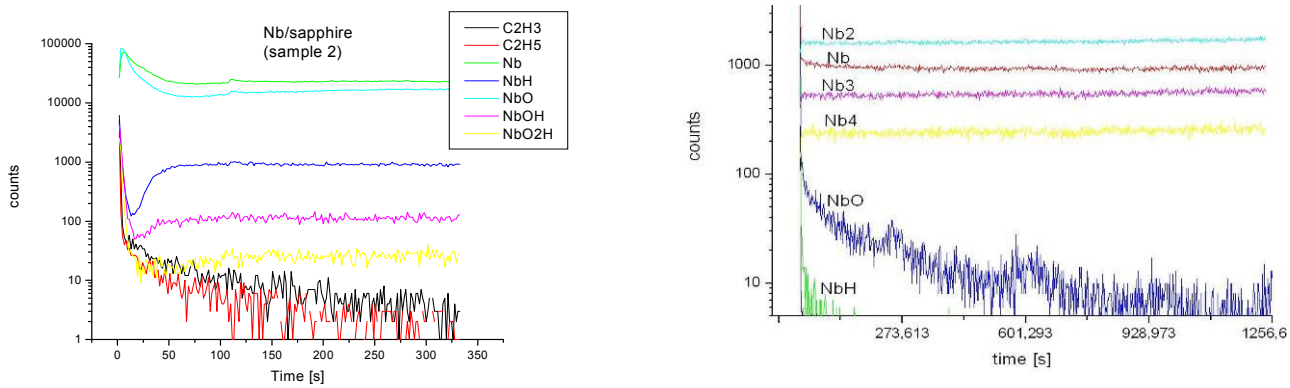

Fig.4.1.5(A,B). SIMS profiles of the Nb films deposited without any microdroplet filter, which were recorded with the use of the oxygen ions (on the left) and argon ions (on the right).

Study of samples coated with the use of a microdroplet filter

In order to prepare for coating of a single cell with micro-droplet filtering (task 4.1.1.7.3) some sapphire substrates were placed outside the Venetian-type filter (see Fig. 4.1.3) and were coated at an arc current of 55 A during 25 minutes. The deposited Nb-film thickness was about 1.5 μm. The obtained Nb-layers were characterized by the surface distribution of micro-droplets, as shown in Fig. 4.1.6.

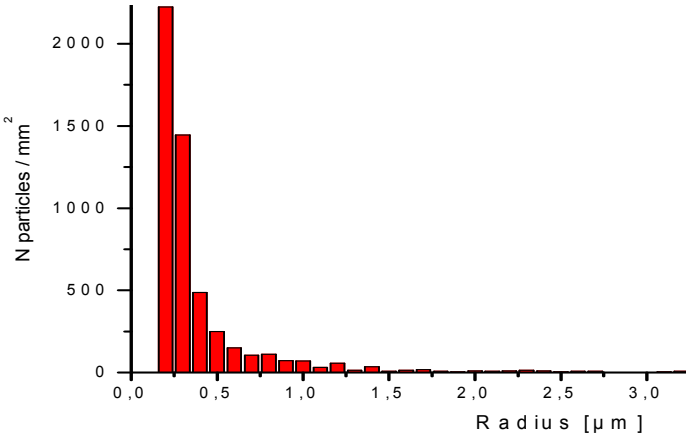

Fig.4.1.6. Micro-droplet distribution upon the filtered Nb-layer.

The amount of the deposited micro-droplets was strongly reduced in comparison to the layer deposited without filtering (see Fig.4.1.4), and about 90% of the micro-droplets have diameters lower than 0.5 μm. The RRR values of these samples are still under investigation at other laboratories.

UHV arc deposition of pure Pb-layers for photo-cathodes

In addition to the planned tasks, the IPJ team has also performed several depositions of pure Pb-layers, which are investigated as potential photo-cathodes for new electron injectors. The preliminary results were presented at EPAC-2006 in Edinburgh (June 2006), the international conference in Alushta (Sept. 2006) and the International Workshop in Legnaro (Oct. 2006), as discussed above.

Task 4.2 – Planar-Arc Cathode Coating

Status of activities

Task 4.2 is focused on the development of a UHV arc system with the planar (truncated cone) cathode configuration, the optimization of micro-droplet filters, and characterization of samples coated under different conditions.

Design and tests of a new T-type filter

The modeling of magnetic field distributions within different filters, which were performed in the collaboration with the IPJ team (as reported in previous Quarterly Reports), has shown that additional correction coils are needed in order to optimize the plasma transmission. In order to improve the filter efficiency a new vacuum planar-arc device with a T-type magnetic filter was assembled and put into operation. The system was equipped with external coils, used for the deflection and guidance of the arc column, as shown in Fig. 4.2.1.

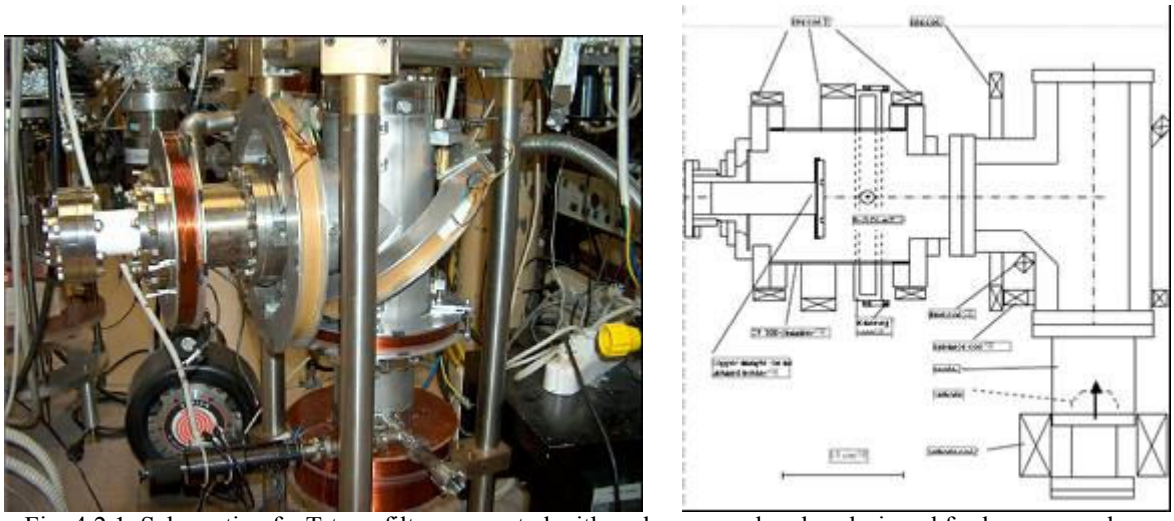

Fig. 4.2.1. Schematic of a T-type filter connected with a planar-arc chamber designed for larger samples and a picture of the system during assembly.

At the typical operating conditions (i.e. arc current of 110 A, and bias voltage - 80 V) the ion current to a large (71 cm^2) sample holder reached 0.5 A. The average ion current density was about 7-8 mA/cm^2, i.e. it was twice as high as that obtained in the 90^0-L filter system used previously.

Improvements of the magnetic field configuration within a cavity-like chamber

Considerable progress has been achieved in controlling arc-plasma dynamics inside a mock RF cavity, which was equipped with insulated collectors to measure the ion current in various parts of its upper half. Two additional magnetic coils, similar to those used in the T-filter system, were mounted on the cavity-like chamber, as shown in Fig. .4.2.2.

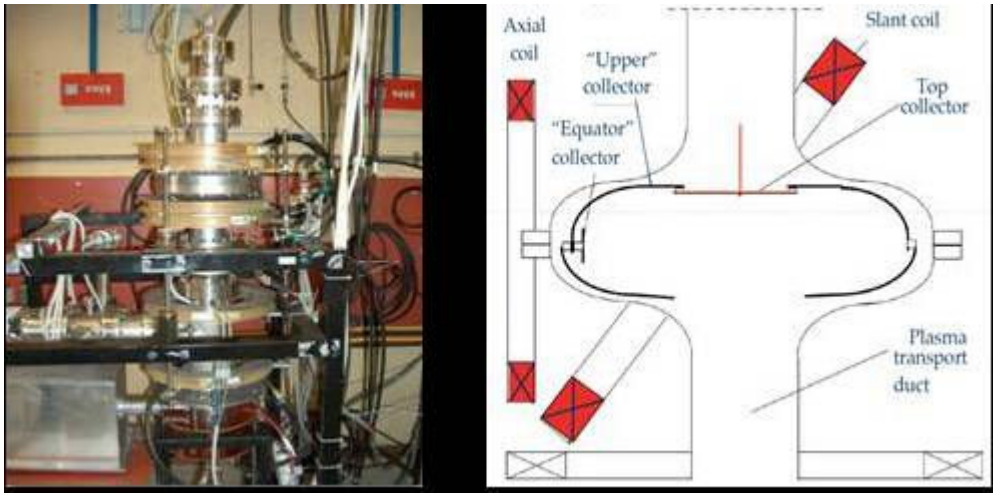

Fig.4.2.2. View of the experimental stand and a schematic of the mock RF cavity equipped with insulated collectors and additional coils used to control plasma flow.

The "slanted" coil, which could generate up to 9 mT magnetic field on the axis, was inclined by approximately 45°, while the second "axial" coil was mounted with its axis oriented in the cavity equatorial plane. It enabled the deflection of the arc-discharge column to be varied considerably. During experiments the collectors were biased (to -80V) separately, and the ion currents delivered to each of them were measured as a function of the magnetizing current (I_{sl}) of the slanted coil, as shown in Fig.4.2.3.

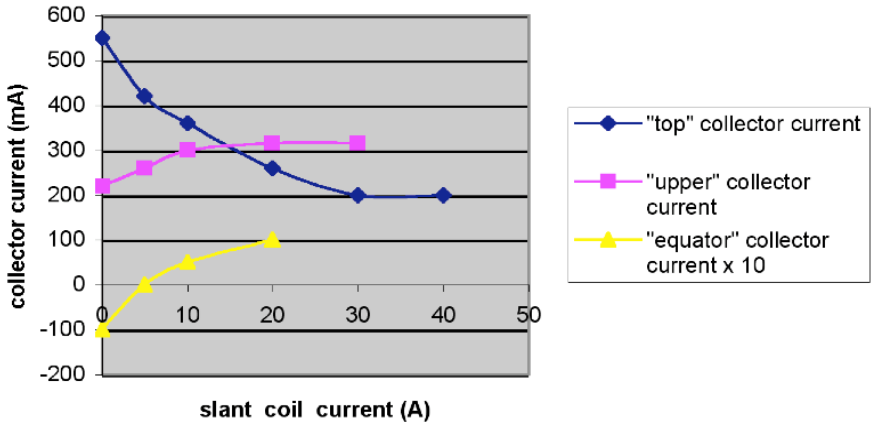

Fig.4.2.3. Ion currents flowing to different collectors within the experimental mock RF-cavity vs. the magnetizing current flowing through the slant coil.

It was found that for I_{sl} = 20 A (corresponding to about 3 mT field at the coil center) the plasma ion current to the "upper" half-cell collector becomes larger than that to the top collector. At the same time a positive-ion current of density exceeding 1 mA/cm^2 is delivered to the equator region. For I_{sl} > 20 A all three collector-currents become saturated. This result suggests that, by rotating the slant coil around the RF-cavity axis, it might be possible to obtain a sufficiently uniform coating upon the upper part of the cavity and the tubular outlet.

Characterization of samples coated at different conditions

To study any influence of the orientation of the coated surface, six sapphire samples were placed at different angles to the z-axis and coated within the planar-arc device equipped with the T-type filter. SEM pictures showed relatively uniform Nb-layers with a reduced amount of micro-droplets, as presented in Fig. 4.2.4.

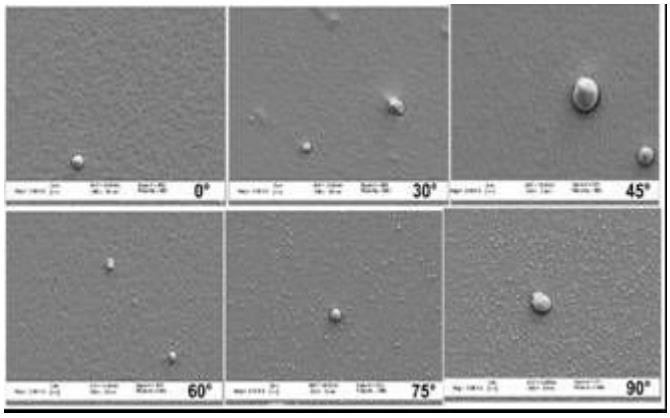

Fig.4.2.4. SEM pictures of the Nb-coated sapphire samples exposed at different angles.

Those samples were also analyzed with other techniques. The obtained data showed that the Nb-layer thickness spread from about 1 μm to 3.5 μm, whereas the RRR values were from 26 to 50 for bias voltages above -40 V. The task concerning the characterization of Nb-coated sapphire samples (4.2.2.2) was completed, as reported in the previous Quarterly Reports, at the workshop in Legnaro (Oct. 2006) and the CARE Annual Meeting in Frascati (Nov. 2006).

Start of coating procedures with pulsed bias

It was expected that the pulsing of bias voltages might help to make the layer thickness (upon the cavity inner-surface) more uniform, but the pulse frequency and duty cycle have to be matched to plasma dynamics. To study this dependence, a new pulse power supply unit was designed and built at IPJ. It has recently been applied at Tor Vergata laboratory, as shown in Fig.4.2.5.

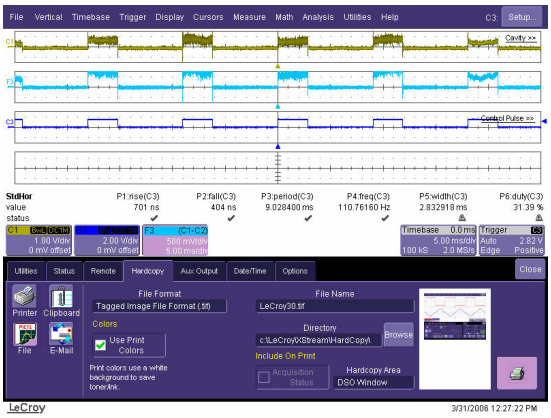

Fig.4.2.5. Traces recorded during test with the pulsed bias: the upper trace - the ion-current upon the cavity wall vs time (at bias -60V, repetition - 110 kHz, 31.5% duty); the middle trace - a differential current readout with noise filtering; the bottom trace – the bias voltage waveform.

Research on the influence of the pulsed bias will be continued in 2007 under different operational conditions.

Characterization of Nb-coated copper samples

The Nb-layers deposited upon copper substrates were investigated by means of the XRD technique. The most important result was that for all the applied bias voltages, which ranged from -20 V to -80 V, the Nb-films upon copper substrates showed the lattice parameters of bulk Nb, as reported at the international workshop in Legnaro (Oct. 2006).

To continue the task (4.2.2.3), four new copper samples of large diameter and the shape used at Cornell laboratory (for Q and RRR measurements) were coated within the UHV planar-arc system in order to collect information about the influence of different surface-preparation processes and effects of the improved plasma column deflection systems (i.e. magnetic filters). The sample positioning inside the experimental chamber was adjusted by changes in the length of the holder, as shown in Fig. 4.2.6.

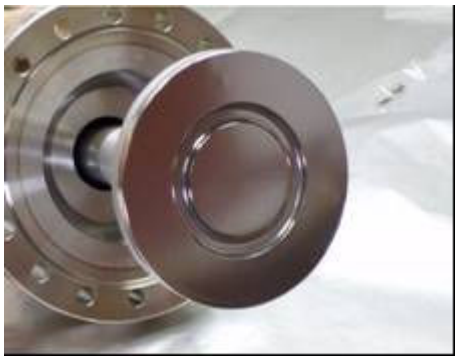

Fig.4.2.6. Large copper sample fixed upon an insulating support (just before the coating).

Studies of other HTC superconducting coatings

A task concerning HTC superconducting coatings (4.2.3) has been continued. The UHV planar-arc apparatus needed to study the production of NbN films has already been modified in order to control accurately the working gas (pure nitrogen) flow into the arc chamber. The triggering and stability of arc discharges at appropriate nitrogen pressures needs further investigation.

Work Package 5: Surface Preparation

Task 5.1: Electro-polishing on single cells Activity status

Sub-task *5.1.1 EP on Samples*

EP on samples like defined in the JAR1 proposal is completed and showed results which will be applied on single cell EP preparation. Basis of this research was the change of mixture in the existing acid components (H2SO4 +HF +H2O). New mixtures basing on different acid compositions like proposed in 5.4 will be examined with the existing test set up as well.
To investigate the phenomena of hydrogen implantation during EP treatments, some samples, treated with different fluorine concentrations and temperatures, have also been electro polished. In order to study H contamination the samples are measured by gaseous chromatography at DESY. This work showed first results on H2 contamination will be continued.

Modelling electro polishing phenomena with COMSOL software has been presented in CARE report-06-010-SRF. This study has been completed. For example, influence of the numbers of species considered in the model has been studied.

Sub-task 5.1.2 + 5.1.3 Single cell cavities:

3 Single cell cavities have been fabricated and will serve as test objects for optimization of EP mixtures.
The EP bench is completed and commissioned. For qualification of the set up a single cell cavity with well know performance is polished and retested at DESY. To calibrate the new infrastructure the polishing process was done under the standard conditions with a 1/9 EP Mixture and @18 V (Fig. 5,1,1).

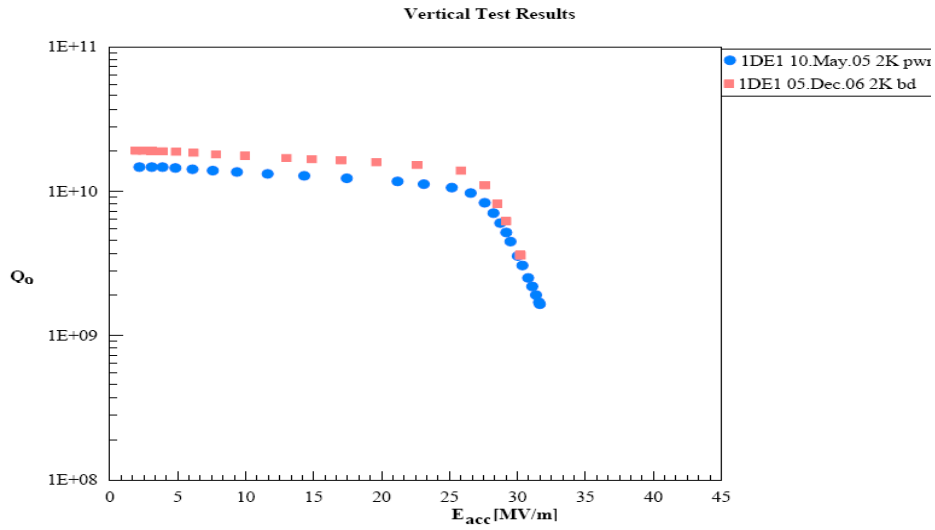

Fig. 5.1.1 Test result of the reference resonator 1DE1
(Blue dots = after EP @DESY Red dots = after EP @ Saclay)

The results show that the EP set up and the handling of cavities and the EP infrastructure is qualified and completed. First test with changed EP Mixtures are on the way.

Task 5.2 - EP on multi cells

Sub-task 5.2.1.1 – 5.2.1.2

The subtasks are finished and the DESY infrastructure for nine cell resonators is running continuously. Basing on the investigations on aging of the EP acid (SRF document 2004-001) an online sensor to control the U/I curves is installed in the DESY EP apparatus. First results show that the sensitivity of the sample is too small to dedicate small variation in the HF Concentration. A new probe with improved surface to distance correlations is build and will be installed during the maintenance shutdown in 2007.

Subtask 5.2.1.1.3

Due to the high investments and the necessary shut down of the DESY EP facility the hot water rinsing after EP treatments will not be installed into the DESY EP apparatus. The goal of the subtask is shifted to a different point of cavity treatment with the same high influence factor on cavity performance. We investigate the effect of hot water high pressure rinsing (UPWHHPR). This new method makes use of the strong bipolarity of hot water and the energy of a high pressure rinse jet at the same time and can be applied at the set up of the new high pressure rinsing facility at DESY. This facility will allow to heat ultra pure water to about 70 C. We will study the effect of removal of acid residues by UPWHHPR .

Subtask 5.2.1.2

Computer software is commissioned. First calculations on simulation of the existing electrode shape show that there is about a factor of 3 differences in the absolute value in the results of the current density distribution calculated from the RF data of cavity measurements and the computer calculations so far, while the distribution of current density shows the same result.

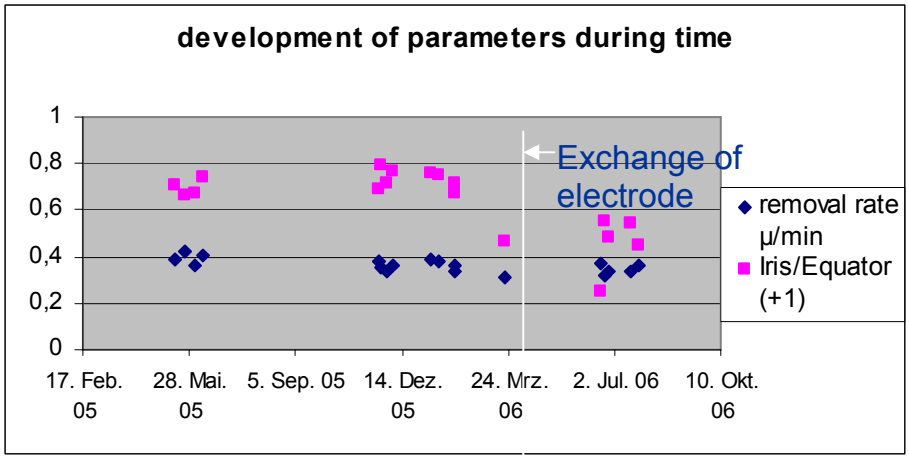

Fig. 5.2.1 Variation of parameters global removal rate and removal rate ration Iris / Equator after exchange of the electrode

One effect will be the hydrodynamic of the acid.
It is found that a change in diameter of the acid ejection holes of the EP electrode leads to a ratio reduction form 1,7 down to 1,5 (Fig. 5.2.1) . This effect will be studied and analysed. Never the less this software with out the liquid modelling module allows optimizing the electrode shape to study the basic influence of the geometry. New designs are under investigation.

Subtask 5.2.1.3.2 + 5.2.1.3.3
Beside the laboratory investigations, which are finished on that laboratory level, an industrial study for quality control and acid management is launched. First results were presented at the TTC meeting in Japan in October 2006. A report on these activities is under preparation.

Subtask 5.2.3.2+5.2.3.3
A design for a nine cell cavity oxi-polishing (OP) set up is finished. The design bases on the usage of the existing nine cells EP hardware. Only a piping system to inject the oxidizing acid into the cavity before starting the oxidation process needs to be fabricated. A test of the set up and the study of the effect of oxi - polishing is depending on the usage of the DESY infrastructure for the on going activities of the preparation for the XFEL and the build up of modules for the flash accelerator at DESY.

Task 5.3 Automated Electro-polishing.

The development of new forming techniques for the fabrication of seamless TESLA-type cavities requires good control of the electro-polishing (EP) process. We have developed a new process for electro-polishing niobium resonators based on a dynamical automated control that takes into account the surface roughness evolution during the EP. The process consists of a dynamical control of the minimum of the differential electrolytic bath conductance extracted from the I-V characteristics (polarization curve). The results obtained are very good, i.e. a smooth and high reflectivity niobium surface is obtainable, even by using electrolytes whose composition is not necessarily known. This last result makes the automated EP tool particularly interesting, especially when searching for alternative electrolytes, where a large amount of new baths need to be tested.

The Electro-polishing Characteristics

Fig. 5.3.1 shows a typical I-V characteristic for the electro-polishing of copper in an orto-phosphoric acid solution for the case of planar and parallel faced electrodes, when edge effects are negligible [Jacquet, P.A., Metal Finishing, 48, 1, 2 (1950)].

The following behaviour is observed at different sections of the polarization curve:

- Over section Va to Vb the current increases as a linear function of the voltage. The copper dissolution happens too slowly. The process is accompanied by the evolution of oxygen bubbles sticking to the anode and promoting local pitting of the copper surface.
- The polishing effect is observed between Vb and Vc; the copper structure is brought into relief, as long as the process takes place. However roughness levelling and a brilliant surface are obtained at the end of the plateau. Here, at voltages close to Vc, there is the minimum of oxygen bubble evolution. Even a minimum amount of bubbles can represent a limitation to the achievement of the desired roughness levelling. Migrating toward the top, oxygen bubbles produce undesired vertical traces depending on the solution agitation.
- At a higher potential the gas evolution becomes stronger and the surface erosion is accompanied by pitting. A better surface quality, although mat, is obtainable at voltages well above Vc, since oxygen bubbles have no time to stick to the surface.

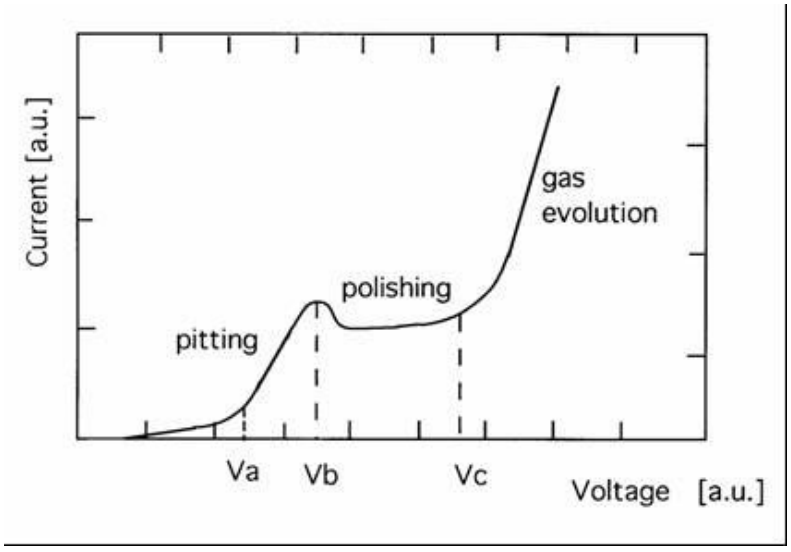

Fig. 5.3.1. Typical I-V characteristic for copper electro-polishing in orthophosphoric acid solution.

The behaviour in Fig 5.3.1 can be found, however, in many metal-electrolyte systems, even if the plateau is extremely narrow, being determined by a minimum of the first derivative of the I-V characteristics.

Several hypotheses exist for explaining the mechanism of electro-polishing in acid solutions. All of them concern the existence of the thin bluish viscous layer of electrolyte formed in proximity to the anode. The simplest explanation is the one proposed by Jacquet [1]. When a current passes across the electrolyte, the anodic film has higher viscosity and higher electrical resistivity than the bulk of the electrolyte. The thickness of such a film on a rough surface (Fig. 5.3.2) differs from site to site: above protrusions the film is thinner than above valleys. Hence protrusions dissolve more rapidly than wells.

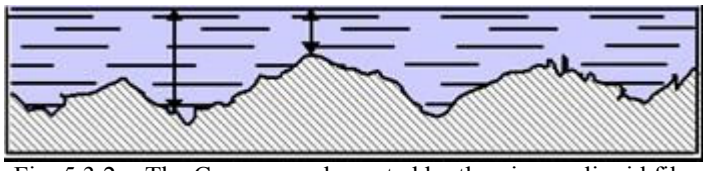

Fig. 5.3.2 - The Copper anode coated by the viscous liquid film.

The thin layer of electrolyte in the vicinity of the anode assumes a bluish color. Moderate agitation of the solution reduces the thickness of the bluish layer while the voltage drops. Vigorous agitation reduces the thickness to a few tenths of a mm and the voltage drops even more. Jacquet assumed that a relationship exists between the formation of the viscous layer in the electrolyte and the polishing effect. According to him, the process should be controlled by maintaining a constant voltage rather than a constant current density; in this case it is unnecessary to calculate the total surface area of the sample to be polished. Rigorously speaking, it would be not possible to control the electro-polishing process solely on the basis of voltage or current density measurements,

The applied voltage V is a function of the anode and cathode potentials, the voltage drop in the electrolyte (I R_{electr}) and the voltage drops in the conductors and contacts (I $R_{Conduct}$), i.e.

$$V = (V_{anode} - V_{cathode}) + I\,R_{electrol} + I\,R_{Conduct}$$

V depends on the electrode potentials, the electrolyte concentration, the anode and cathode surfaces, the arrangement of electrodes in the bath and the shape and size of the bath. Hence, the "applied voltage" used by Jacquet as a control parameter would not always correspond to the optimum polishing conditions. On the other hand, the potentials of the anode and of the auxiliary electrode do not remain constant. They change as a function of the time of electrolysis and the composition of the electrolyte.

Given that the plateau region in the I-V characteristics gives the best polishing conditions, it is important to examine the effect on the plateau of the process parameters. The four most important parameters are the electrolyte temperature, acid concentration, viscosity and stirring. The temperature does not affect the plateau voltage range, but only the current density; the same holds for acid concentration, the plateau voltage remains unchanged, while the current density increases; the current density is inversely proportional to viscosity; while stirring increases almost linearly the current density.

We have proposed one useful technique that makes it easy to automatically find the optimum electro-polishing conditions. The technique consists of locking the minimum of the differential conductance found by numerically differentiating the polarization curve. The idea is that, since the viscous layer has higher viscosity and greater electrical resistivity with respect to the bulk of the electrolyte, by finding the minimum of the differential conductivity of the I-V characteristics, one automatically obtains the right electro-polishing voltage. Computer control helps in finding this ideal working point and constantly tuning the process following the evolution of this point.

The I-V characteristic is monitored and controlled by the use of a PLC field-point programmed in Labview. Working with a PLC gives the big advantage of not loosing the control of the working point during the locking procedure around the minimum of the EP bath differential conductivity. This was indeed the main problem we faced during our preliminary attempts at dynamic control of the EP differential conductivity by a simple PC, due to the fact that standard PCs often interrupt the process just when refreshing so that the dynamic control is often lost. The process is driven by voltage. An automatic program displays the numerical derivative of I versus V. The working point is chosen as the minimum of such a derivative, i.e. the minimum of the bath differential conductance.

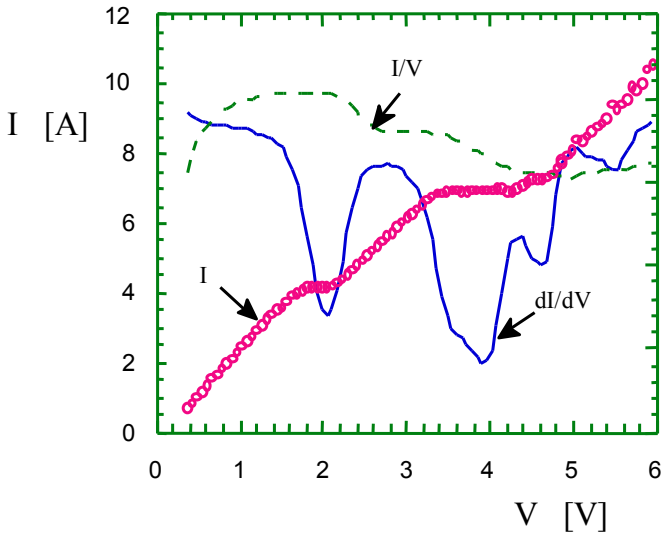

Figure 5.3.3: I-V characteristic for a standard electro-polishing process (circles); The differential conductivity dI/dV (continuous line) and the ratio I/V (shaded line) are displayed versus voltage. We interpret the first minimum in differential conductance as due to edge effects and to the non uniform distance between electrodes.

In Fig. 5.3.3, we display the differential conductance compared to the ratio I-V and together with the I-V characteristic. Some literature approximates the minimum of dI/dV with the minimum of I/V. Already from fig. 4, it is clear that the two minima differ quite substantially in voltage. In any case, an electrolytic cell is a non-linear circuit, hence the solution conductivity is a differential quantity while, the ratio I/V has no any physical sense in such a case. The I-V characteristic evolves with time. Fig. 5.3.4 displays the evolution of the current plateau.

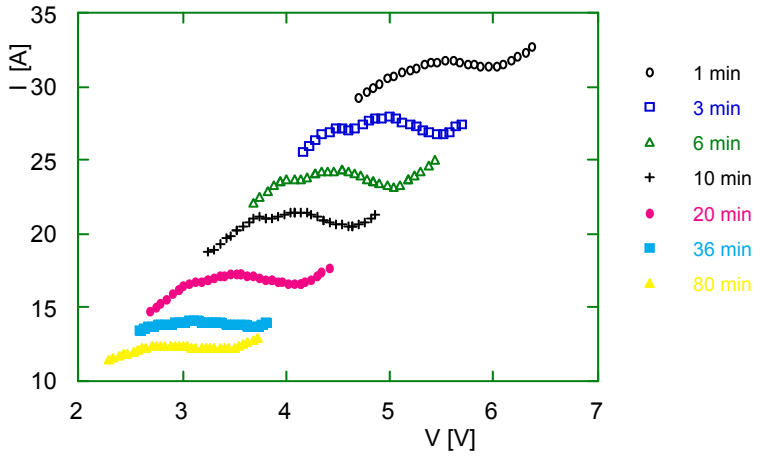

Figure 5.3.4: Time evolution of the I-V characteristic plateau.

The reason for the plateau decreasing is twofold. The levelling action decreases the roughness, but also the surface area decreases. Moreover, under the hypotheses of an anodic, passivating oxide film, the longer the process lasts, the more stable is the film and the weaker is the etching. By locking the minimum of the differential conductance, we could lower the plateau up to very low values of metal dissolution rate. Hence when the viscous layer becomes too thick, equivalently the voltage becomes too low, the process is reset by a sudden increase of the supplied voltage and by starting the process again from the beginning by plotting the I-V characteristics. In other words, whenever we need to remove hundreds of microns of metal, we apply the method of locking the minimum of differential conductance for one hour, than for a few minutes we work at a much higher voltage in order to destroy the passivation layer, then we restart locking the minimum for another hour and so on.

At the minimum of the differential conductance there is already low gas evolution. However as soon as the process is started and the plateau starts to get lower, at a certain voltage threshold, gas evolution can even disappear. We have written a computer program that automatically locks onto the minimum of the bath differential conductance. In this way not only is the process constantly driven according the best parameters, but also we can directly find the best electro-polishing current density, without the need to know them a priori. The method applies to any metal (copper, niobium, magnesium, aluminium, titanium and its alloys, gold alloys, and many technical alloys), and the operator does not even need to know what electrolyte he is using.

The automated EP Labview program

The rotating cavity EP System built for electro-polishing cavities is a standard closed loop circuit and it is seen in Fig. 5.3.5. Mono-cell and three-cell cavities can be easily treated. Copper and niobium cavities can be simultaneously treated. The architecture of the automated EP is sketched in Fig. 5.3.6. The best working point of the I-V characteristic is searched for and dynamically followed during the whole EP process.

.5.3.5 – The rotating cavity EP system built for the treatment of both Niobium and Copper.

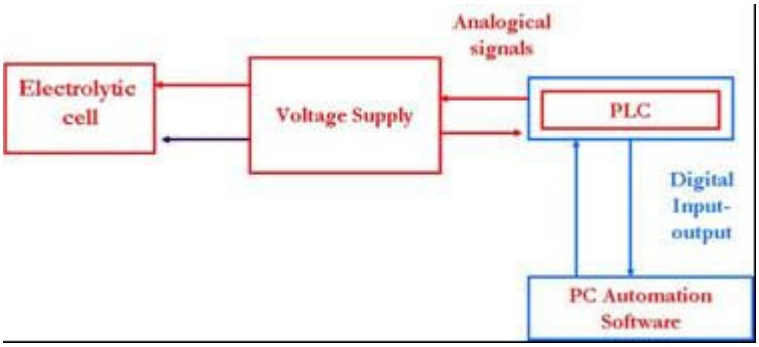

Fig. 5.3.6 - Scheme of the automated EP

The apparatus is composed of:

- An industrial power supply controlled by means of an analog current signal;
- A special PLC, the FieldPoint® FP-2010 from National Instruments, that uses the software written by LabView® 7.1;
- The LabView® program written on a computer, and then transferred onto the memory of FieldPoint®.

The Hardware consists in an ALINTEL S4000 power supply (100V max - 40V max) with a remote controller. The 0-10 V applied to the pins at the interface produces 0-100 V in output. The analog readings from the power supply are converted to digital signal in a PLC and treated by the automation software. The digital output from the automation software is converted to voltage signals that drive the power supply.

The PLC is a LabView® programmable National Instruments Field Point 2010 and it is composed of 2 modules; 1 supply; 1 RS-232 Serial interface; 1 Ethernet 10/100 Mbps. It is possible to drive the process by several PCs connected to the PLC in a network as shown in Fig. 5.3.7.

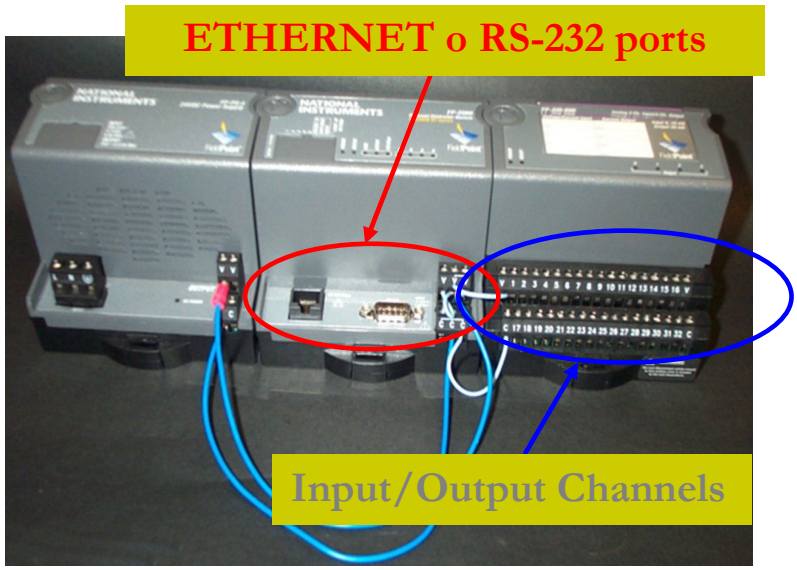

Fig. 5.3.7 - The LabView® programmable National Instruments Field Point 2010

The control software for electro-polishing is written in LabView 7.1, which is a graphical language specifically designed for interface and control of the instruments of National Instruments. This language combines with a simple graphic interface and a powerful set of functions. The core of the program is the algorithm for the search and recognition of the working point. The program initially makes a large scan from two values set by the user. After the scan, the software calculates the derivative of the I-V curve, and sets the voltage that matches to the minimum point as shown in Fig. 5.3.8. Then the program maintains the voltage for a time set by user, after it makes a little scan around the minimum voltage. By recalculating the derivative, the program follows the new voltage minimum. After a time, set by user, the program uses the initial data to rescan the characteristic curve. This system allows the program to adjust the minimum if the working point moves away from plateau. If the point found by program is not at the right place, the user can stop the automatic search and manually set a new minimum. The program continues the automatic search around the new minimum. All parameters can be changed in real time.

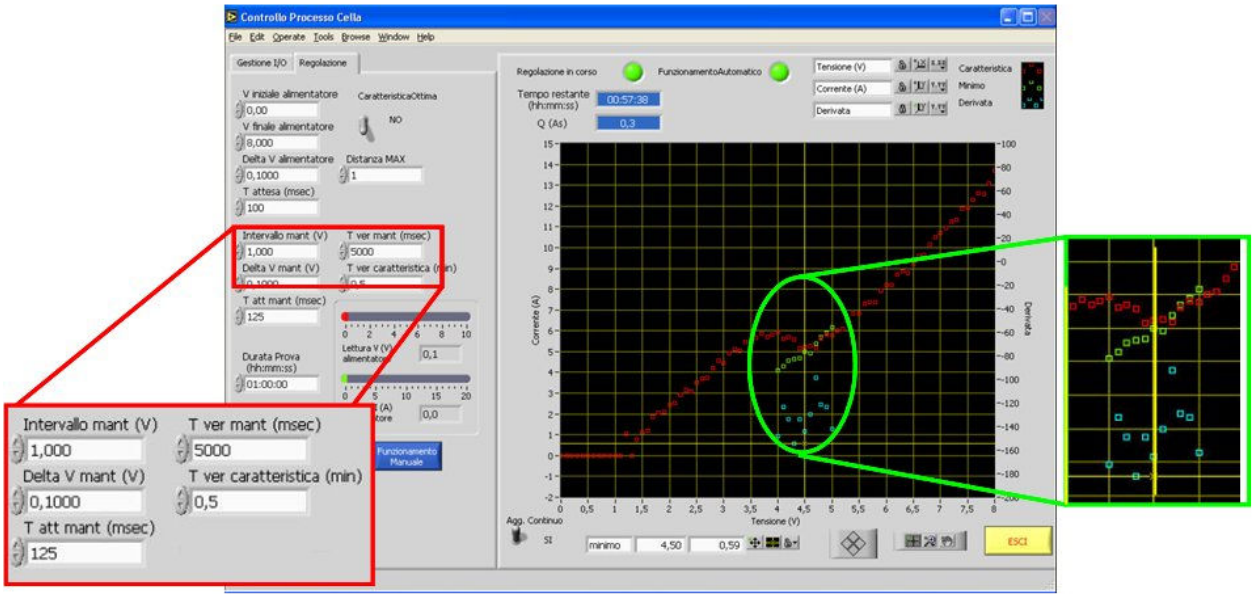

Fig. 5.3.8 - Typical I-V characteristics (red dots), displayed on the computer screen, controlling the electro-polishing processes. The curve drawn by the blue dots is the derivative of current versus voltage. The numbers on the left are the process parameters; the knobs at the bottom-right are needed for setting the starting point.

The program tested on niobium, displays the typical oscillations given by the forming and the cracking of the forming oxides and displayed in Fig. 5.3.9. Oscillations create difficulties on setting the working point, but it is sufficient to directly start the acquisition of the polarization curve after the oscillation and to search the working point on the plateau after the oscillating regime.

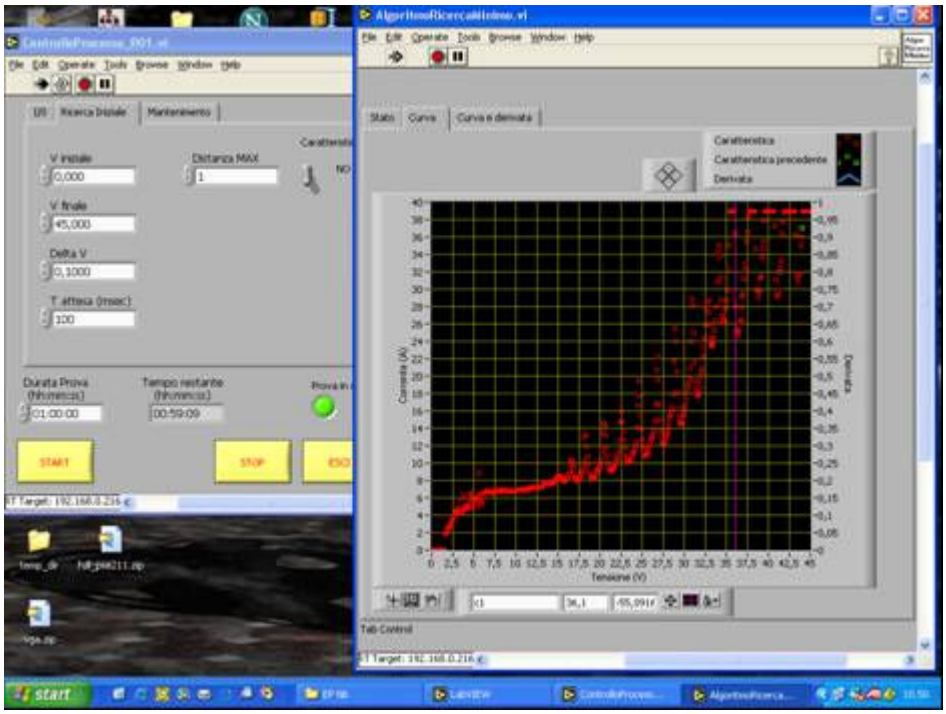

Fig. 5.3.9 – Typical oscillating regime in the I-V characteristics when electro-polishing niobium.

The programme has been successfully used for the electro-polishing of a mono-cell cavity and it is a unique tool for the development of the research of new hydrofluoric-free electrolytes

for the electro-polishing of niobium. The Automated EP tool has been satisfactorily used by our laboratory and it is available for all CARE partners working on work-package 5.3 on electro-polishing.

Task 5.4 Dry Ice Cleaning

A jet of pure carbon dioxide snow loosens and removes different types of surface contaminations by its unique combination of mechanical, thermal and chemical effects. The cleaning process acts locally, is mild, dry and without residues requiring no additional cleaning agent. The spontaneous relaxation of liquid carbon dioxide leaving the nozzle results in a snow/gas mixture with 45 % snow and a temperature of 194.3 K (-78.9°C). This jet is surrounded by supersonic nitrogen, which, firstly, provides an acceleration and focussing of the jet and, secondly, prevents the condensation of humidity at the cleaned object. The cleaning effect is based on thermo-mechanical and chemo-mechanical forces. The former are created by three effects: brittling of the contamination as a result of rapid cooling (shock-freezing), the tough pressure and shearing forces due to the high momentum of the snow crystals hitting the surface and the powerful rinsing due to the 500 times increased volume after sublimation. Particles down to 100 nm can be removed. Chemo-mechanical forces occur when high momentum snow particles hitting the surface are melting at the point of impact. In its liquid phase carbon dioxide is a good solvent for non-polar chemicals, especially for hydrocarbons and silicons. The thermal effect of shock-freezing is thereby directly correlated with the snow intensity, while the mechanical effect however depends on the velocity and angle of the jet. The chemical effect depends on the momentum of the crystals. An optimal cleaning impact is achieved if the thermal gradient between contamination and substrate is high. To avoid recontamination an effective and well-defined exhaust system is necessary. In summary the advantages of the carbon dioxide dry ice cleaning are:

- dry cleaning process,
- no cleaning agents,
- removal of particulate and film contaminations,
- no polluting residues.

The basic cleaning parameters are shown in Table 1.

Table 1: Dry ice cleaning parameters

CO_2-pressure	~ 50 bar
N_2-pressure	12 – 18 bar
Particle filtration	< 0.05 µm
Temp. of liquid CO_2	-5° - -40° C
Enviroment of cleaning	Laminar flow class 10

In order to achieve high gradients for future accelerators like XFEL, ILC, etc., without field emission loading, advanced cleaning and handling procedures must be applied. Surface contaminations like particles, hydrocarbons, etc. and mechanical damages like scratches have been shown to cause enhanced field emission limiting the usable gradient of accelerating structures. Although high pressure rinsing with ultra-pure water has been proven to be a powerful technique to reduce the enhanced field emission of cavities, dry–ice cleaning might have additional cleaning potential. Moreover it avoids a wet cavity surface with its enhanced sensitivity against recontamination. It should be applicable to ceramics (coupler windows)

without loosing the gain of an earlier conditioning. Due to these properties dry-ice cleaning is considered as very attractive for the final treatment of horizontally assembled cavities with their power couplers.

Description of Work

After successful pre-tests on samples and cavities in 2002 and 2003 using the facilities of Fraunhofer Institute IPA, Stuttgart (Germany), in early 2004 the infrastructure installation at DESY started. An ultra pure gas supply system for both carbon dioxide and nitrogen was installed and successfully tested in the existing clean room (Fig.5.4.1). At the end of 2004 / beginning of 2005 the CO_2 cooler/purifier unit (Fig.5.4.1, 5.4.2) was ordered as an important component in order to filter, purify and liquify the CO_2.

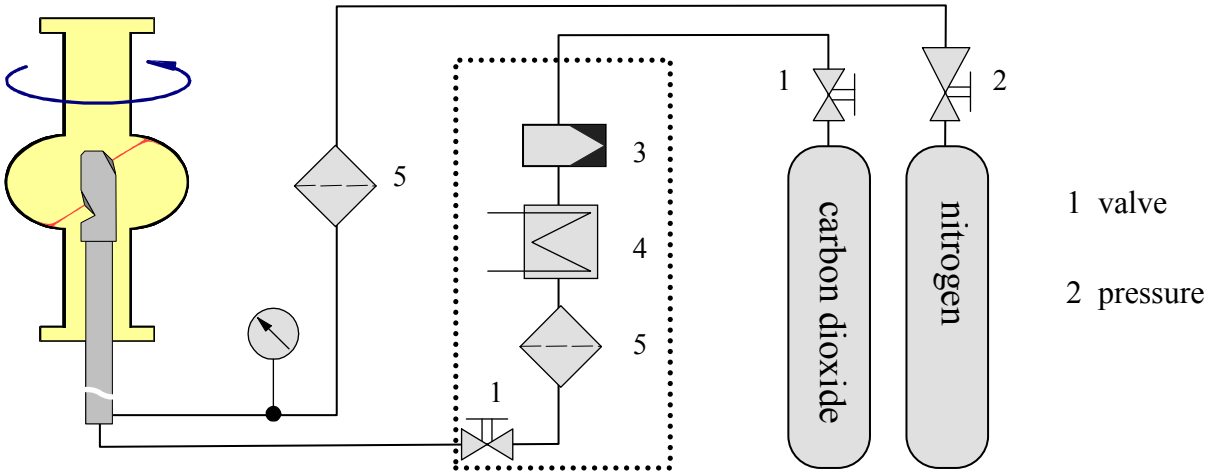

Figure 5.4.1: Schematic of the prototype set-up for dry-ice cleaning of a mono-cell cavity.

As described in the introduction, dry-ice cleaning should be well suited for horizontal cleaning of SC cavities. Therefore the set-up for cleaning of 1-3-cell cavities was designed for horizontal cleaning differing from the proposal for task 5.4. In 2005 the horizontal motion unit using the existing spraying cane and a new motion unit started operation (Fig 5.4.2). Due to man-power problems, caused by unexpected repair work at the DESY HERA accelerator, the complex control system of the cleaning unit was delayed significantly. This delay has not been compensated to date.

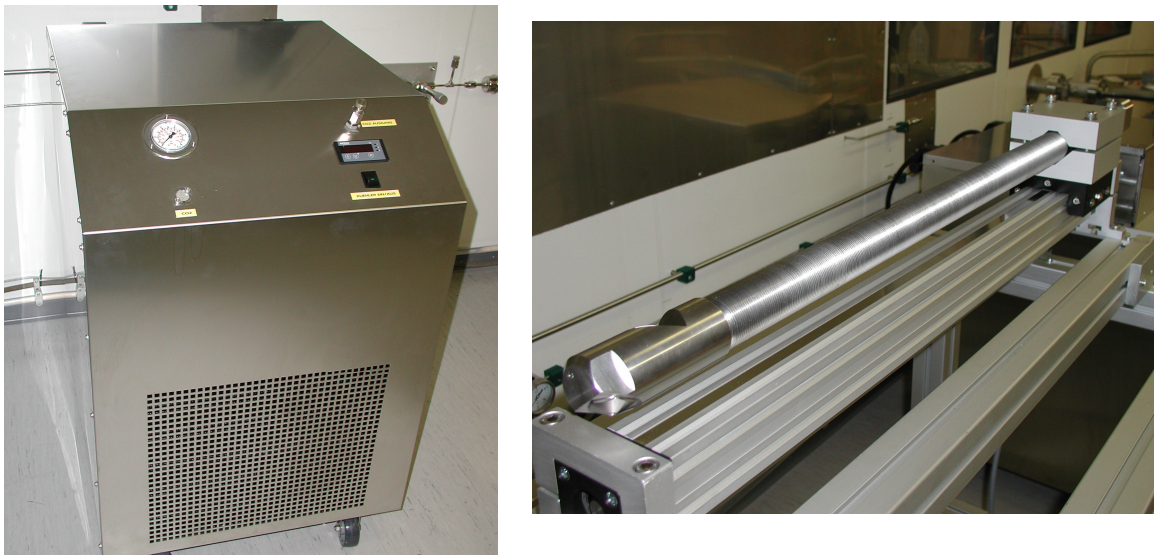

Figure 5.4.2: CO_2- cooler/purifier unit (left) and horizontal motion unit with the spraying cane assembled on the linear drive (right).

The heat removal from the cavity during operation of the dry-ice jet makes it necessary to apply a heater system to avoid cooling and freezing of the cavity. Several options have been considered. With respect to clean-room requirements and for simple assembly, a prototype of an IR heater system was tested. After first operational tests it turned out, that the power was insufficient. Furthermore the assembly procedure after cleaning of the integrated heating and exhaust box was too complicated. A new dedicated design of an optimized, high power IR heater (Fig 5.4.3, 5.4.4) had to be developed, constructed and installed. This caused a delay during commissioning of approximately six months. The new heater system fully meets its requirements and allows continuous dry-ice cleaning almost without freezing of the cavity.

Figure 5.4.3: Dry-ice cleaning system with the new IR heater

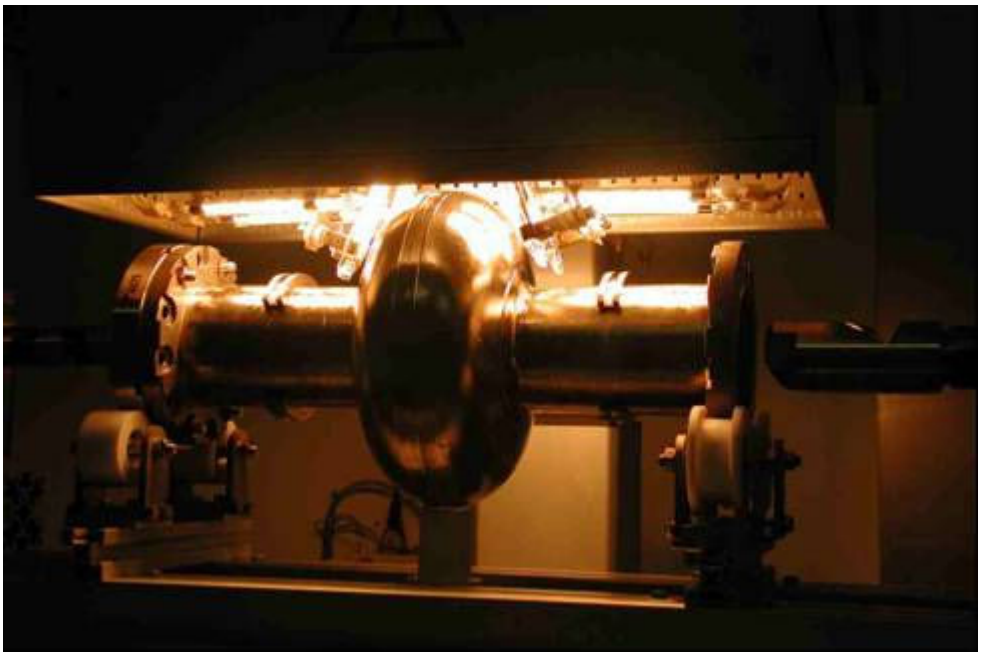

Figure 5.4.4: The new IR heater system in operation

To fulfil the requirements of personnel safety for routine operation a gas alarm system was installed. During the installation phase the commissioning continued under special safety conditions.
Recently, new capillaries with lower diameter have been tested in order to reduce the cooling of the cavity and the consumption of CO_2. The former is important to keep a high temperature gradient on the inner surface for an optimum cleaning efficiency. A reduced CO_2 consumption enhances the usable time of one set of pressurised bottles and is in general preferable with respect to safety aspects. A capillary with 12% reduced diameter has been used since November 2006. In addition, the assembly procedure of the cavity to its vacuum and RF connections ("antenna") is improved by a simple, but effective new fixture.
In 2005 and 2006 the commissioning of the dry-ice cleaning system was continued successfully (Fig. 5.4.5). Several cavities have been cleaned both for system tests and for RF measurements of the cavity. Additional samples have been cleaned and tested (see WP 6.3). The cleaning parameters and cavity results are discussed in the next chapter.

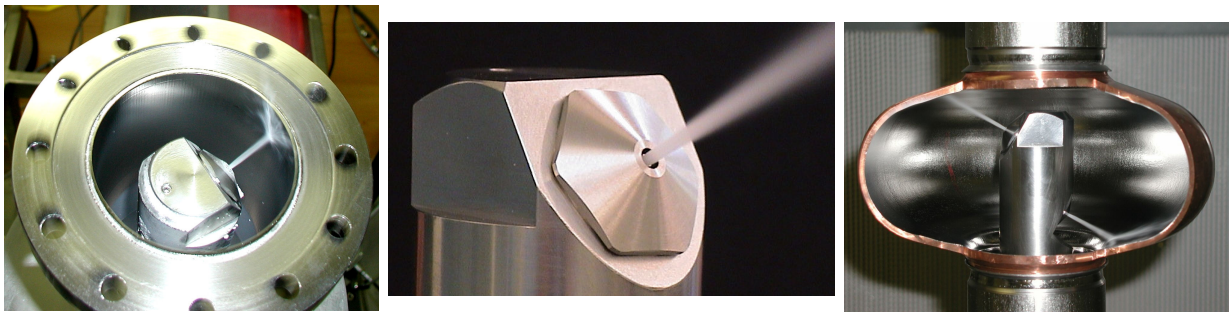

Figure 5.4.5: Commissioning of the dry-ice system: Optical checks of the jet under different conditions.

Discussion of Work

The dry-ice cleaning system is operable and a preliminary cleaning parameter set is established. With respect to the results there is still some contradiction between excellent cleaning results on samples (WP6.3.) compared to most of the cavity tests which still suffer from field-emission loading (Fig 5.4.6). The reason can be either due to the cleaning parameters or a contamination of the cavity during the final assembly after the dry-ice cleaning. After the recent modification of the CO_2 – capillary and assembly fixture an excellent cavity result, with no field-emission loading up to 33 MV/m, was achieved (Fig. 5.4.7). The goal of the next tests will be the reproduction of this result.

In spite of this good result the preparation of the construction of the nine-cell cleaning apparatus requires a careful re-investigation of the nozzle system and cleaning parameters together with the experts in dry-ice cleaning of the Fraunhofer Institute for Manufacturing Engineering and Automation (Fraunhofer IPA). This will continue until the middle of 2007. In addition, further sample measurements on various niobium materials are foreseen in close collaboration with task 6.3.

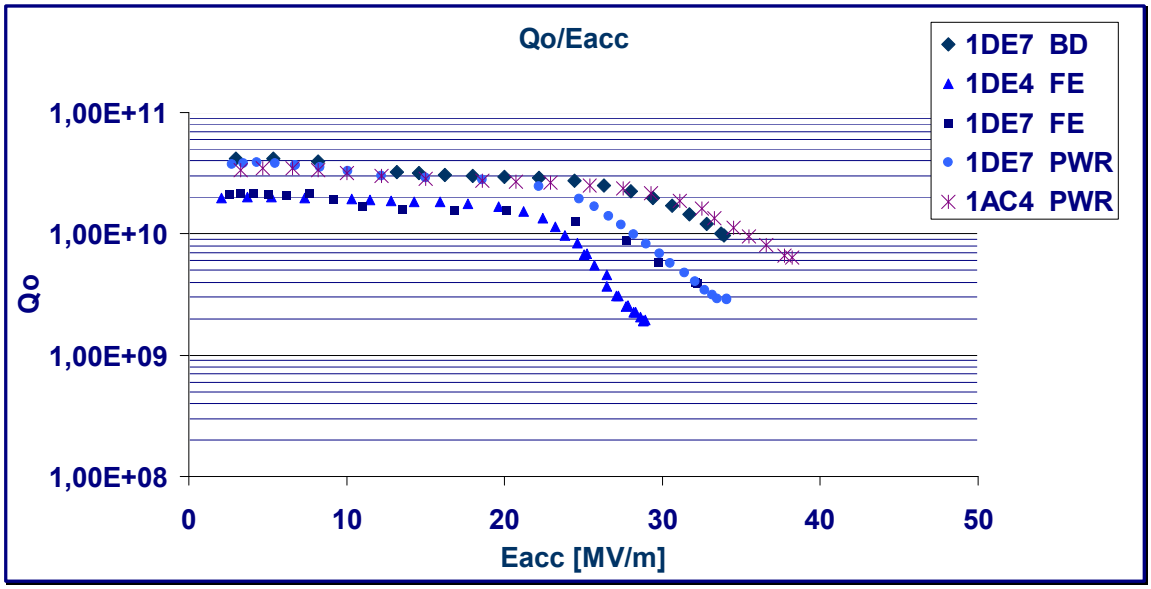

Figure 5.4.6: $Q_0(E_{acc})$-performance of latest rf-tets after dry-ice cleaning

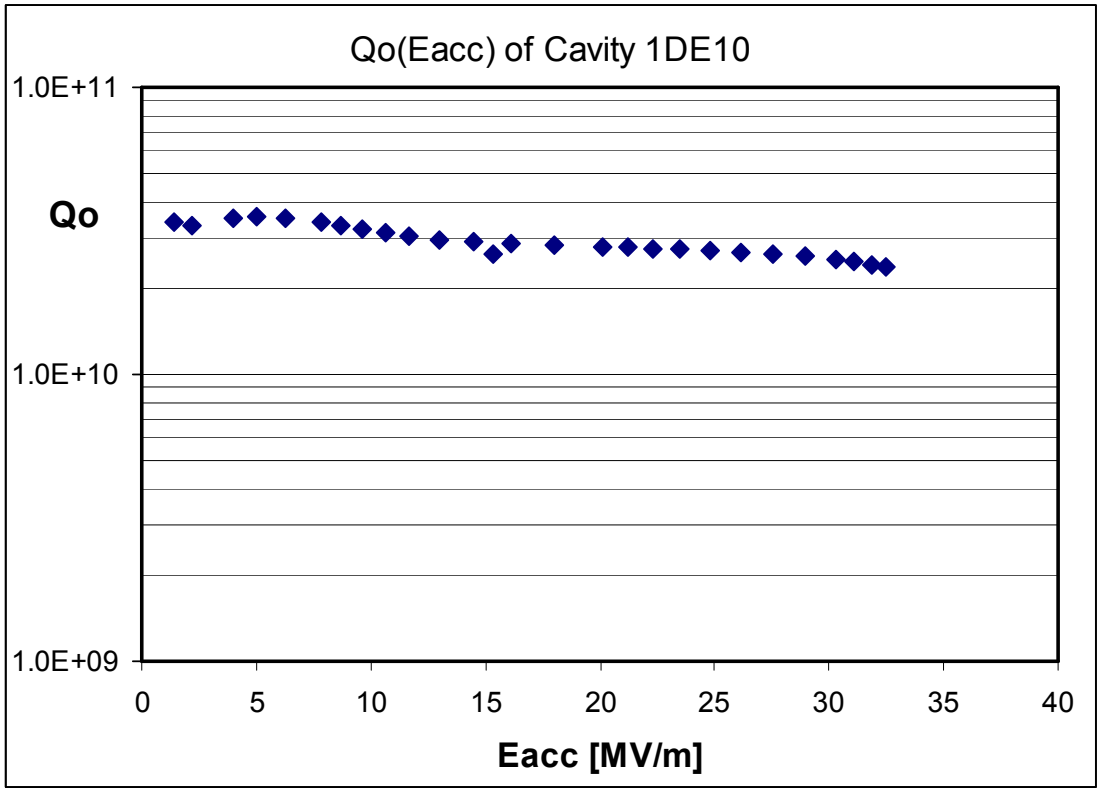

Figure 5.4.7: Recent best $Q_0(E_{acc})$-performance after dry-ice cleaning with the new capillary.

Conclusions and Future

Dry-ice cleaning has shown its capability for successful cleaning of SRF cavities. Nevertheless, the results are not as reproducible as is necessary for multi-cell applications.
The next steps in the near future will be the evaluation of the cleaning parameters described above and the understanding of critical conditions during cavity cleaning. Although the multi-cell cleaning apparatus is significantly delayed, this is a necessary pre-condition for the successful construction of a next generation set-up. Reproducibility of the cavity cleaning is essential for the envisaged applications. Only minor modifications of the existing apparatus

are planned. An additional heater of the gas pressure bottles will avoid the cool-down of the bottles in order to stabilize the CO_2 pressure during operation.

References

1) "Dry-ice cleaning for SRF Applications", D. Reschke et al., Proc. of the 9th Workshop on RF superconductivity, KEK Proc. 2003-2, Tsukuba-shi, Japan (2003)
2) "First experience with dry-ice cleaning on SRF cavities", D. Reschke et al., Proc. Of the LINAC 2004, Lübeck, Germany (2004)
3) Presentation at the ELAN Meeting, May 4th – 6th 2004, Frascati, Italy
4) "Further improvements with dry-ice cleaning on SRF cavities", A. Brinkmann et al., Proc of the 11th Workshop on Rf superconductivity, Cornell, USA (2005)
5) "Dry-ice cleaning on SRF cavities", A. Brinkmann et al., Proc. of the EPAC 2006, Edinburgh, Scotland (2006).

Work Package 6: Material Analysis

Task 6.1 Development of SQUID based equipment for detection of defects in niobium

Scanning of artificially produced defects

A niobium test sheet with artificially imbedded flaws (tantalum inclusions of size 0.1-0.05 mm close to the surface) was produced and scanned with a SQUID scanner developed and built at WSK (Fig.6.1.1).

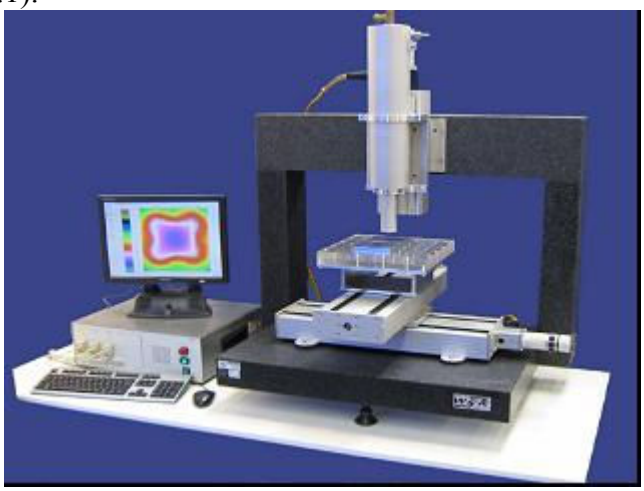

Fig.6.1.1. SQUID scanner developed at Fa. WSK

Holes of different diameters and depth were drilled and filled with tantalum. After, these locations were heated by a defocused electron beam up to the melting point. Finally, grinding of the complete sheet surface was done so that the defect positions were barely visible (Fig. 6.1.2).

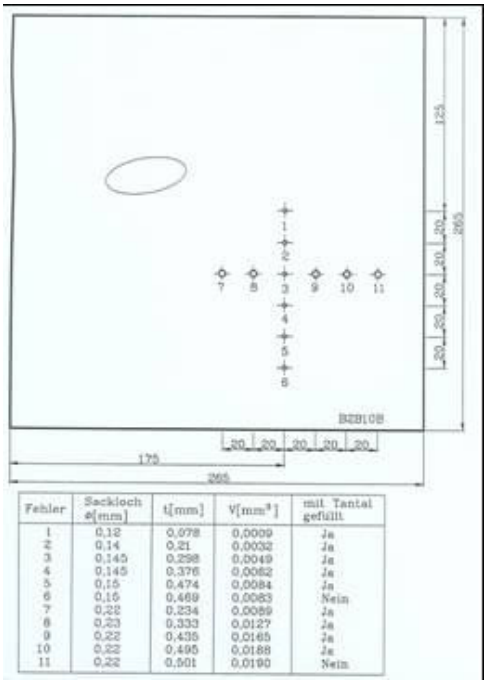

Fehler	Sackloch ø[mm]	t[mm]	V[mm³]	mit Tantal gefüllt
1	0,12	0,078	0,0009	Ja
2	0,14	0,21	0,0032	Ja
3	0,145	0,298	0,0049	Ja
4	0,145	0,376	0,0062	Ja
5	0,15	0,474	0,0084	Ja
6	0,16	0,469	0,0083	Nein
7	0,22	0,234	0,0089	Ja
8	0,23	0,333	0,0127	Ja
9	0,22	0,435	0,0165	Ja
10	0,22	0,495	0,0188	Ja
11	0,22	0,501	0,0190	Nein

Fig. 6.1.2: Nb test sheet with tantalum inclusions.

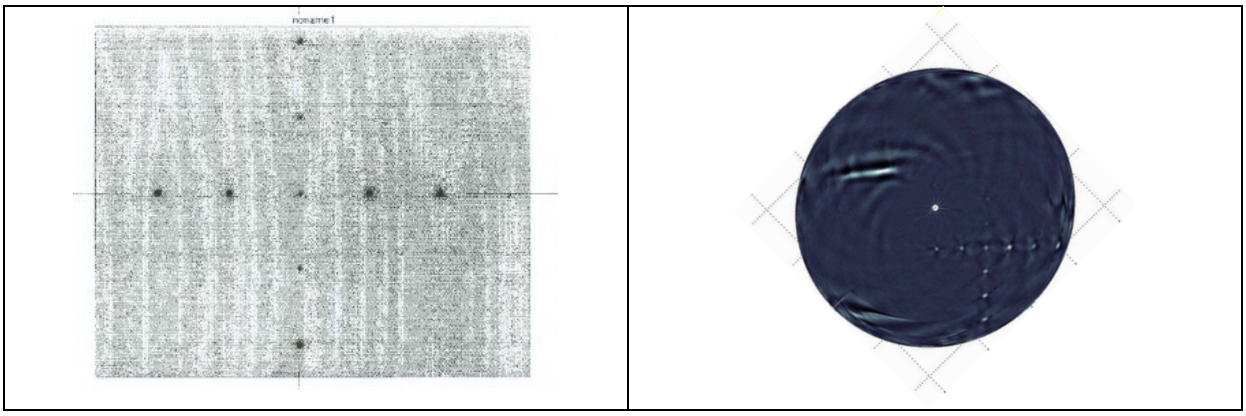

Fig. 6.1.3. NAA Neutron activation analysis and eddy current images of the test sheet

The neutron activation analysis and eddy current images of the test sheet are shown in Fig.6.1.3. All artificially produced defects can be located.
SQUID scanning was done with an excitation coil of 1 mm diameter and 40 windings. The scanning speed was around 10cm/sec. The excitation frequency was 6 kHz. The scanning results can be seen in Fig. 6.1.4. All artificially produced defects were identified.

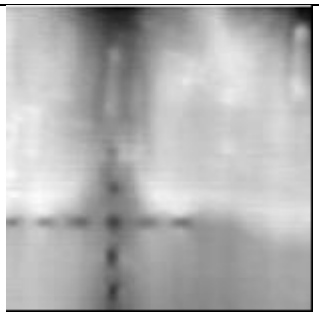

Fig. 6.1.4a: SQUID scanning results of Nb test sheets.

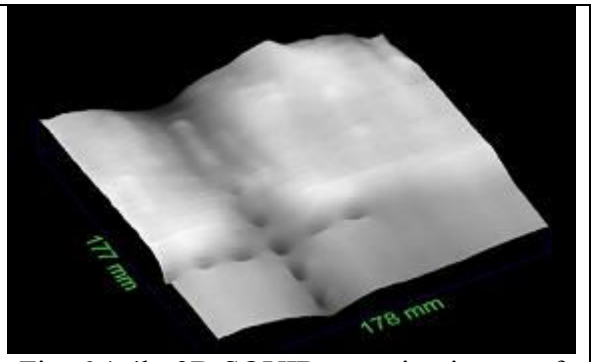

Fig. 6.1.4b: 3D SQUID scanning image of Nb test sheet with artificial Ta defects.

Fabrication of more systematically produced artificial defects is in progress. A drawing of the defect distribution can be seen in Fig. 6.1.5. The following materials are foreseen to be imbedded; tantalum, cooper, iron, niobium, stainless steel.
Unfortunately this work has been delayed. The contract for the production of holes for defects with very small diameter was placed with the company Swiss-Laser, which is now insolvent. The company Rofin-Sinar-Laser Micro took over the contract and the fabrication of the holes is foreseen for beginning of 2007. After that the holes will be filled with implanted material and closed by a defocused electron beam at DESY. Scanning of the sheets with the artificial defects is foreseen to start after grinding at WSK.

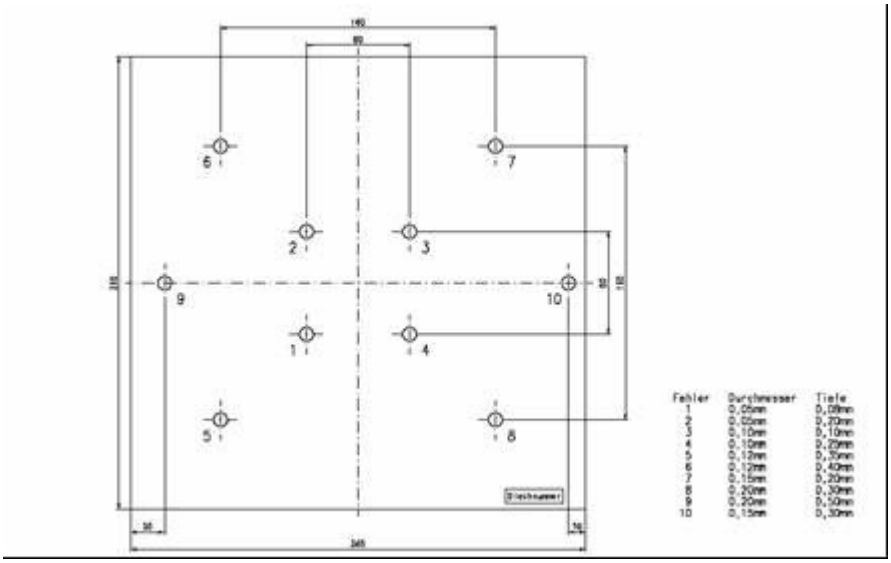

Fig. 6.1.5: Drawing of niobium sheet with imbedded defects

Scanning of industrially produced niobium sheets for 1.3 GHz resonators

Twenty niobium sheets from the Fa. Plansee for the cavity AC115 were scanned before annealing with the WSK SQUID scanner. The excitation frequency was 6.3 kHz.

- Surface structures (increasing of surface roughness), detected in sheets Nos. 14, 24 and 26 is probably caused by the rolling.
- Sheets 12, 17, 18 und 20 demonstrate small density gradients in corners.
- All sheets (excluding sheet No. 28) are defect free. Sheet No. 28 has a de-lamination in the lower left corner penetrating from the surface into the bulk (Fig. 6.1.6). This sheet was removed and not used for cavity fabrication.

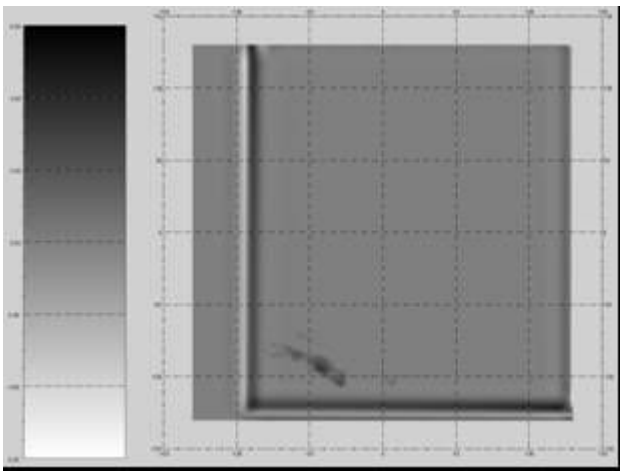

Fig.6.1.6. De-lamination detected in a sheet by SQUID scanning.

Task 6.2: Flux gate magnetometry

The activity on flux gate magnetometry has proceeded comparing what can be obtained by a flux gate and what can be obtained by the same EP process by a GDR. We have applied the magnetometer to an Electropolishing cell section (Fig. 6.2.1).

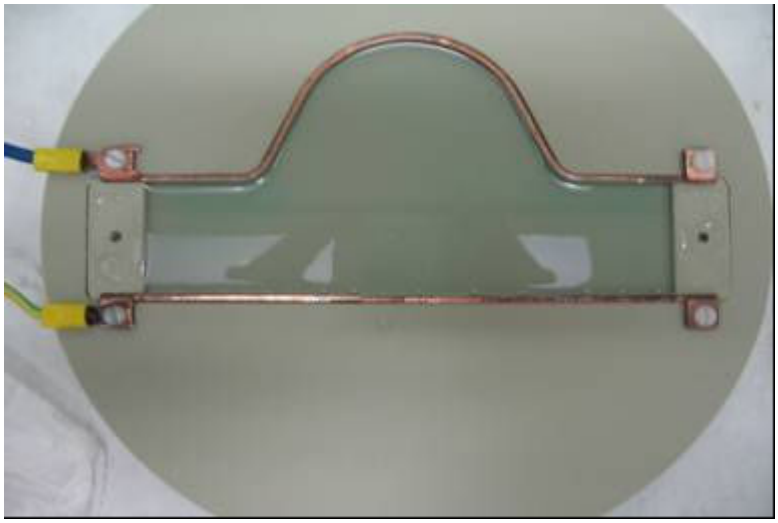

Fig. 6.2.1 Experimental Arrangement for magnetometric investigation of EP current distribution.

The left picture (Fig. 6.2.2) is the field distribution obtainable by a Flux gate 1st order gradiometer. The right picture is the current distribution GMR 2nd order gradiometer, showing that room temperature non destructive evaluation can easily make electrochemistry diagnostics.

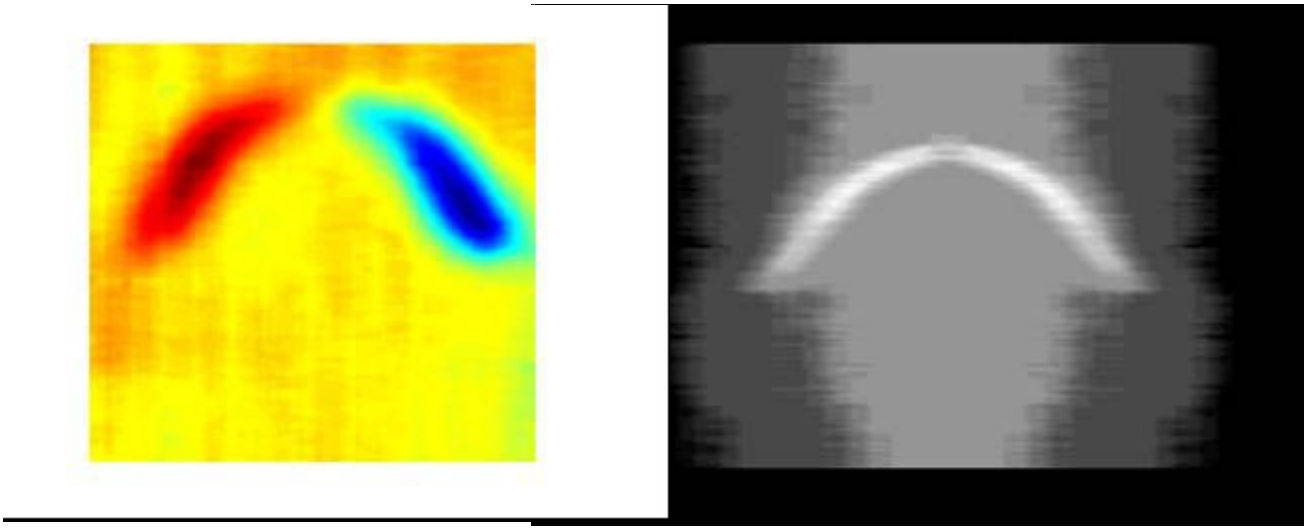

Fig. 6.2.2 Field and current distribution of EP cell.

Task 6.3: DC Field Emission Studies of Niobium samples

Quality control field emission measurements were performed on a standard Nb sample, electro polished and high pressure rinsed, inside a nine-cell cavity at DESY. Also, to study the improvement of surface quality by applying dry ice cleaning (DIC) as a final surface

cleaning procedure, a series of successive field emission scans and local FE, SEM and EDX measurements of emitters were performed on two circular Nb samples (28 mm diameter). The curvature and surface roughness of the samples were measured by means of a new optical profilometer. Moreover, we also started to study the FE properties of two single-crystal Nb samples cut from ingot plates and chemically polished only. A series of systematic field emission scans on these circular Nb samples (28 mm diameter) at surface fields of up to 200 MV/m was performed and was followed by local measurements of the emitters found. The surface treatments and measurement details of the samples are listed in the table below.

Sample names	Suface treatment	Parameters	Measurement, Analysis
SEP1†	Dry ice cleaning (EP+HPR before)	T (liquid CO2)= -5 to - 40 0C CO2 pressure = 45 bar N2 pressure = 12-18 bar	FE measurement, SEM, EDX Profilometer scans
SEP2*†			
QCNb1	Sample prepared (EP+HPR) inside a 9-cell cavity	Standard for cavities at DESY	FE measurements Profilometer scans
SCNb1	BCP + HPR	# Single crystal or large grains Only 30µm removal by BCP ⇒ Mirror like surface	FE measurement, SEM, EDX
SCNb2			
CryNb1			
CryNb2			

The main results of this work are summarized as follows:

Quality Control Nb sample EP+HPR inside 9-cell cavity:

The electro-polished Nb sample showed a very smooth surface with step heights of ~ µm due to the grain structure and a very small micro-roughness of less than 0.2 µm, as measured with the profilometer (Fig.6.3.1).

No field emission was observed in the voltage scans up to a surface field of 120 MV/m over a $(10mm)^2$ area; while at 150 MV/m the number density of emitters observed is $9/cm^2$ (Fig.6.3.2). This is the best result observed to date on polycrystalline EP/HPR Nb samples.

Suppression of FE on EP Nb samples after HPR and DIC:

Treatments on Nb:	EP	EP + HPR	EP+HPR+DIC
E onset (1 nA)	40 MV/m	60 MV/m	90 MV/m
N @120 MV/m	30/cm2	14/cm2	< 2/cm2
β values	(31-231)	(17-167)	(17- 80)

High resolution SEM on Nb samples revealed two types of emitters: particulates of 500 nm to 20 µm size and scratch-like surface defects. Most of the particulates show foreign elements.

SEM images (Fig.6.3.3) of an emitter before and after DIC, show the destructive effect of DIC on one of the emitters which could not be removed by HPR.

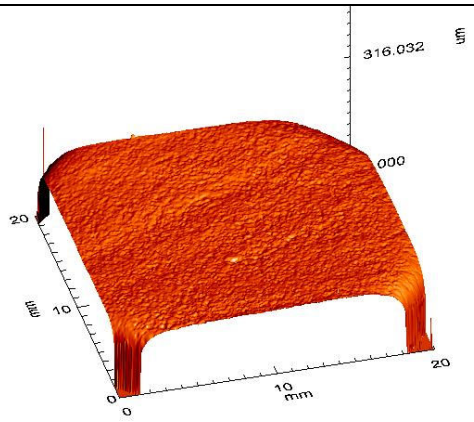

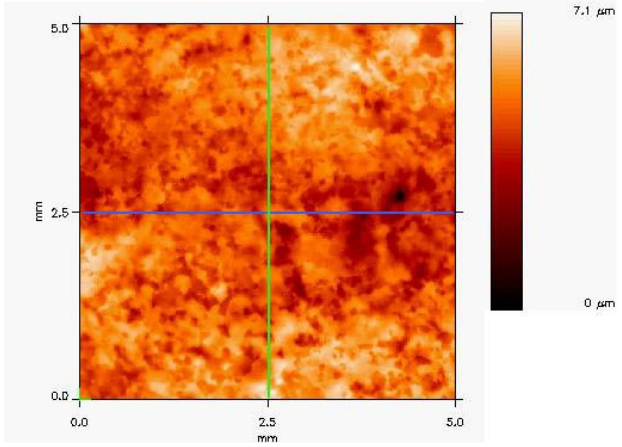

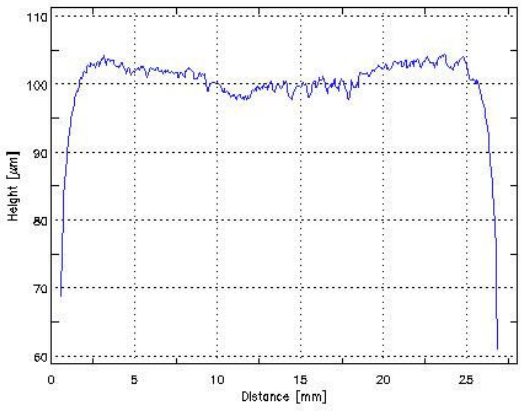

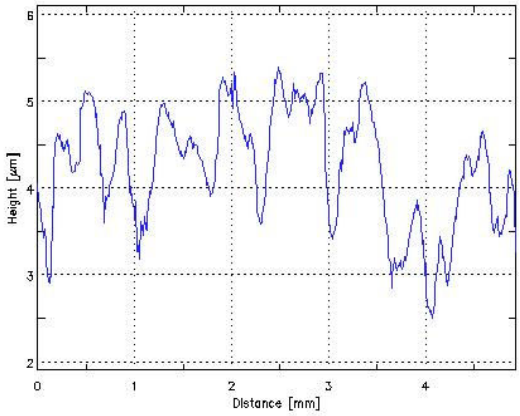

Profile:
Curvature: 6.7 µm over 20 mm

Horizontal profile:
Height steps: < 1.5 µm over 0.5 mm
Microroughness: < 0.2 µm

Fig.6.3.1. Profiles of electropolished quality control sample (NbQcEP*1)

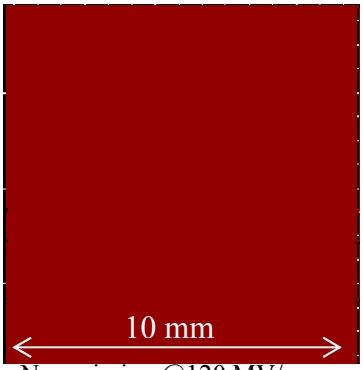

No emission @120 MV/m

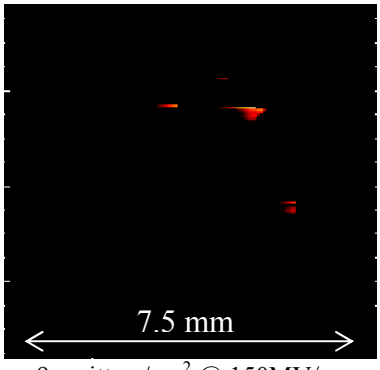

9 emitters/cm^2 @ 150MV/m

Fig.6.3.2. Regulated voltage scans for Nb sample electropolished inside the 9-cell cavity.

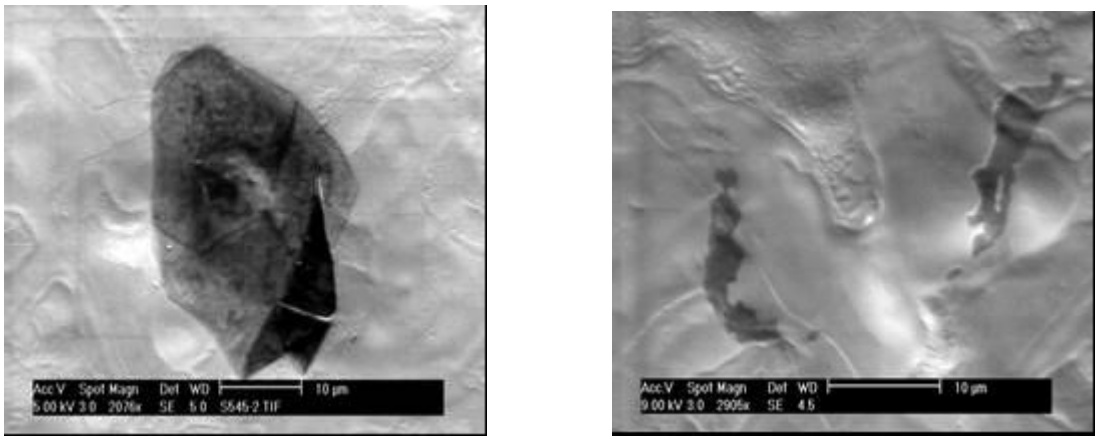

Fig.6.3.3. SEM images of an emitter after HPR and after dry ice cleaning. Most of the part of the emitting particle has been destroyed by DIC, but remnants still emitting with reduced strength.

Single crystal and large grain Nb samples:

Crystalline Nb samples were only 30 µm BCP treated and high pressure rinsed, giving the visual appearance of a mirror like surface, i.e. surface roughness <<1 µm. Two samples were of single crystal Nb (SCNb1, 2) and another two samples were of large grain Nb with only three grain boundaries on the sample (CryNb1, 2). The grain boundaries observed in SEM are shown in Fig. 6.3.4.

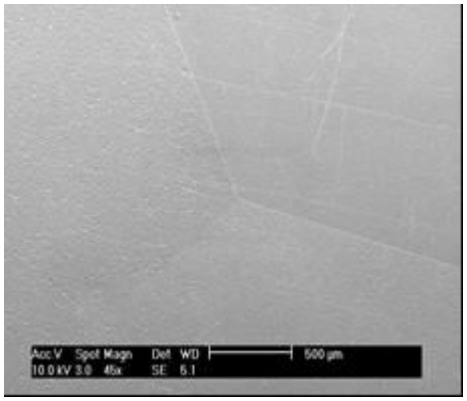

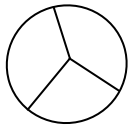

Fig.6.3.4. SEM image of the intersecting grain boundaries at the center of the sample surface (CryNb2)

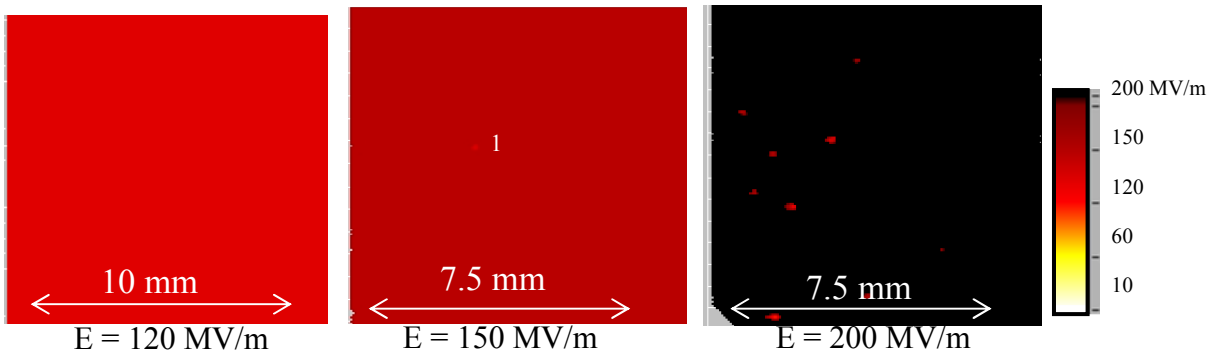

Fig.6.3.5. Regulated voltage scans on a single crystal Nb sample.

FE results on large grain samples are summarized as:

1. The onset of FE was observed in the regulated V-scan for 2 nA current at 150MV/m (Fig.6.3.5) and the emitter density at 200MV/m is (18, 21) and (9, 16) /cm^2 for large grain and single crystal samples.

2. Locally measured emitters show stable FN behavior after conditioning at $I_{max} < 35$ nA. The onset field lies in the range of 64 to 175 MV/m, β values in (22 – 75) and S-parameters in (10^{-5} to 10^{-8} μm^2) range, which are typical for particulates and surface irregularities.

Comparison of emitter statistics on all measured samples:

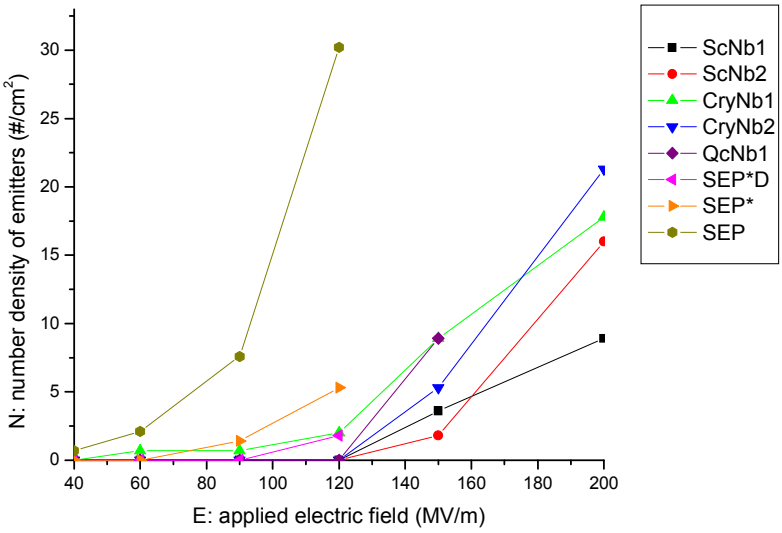

Fig.6.3.6. Emitter statistics on various investigated Nb samples. Single crystal Nb samples show least emitter number densities and minimum onset field. (SEP: EP in Saclay, SEP*: EP+HPR, SEP*D: EP+HPR+DIC, QcNb: EP+HPR inside cavity for quality control)

In conclusion of all the above measurements, single crystal Nb samples (only with 30 μm BCP + HPR) provide better performance than the best EP Nb sample measured yet (Fig.6.3.6).
Measurements on dry-ice cleaned large grain samples are in progress. Further, a series of measurements on EP Nb samples prepared inside 9-cell cavities for quality control scans are planned. Moreover, the effect of heat treatments on FE will be studied for the best Nb samples.

Work package 7: Couplers.

Work-package 7 concerns the development of power couplers. This WP is broken down into three main tasks:

7.1 – New proto-type couplers.
7.2 – Fabrication of a titanium-nitride coating bench for the coupler ceramic windows.
7.3 – Conditioning studies of proto-type couplers.

For task 7.1 we have designed two new proto-type couplers named TTF-V and TW60 respectively. Both types of coupler are being produced in industry and were received in summer-autumn of 2006. Four couplers of each type have been delivered by ACCEL. A new test transition for these 8 couplers has also been built.

A first pair of TTF-V proto-types was tested at low power. This revealed an important shift in the matched frequency (~ -80 MHz) with respect to the calculated value of 1300 MHz. The second pair shows a shift of about -45 MHz (Fig 1).

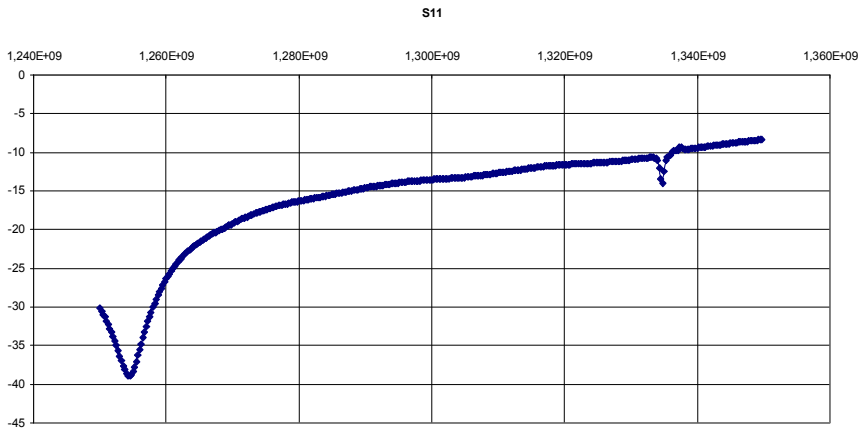

Fig. 7.1: S11 parameter low level measurements for the second pair

With a return loss of ~ 14 dB at 1300 MHz we attempted power conditioning. The klystron is protected with an interlock and a circulator in the wave-guide distribution system. This conditioning showed a very slow power ramping time and finally it was interrupted.
To solve the problem of the frequency shift three actions are planned:

1) Mechanical measurements and checks.
-All the mechanical dimensions in the drawings were re-checked. The checked dimensions were re-evaluated in the HFSS simulations. A new version of HFSS is operational and it allows also a full simulation of an entire pair of couplers on their test stand. In the most critical points (ceramics, short circuit….), to increase the precision, the simulation was performed locally with an increased number of lattice nodes. All these simulations confirmed the original results with the reflection minimum at 1.3 GHz.
-The mechanical dimensions were measured (within the limit of accessibility) to check also if the tolerances were respected. Some discrepancies were found especially in the antenna penetration and in the transition box. These measured dimensions were re-inserted as input for new simulation but they do not show any drastic effect that can explain the frequency shift. A full documentation has been produced and exchanged with the industry to collaborate in understanding the origin of the problem.

2) Simulation
- Besides the above mentioned simulations other computational work was performed to understand the effect of different parameters on the resonance frequency. Different simulations were performed for various values of the properties of the ceramics, the penetration of the antennas, and the position of the short circuit. Considering each parameter in turn we do not find any explanation to the problem since the calculated shift in frequency is not of the same order of the measured one. Only a strong coherent variation of the ensemble of different parameters can justify the frequency shift but this seems strongly improbable.

3) Low level measurements.
- Apart from the activities carried out to understand the problem an empirical approach was adopted to find a solution. Different low level measurements were taken while trying to vary the antennae penetration (compressing or stretching the bellows or inserting different thickness plates between the test stand and the cold part flange). Promising results were

obtained but they are affected by a mechanical inclination of the couplers. A new measurement is envisaged with a mechanical support to block the inclination of the couplers and especially the bellows.

A high power conditioning attempt also for the second pair is foreseen for the beginning of 2007.

The TW60 proto-type was also expected before summer but it has a delay in production. They were received in October with a certain delay due to difficulties encountered in the TiN coating. Mechanical and endoscopic checks were performed. A number of anomalies were noticed and the manufacturer was so informed. A major fault in the tolerances of the cold part flanges prevents any mounting for low level tests. The cold parts were sent back to ACCEL for mechanical modification. They are expected back before the end of 2006.

As far as the task 7.2 is concerned we have to announce a certain delay (4-5 months on the last milestone) on the time schedule due to the difficulty of finding an industrial partner that could assure the construction of the prototype with the required performances in a reasonable time schedule and budget.
Finally we have established a collaboration with an Italian research consortium that can meet our needs. This collaboration will also mean the participation of LAL personnel to the development and testing phases of the coating station. A device using the sputtering solution seems to be the preferred choice.
The TiN coating will be performed by sputtering under vacuum using a magnetron. The machine has been designed to have an oil free pumping system to adjust the pressure to the order of $1x10^{-7}$ mbar. A nitrogen (99.999% pure) inlet has been foreseen designed to facilitate vacuum breaking. Nitrogen and argon bottles will be of 99.999% purity. All gas entrances have to be designed with filters filtering particles with a diameter bigger than 0.2 μm and the filters will be inserted as close as possible to the chamber. A vacuum measurement system will operate from atmospheric pressure to $1x10^{-7}$ mbar or from 10 mbar lower vacuum. All flanges with a low probability to be dis-assembled, such as pumps, instrumentation etc.. will be CF flanges with metallic seals, while only the coupler entrance porthole, the magnetrons and the UHV gate valve will use rubber seals. Those parts that constitute the internal part of the vacuum chamber will be made of; 316L stainless steel (a part the magnetron AISI 304); Copper for UHV; beryllium-copper, pure titanium and titanium nitride and ceramics.
Fabrication drawings: Conceptual drawings of a planar magnetron and target have been made. The vacuum design is now complete, while the plasma chamber mechanical drawings have been started and they are expected before the end of 2006.
The sputtering system will be turbo pumped. The rough vacuum will be done by a Scroll pump. Vacuum gauges will be of the Pirani, capacitive and ionization types.
In the meanwhile we have performed some testes on different samples to validate the sputtering technique for TiN coating on alumina. The results were extremely encouraging. A diffractometer analysis showed the deposition of a nearly stochiometric layer of TiN. The same results were obtained on an 800 nm coated sample analysed by ESCA and SIMS techniques (Fig. 2). In this last analysis contaminants were found, more precisely oxygen and some contamination. Both can be fully explained by the low vacuum quality in the device used for the sputtering and in a minor accident that produced a limited quantity of carbonates.

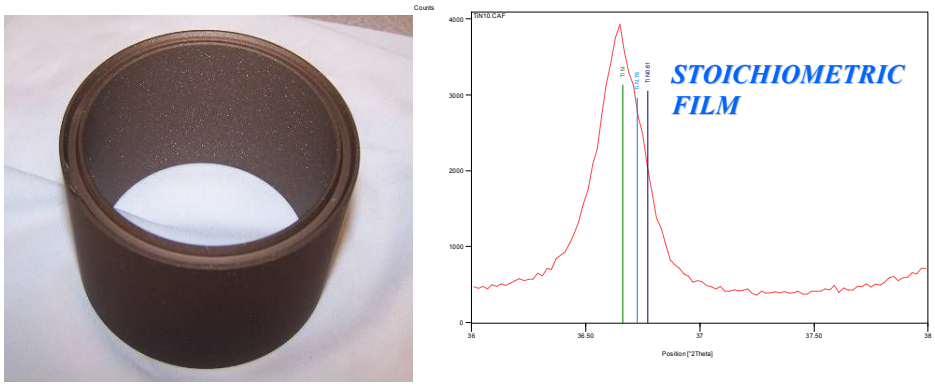

Fig. 7.2: (Left) Tin coated ceramic window, thickness = 800nm. (Right) results of the diffractometry are shown. The film appears to be stochiometric.

Concerning Task 7.3 we are still waiting to condition the new prototypes. In the meantime, preparation for the new tests have been performed. A lot of simulations have validated the models as far as the thermal response, multipacting activity and the Q_{ext} parameter are concerned. Multipacting for TTF-V was simulated and shows a possible 2^{nd} order 2-point multipacting threshold at ~ 700 MHZ. Presently, we are calculating the transverse kick effect on the beam of the coupling field of the prototypes couplers on the cavity.
A number of technical modifications have also been implemented in the conditioning station to be able to receive the new prototypes..
A great deal of experience has been acquired working on the conditioning of the TTF-III couplers and a strong evidence of conditioning time reduction is the result. The conditioned pairs have been also installed and tested on a SC cavity giving excellent results. All the improvements on the conditioning procedure that have been studied in this activity will be applied to the new prototypes. We have tested a pair of fully TiN coated TTF-III couplers. The result was strongly affected by multipactor in only one cold part. An endoscopic analysis of the concerned part is expected. Different tests were also performed to bias the TTF-III antennas. The capability to suppress the electronic activity in the biased region was clearly demonstrated.

Work Package 8: Tuners

Task 8.1: The UMI Tuner

A coaxial (blade) tuner solution has been developed for the compensation of the Lorentz force detuning of the superconducting cavities under the high gradient pulsed operation foreseen for ILC operation. The device is based on the prototypes successfully tested at DESY in 2002 both on CHECHIA and on the superstructures inserted in the TTF string. In order to compensate the Lorentz force detuning foreseen at 35 MV/m, fast elements, such as piezo ceramics, have been integrated into the tuning system. Each tuner can accommodate up to four piezo actuators. Two existing blade tuner assemblies have been equipped with a revised leverage system, and two modified Helium tank systems have been manufactured by Zanon in order to include the piezo active elements (see Figure 8.1.1, Figure 8.1.2 and Figure 8.1.3).

Figure 8.1.1: TTF cavities modified Helium tanks

Figure 8.1.2: Complete assembly provided with leverage mechanism and stepping motor.

The ring-blade assembly that provides the slow tuning of the cavity is shown in Figure 8.1.2 together with the leverage system. This is the main tuner mechanism and consists of a three-ring bending system. One of the external rings is rigidly connected to the helium tank, while the central one is divided in two halves. The rings are connected by thin, welded titanium plates (the so called "blades") at an angle which transforms the azimuthal rotation (in opposite directions) of the two halves of the central ring, into a variation of the distance between the end rings, producing an elastic change of the cavity length.

Each tuner can accommodate up to four piezo actuators with length of up to 72 mm and a section of up to 15 mm^2. This part, during operation, can provide the fast tuning capabilities needed for Lorentz force compensation and micro-phonic stabilization. In Figure 8.1.2 a 40 mm long aluminum dummy piezo is also shown mounted on its support in order to verify the mechanical constraints without risking damage to the real piezo actuators, while in Figure 8.1.3 a 3-D drawing of the cavity-tuning system assembly is shown.

Figure 8.1.3: The cavity dressed with the modified helium tank and piezo blade tuner.

The cavity elasticity is used to provide the piezo pre-load. During the first cold tests in a horizontal cryostat, foreseen at DESY and Fermilab for the beginning of 2007, two 15 mm^2 cross section and 70 mm long NOLIAC piezos will be employed for each tuner.

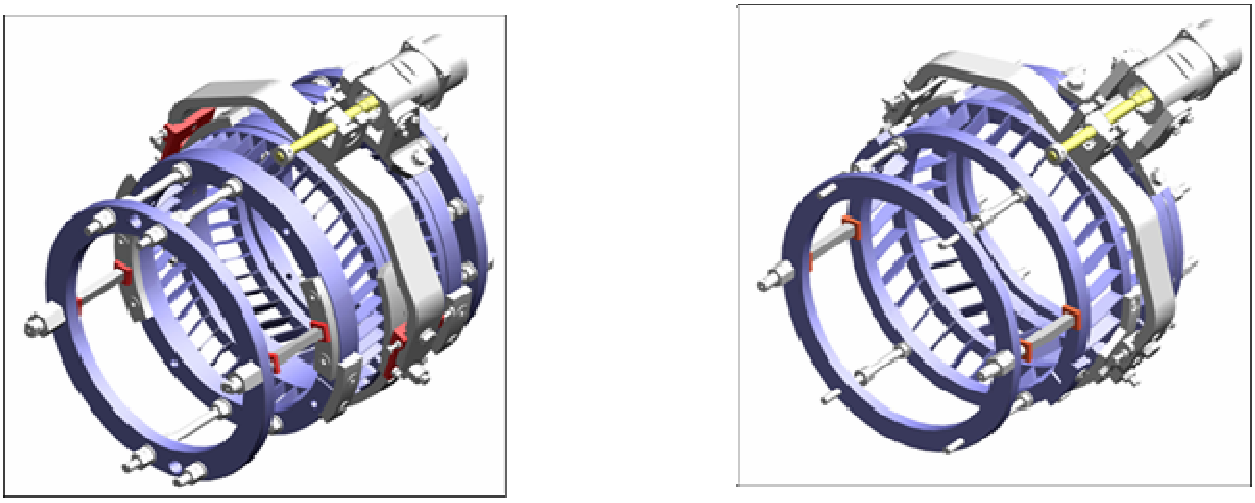

Figure 8.1.4: The piezo blade tuner (left) compared with the "lighter" one (right).

Meanwhile, we have started to analyze design modifications to the coaxial blade tuner concept in order to reduce manufacturing costs and simplify the manufacturing process, in view of large scale industrialization for the ILC. All of this, keeping in mind the perspectives of the large scale production foreseen for the collider (> 16,000 components for the baseline 500 GeV design).

This consideration led us to begin exploring possible simplifications and cost reduction efforts for an industrial scale blade tuner. By lowering the requirements on the ring-blade stiffness, on the basis of the considerations that the overall combined tuner stiffness (as provided to the cavity) is essentially limited by the leverage mechanism, especially in terms of slack and tolerances, and by the helium tank conical end plates, a "lighter" version was devised. This version reduces the required material and the number of machining and welding procedures. The width of the Ti rings has been reduced, as well as the number of blade elements. Now the system has an array of 14 "packs" of 2 blades on each side, for a total of 112 flexural elements (blades), with a 40% reduction in the number of blade packs, and a consequent reduction of the assembly time and number of EB welds. This leads to a corresponding decrease of the nominal stiffness of the ring-blade mechanism that is still consistent with the overall stiffness requirement dominated by the other system components (see above). The blade length and width have also been adjusted to improve the tuning range in order to relax

the pre-tuning requirements. The current tuner 3-D drawing is shown in Figure 8.1.4, together with the lighter one.
Once installed the new coaxial blade tuner will be the core of a complex control system designed to ensure a stable resonant frequency to the superconducting cavity. The whole system must be able to implement an affordable control with good performance, involving both feed-back and feed-forward architectures. For this purpose a complete electronic platform based on a SIMCON 3.1 FPGA board (courtesy of the TESLA LLRF group) is now under development and will allow us to quickly implement a first prototype of the blade tuner control system. The block diagram of the tuner control system is shown in Figure 8.1.5.

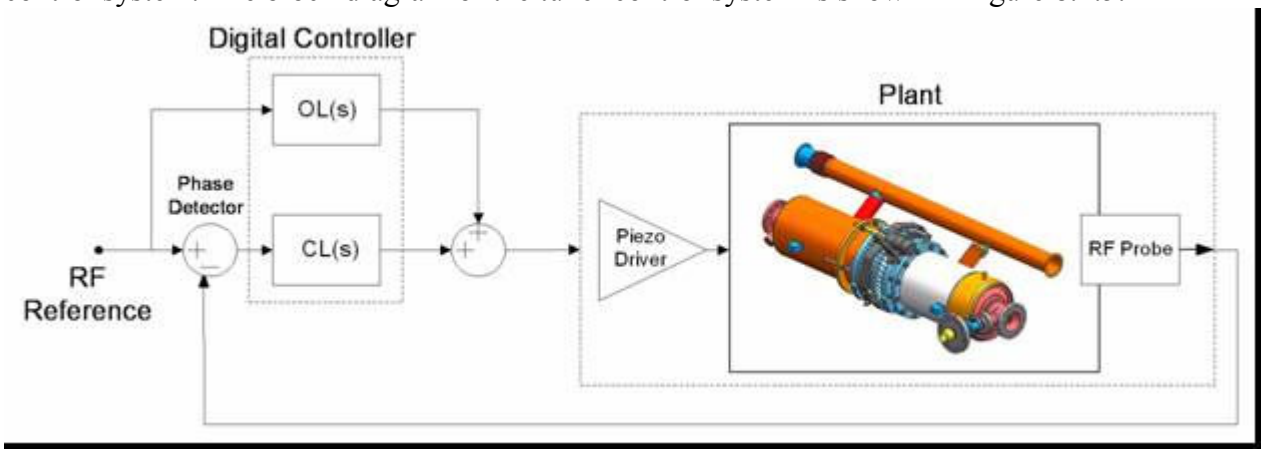

Figure 8.1.5: Tuner control system schematic view.

Last, but not least, we obtained, from Celmi, and tested a cryogenic (i.e. realized using strain gauges and glue suitable for cryogenic applications) load cell of reduced dimensions. This device is of size comparable to the piezo-ceramic support and will allow us to measure forces exerted on (or by) piezo elements directly inside cryogenic environments. The new load cell (compared to the former, bigger one) can be seen in Figure 8.1.6.

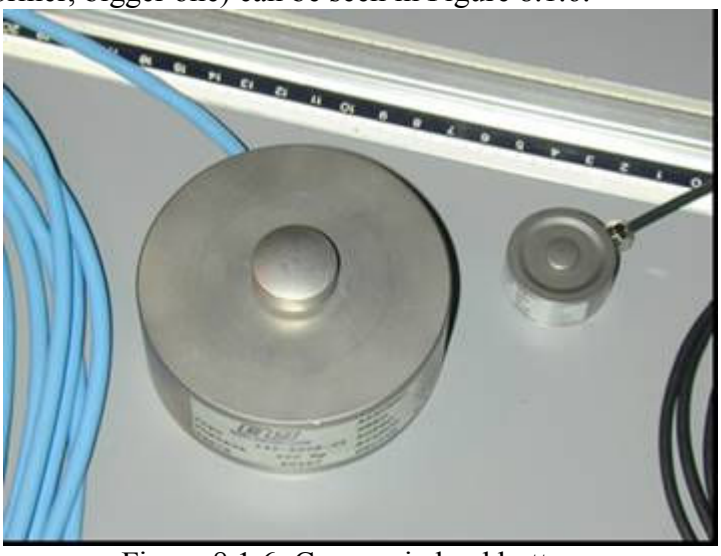

Figure 8.1.6: Cryogenic load buttons.

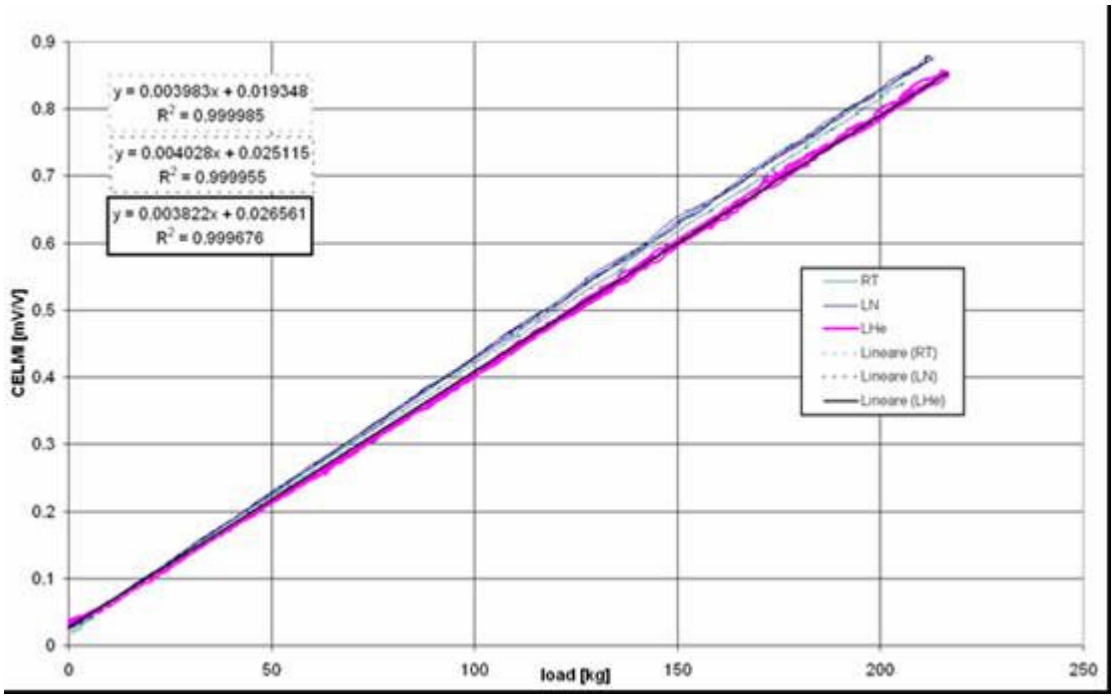

Figure 8.1.7: Characteristics of the new cryogenic load cell for different working conditions.

The tests of the new load cell in liquid helium have been successful and the device characteristics taken at different temperatures all shown good linearity and repeatability, as one can see from Figure 8.1.7.

Task:8.2 The Magneto-strictive Tuner

The prototype of a magneto-strictive tuner is ready for tests with a cavity. The control system aswell as the driver is already prepared. Due to the movement of the CRYHOLAB test stand the specific experiment with magneto-strictive tuner has been postponed. According to the recently updated schedule, the test will be performed in middle of 2007. Moreover, the huge progress which was made with piezoelectric stack indicates that this alternative solution will not be used for the XFEL.

The control algorithm was developed for both piezostack and magnetostrictive operation. The test with piezostack mounted in the VUV-FEL shows that the Lorentz force was compensated in at least 4 steps by 90% for a gradient of 20MV/m. Further developments are focused on implementation of the algorithms employed in the FPGA based board used for LLRF control. Currently, the online Lorentz force detuning algorithm has been successfully implemented and tested in a module test stand with ACC6. Further research will be focused on microphonics compensation.

A new amplifier for piezo element control has been developed. It is based on the single APEX PB58 power amplifier. It is suitable for resonant compensation, since it can supply current up to 300 mA and voltage up to 50 V. As it uses only one chip, instead of two as previously, it is a cheaper solution. The amplifier successfully passed a preliminary test with a dummy load. At the present time tests in a real system are being performed. The results will be presented in January 2007.

Task 8.3: The CEA Tuner

The fabrication of the new CEA tuner is finished. The tuner was mounted in CRYHOLAB and then tested. The detailed report of this study is covered by the report of WP 10.

Task: 8.4 IN2P3 activities

The IPN-Orsay has prepared two piezoelectric actuators PICMA#6 and PICMA#7 (see Figure 8.4.1) for their integration (sub-task #8.4.5) in the new Piezo-Tuning System (PTS) developed at Saclay. As it is a critical part of the PTS, the fixture of the actuators was carefully designed in order to avoid shear forces and/or torsion forces to the actuator and fit very precisely (e.g. ~10 µm) into the PTS in order to avoid loss of mechanical contact during cool down to 2 K. To fulfil these requirements, a cone-on-sphere system is used. In the actual PTS, the cavity, acting as a spring, is used for preloading the piezostacks.

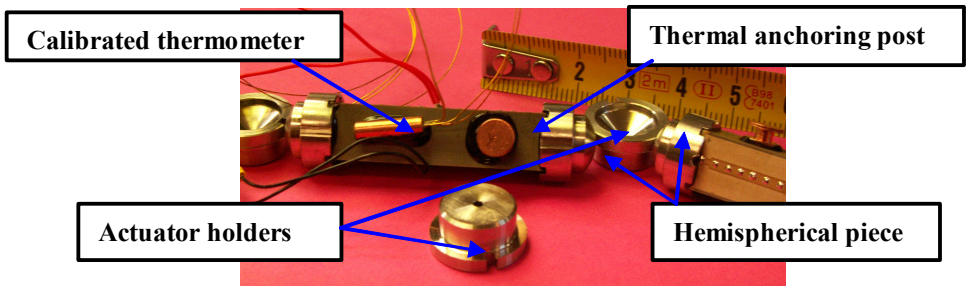

Figure 8.4.1 : Piezoelectric actuators ready for integration into Saclay PTS.

The critical dimensions were measured with high precision in industry (micrometer and 3-D machine). In particular, the following overall lengths (see figure 8.4.2) (actuator with their holders) were measured: L_6=51 mm $_{-0}^{+5\mu m}$ and L_7=51 mm $_{-0}^{+7\mu m}$ for the piezostacks PICMA#6 and PICMA#7 respectively.

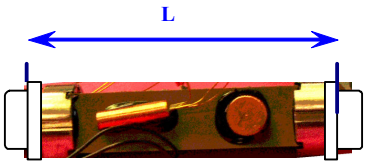

Figure 8.4.2: Definition of the overall length L

Moreover, each actuator is equipped with an Allen-Bradley thermometer which was calibrated (see Figure 8.4.3) on an IPN-Orsay facility in the temperature range 1.56 K - 71 K.

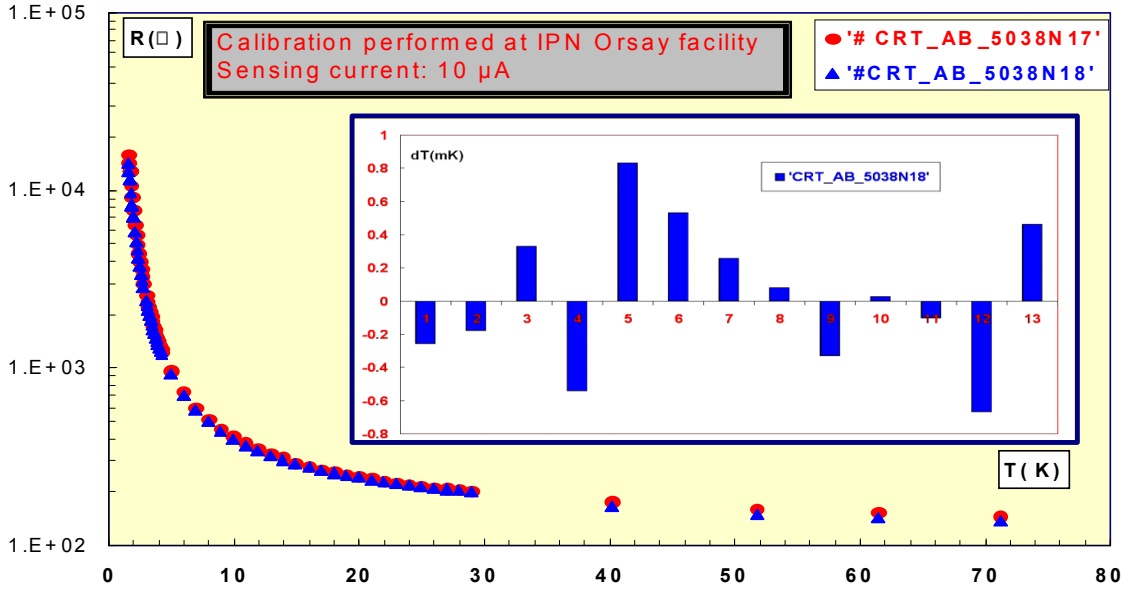

Figure 8.4.3: Calibration curves and fit error histogram (insert) in super-fluid helium region (1.56 K-2.1 K).

The actuators were integrated into the PTS and then the assembly was mounted on the cavity C45 and installed in CRYHOLAB test facility (see Figure 8.4.4).

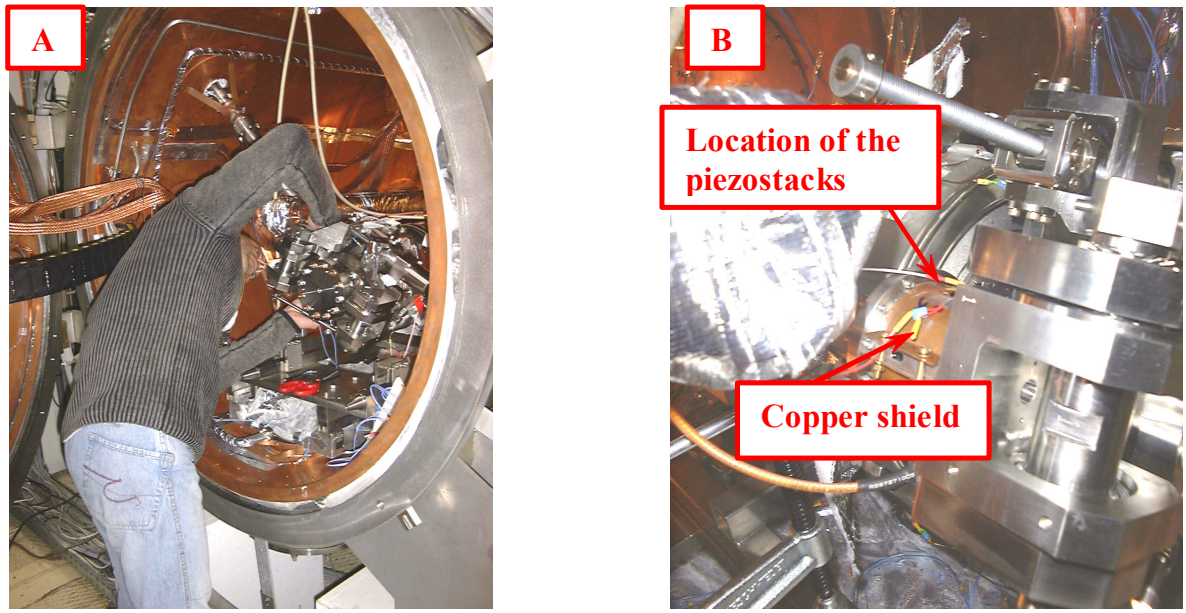

Figure 8.4.4: (A) Mounting the PTS in CRYHOLAB, (B) close up view of the fixture of the actuators.

In order to investigate (subtasks #8.4.6 and #8.4.7) the electro-acoustic behavior of the TESLA cavity #C45 and to measure the performance of the PTS developed at Saclay with PICMA actuators, the following tests in CRYHOLAB were performed during three weeks (10-27 April 2006):

1) Measurements of the transfer functions.
2) Study of the mechanical modes of the cavity including quality factors.
3) Measurements of the actuators response to the applied preloading force.
4) Study of Lorentz detuning and detuning compensation with PTS (Pulsed RF tests).

The experimental data were reported at LINAC2006. The pulsed RF tests were started: the status of this activity is summarized in WP#10 quarter report QR's 1 & 2/2006 (Cryostat integration tests). Finally, the sensitivity of PICMA piezo stacks to a preloading axial force at cryogenic temperature were investigated and the corresponding results were reported and discussed in detail (CARE Note and EPAC06). The variations of the relative capacitance $\Delta Cp = Cp\text{-}Cp_0$ (Cp_0: capacitance at zero preload (F = 0)) as function of the preloading force F at T = 2 K are shown in Figure 8.4.5. Non-linear effects are observed at low pre-loading force when F is increased from zero: they are due to friction, stick-slip among non linear phenomena in the pre-loading device mechanism (rotating arm, bellows, etc). Further, these data clearly show a large hysteresis for an increase and decrease of the pre-loading force. This behaviour could be attributed to the intrinsic irreversibility in the piezoelectric material itself.

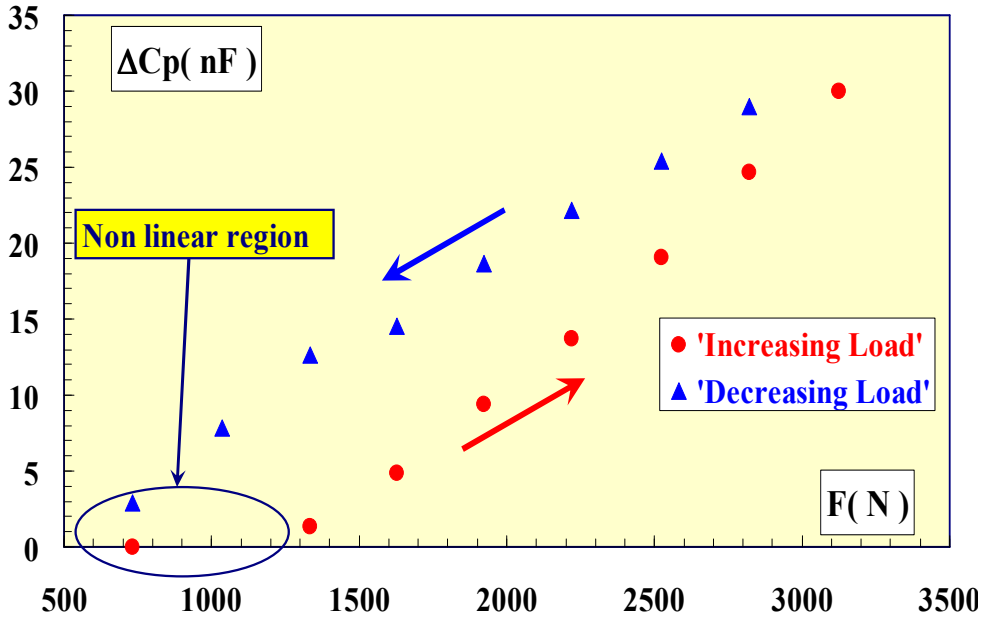

Figure 8.4.5. Capacitance versus preload at T = 2.05 K

At T = 2 K, the measured sensitivities to preloading for the force increasing and decreasing are 16 nF/kN and 10 nF/kN respectively. The behavior of the piezostacks as a dynamic force sensor was also studied. The transient response of a PICMA type actuator to a steep preload variation ΔF at T = 2K is presented in figure 8.4.6:

1) a steep voltage increase (capacitor charging) followed by an exponential decrease (capacitor discharging) is observed,
2) the peak actuator voltage ΔV_p ($\Delta V_p \propto \Delta F$) is reproducible to within 3 %.

The actuator is a very sensitive dynamic force sensor with a strong temperature dependence: $\Delta V_p/\Delta F$ = 4.7 V/kN at T = 2 K and $\Delta V_p/\Delta F$ = 21.4 V/kN at T = 4.2K.

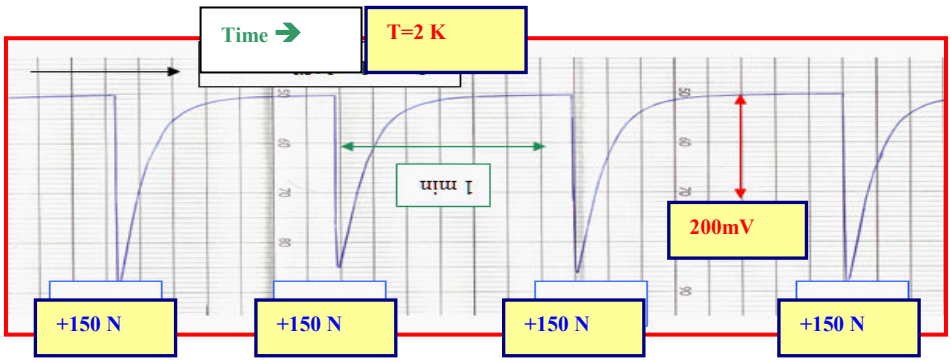

Figure 8.4.6: Transient response of a PICMA type actuator to a steep preload variation □F=150 N at T= 2 K.

Work Package 9 Low Level RF

Task 9.1 Operability and technical performance

9.1.1 Transient detector

Progress: In line with schedule.

During the reporting period the activities were focused on improving the transient detection system. It was equipped with fine-tuning circuitry for an RF feed-forward comb filter (Fig. 9.1.1) and it uses an IQ modulator for precise filter adjustment. The system was moved from building 28F to the injection area in Hall 3 in order to reduce the cable lengths. It was also connected to all cavities in module ACC1 (Fig. 9.1.2). All these upgrades enable the measurements and tests with any cavity in module ACC1.

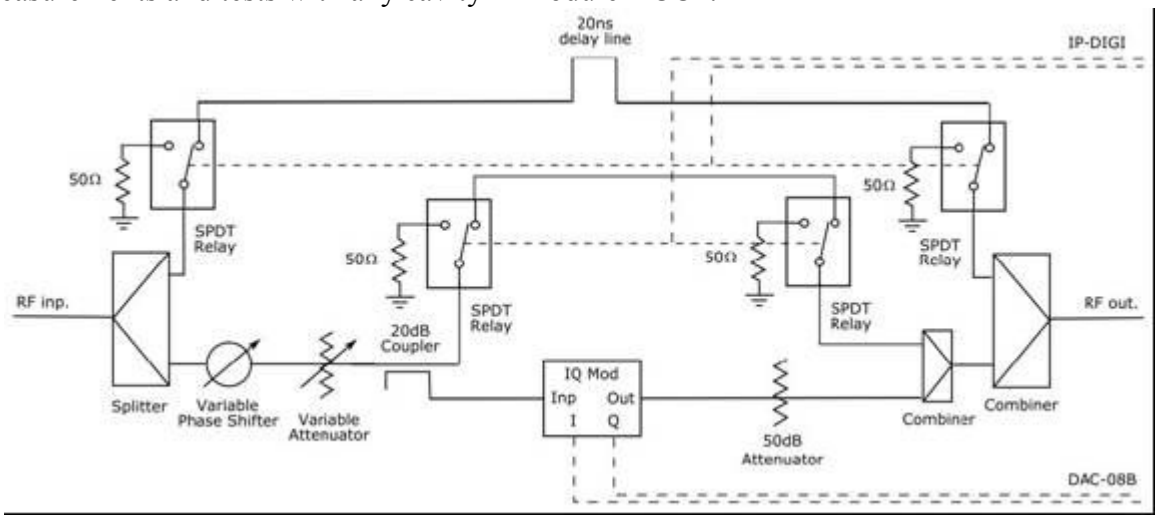

Figure 9.1.1 Schematic diagram of the RF feed-forward comb filter with fine-tuning circuitry

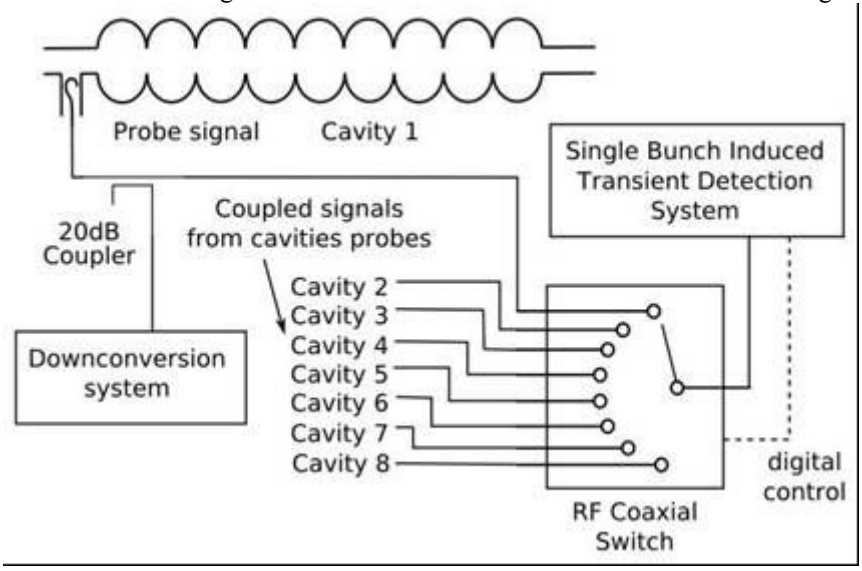

Figure 9.1.2 Transient detector connection in ACC1

Milestones and deliverables: None defined in contract for this period.
Significant achievements and impact: Filter for transient detection was improved with fine-tuning circuitry. This circuitry allows filter adjustment to keep required attenuation transparent to normal operation.

Deviations from schedule: None

9.1.2 LLRF Automation
Progress: In line with schedule.

During the reporting period a new solution was developed to facilitate automation of the RF-power station. The main effort was focused on elaboration of a general conceptual architecture and its preliminary implementation. Major changes concern relinquishing of the Harels FSM computation model and expansion of the environment driven aspect of the project. The implementation of the FSM is currently done using Prolog language. A general conceptual scheme of the solution is presented in Fig. 9.1.3.

The other task in progress was the identification of the high power chain (klystron and its pre-amplifiers) non-linearities and development of a method for their compensation. The developed method distorts the klystron input signal in a way that compensates the klystron non-linearities. The measurements of the high power chain characteristics with application of a pre-distorter method shows good compensation levels both for phase and amplitude characteristics (Fig.9.1.4).

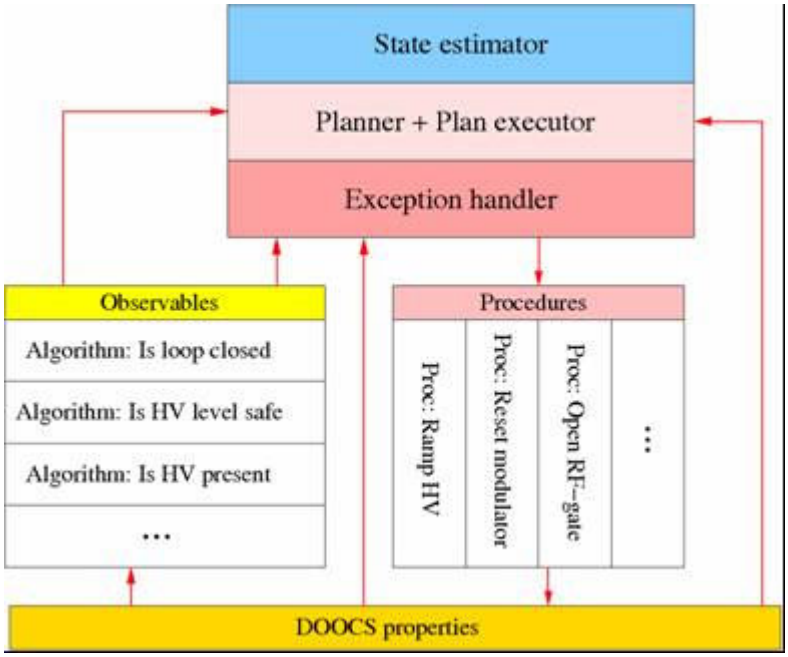

Figure 9.1.3 General conceptual scheme of automation module

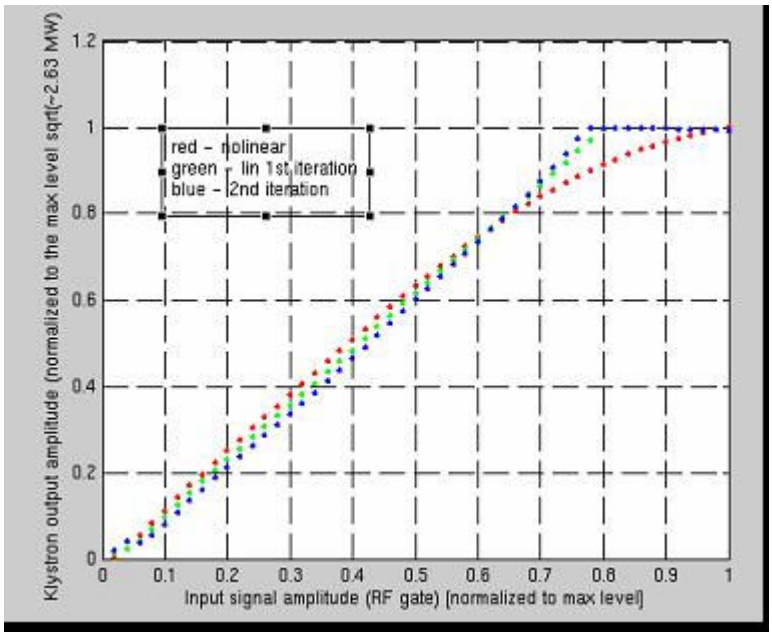

Figure 9.1.4. Results of measurements of klystron amplitude characteristics (application of self-adapting predistorter method)

Milestones and deliverables: Final report on "Automation".
Significant achievements and impact: The development of the FSM for the RF power station and its implementation in Prolog language. The implementation of the pre-distorter method of klystron linearization in FPGA (SIMCON3.1).

Deviations from plan:None

Task 9.2 LLRF cost and reliability

9.2.1 Cost and reliability study

During the reporting period several possibilities for cost reduction were investigated.

- Automation procedures using knowledge database (rule-based) to reduce cost of operation.
- Application of standard crates (ATCA or μTCA).
- Cabling from the rear side of the crate.
- Reduction in the number of signals.
- In-house development of boards.

Milestones and deliverables: None defined in contract for this period.
Significant achievements and impact: Investigations of overall cost reduction and reliability of the system.

Deviations from plan: None
9.2.2 Radiation damage study

During the reporting period the on-line radiation-level monitoring system (RADMON) was installed and operated in the FLASH tunnel. It was integrated with the existing DOOCS

control system and now the results of radiation level measurements are accessible remotely (Fig.9.2.1). Also several techniques for designing SEU-tolerate circuits were worked out and implemented (e.g. SEU tolerant IQ detection algorithm – Fig. 9.2.2).

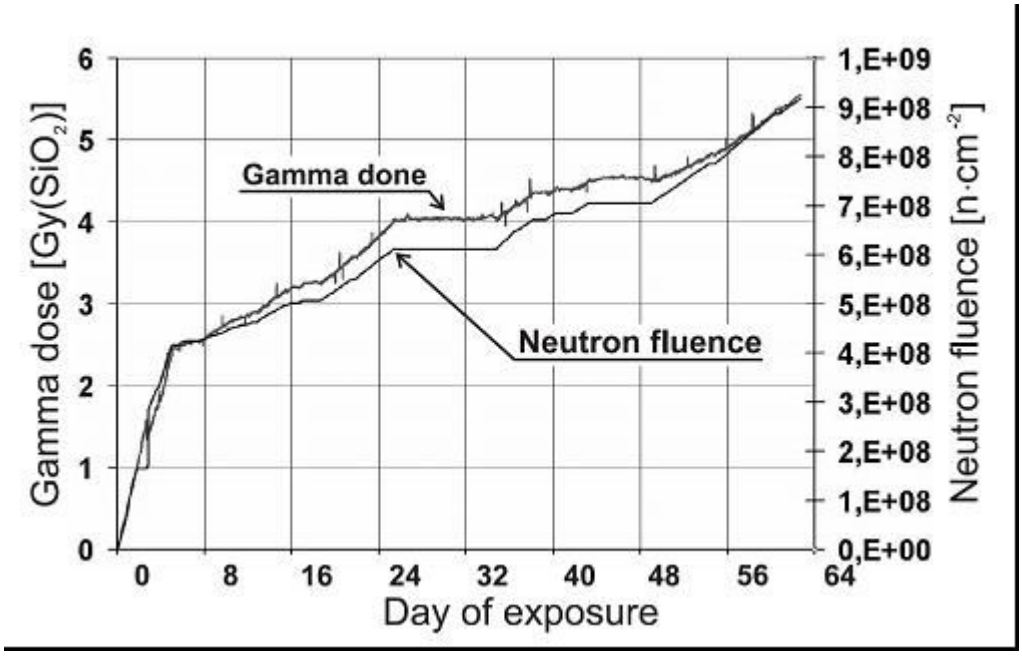

Figure 9.2.1. The accumulated dose of gamma radiation and neutron fluence registered on FLASH.

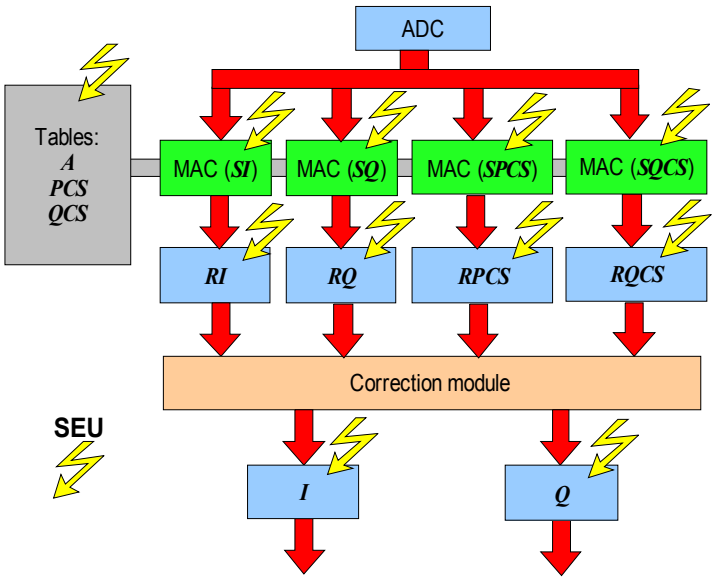

Figure 9.2.2. Block diagram of the SEU-tolerant IQ detection algorithm

Milestones and deliverables: None defined in contract for this period

Significant achievements and impact: Development of a new version of SRAM based radiation on-line monitor RADMON. Development of design techniques for radiation tolerant systems.

Deviations from schedule: None

Task 9.3 Hardware

9.3.1 Multichannel downconverter

During the reporting period new down-converter boards were designed and manufactured. The digital motherboard (Fig. 9.3.1) carries mezzanine boards with down-converters and integrated 16-bit resolution fast ADCs. The whole board is a digital down-converter that can perform IQ detection algorithms and provide digital output data.

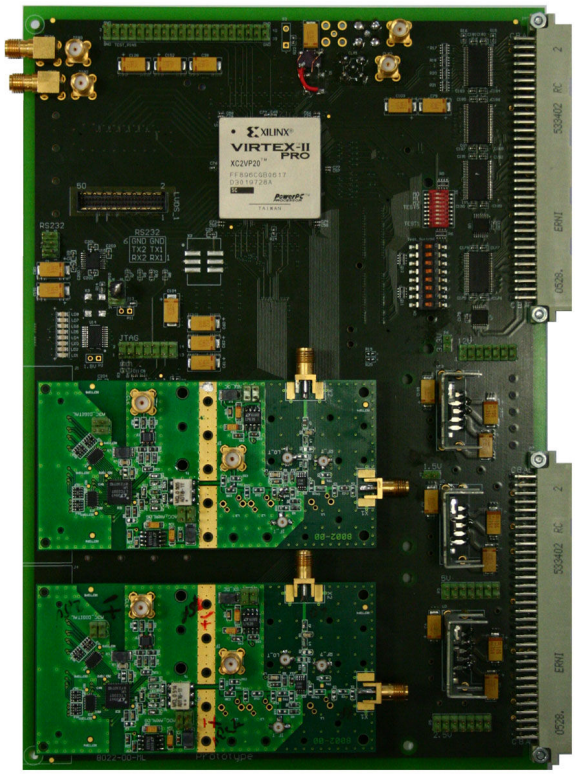

Figure 9.3.1. Digital motherboard with down-converters boards integrated with ADC

Milestones and deliverables: None defined in contract for this period
Significant achievements and impact: Development of new down-converter boards.
Deviations from plan: None

9.3.2 Third generation RF control

During the reporting period two new boards were designed and manufactured. The SIMCON 3.1 DSP board (Fig. 9.3.2.a) is the upgrade of the SIMCON 3.1 board with a DSP chip for real-time floating point operations and 4 additional DACs (8 in total on the board). The second board (Fig. 9.3.2.b) is the concentrator board with 8 fast optical links, Virtex II pro and Flash memory slot. The board can exchange data between other SIMCON boards through optical links and VME (it can be VME master) and is meant to be used as a part of distributed, multi-channel, cavity control system.

a) b)

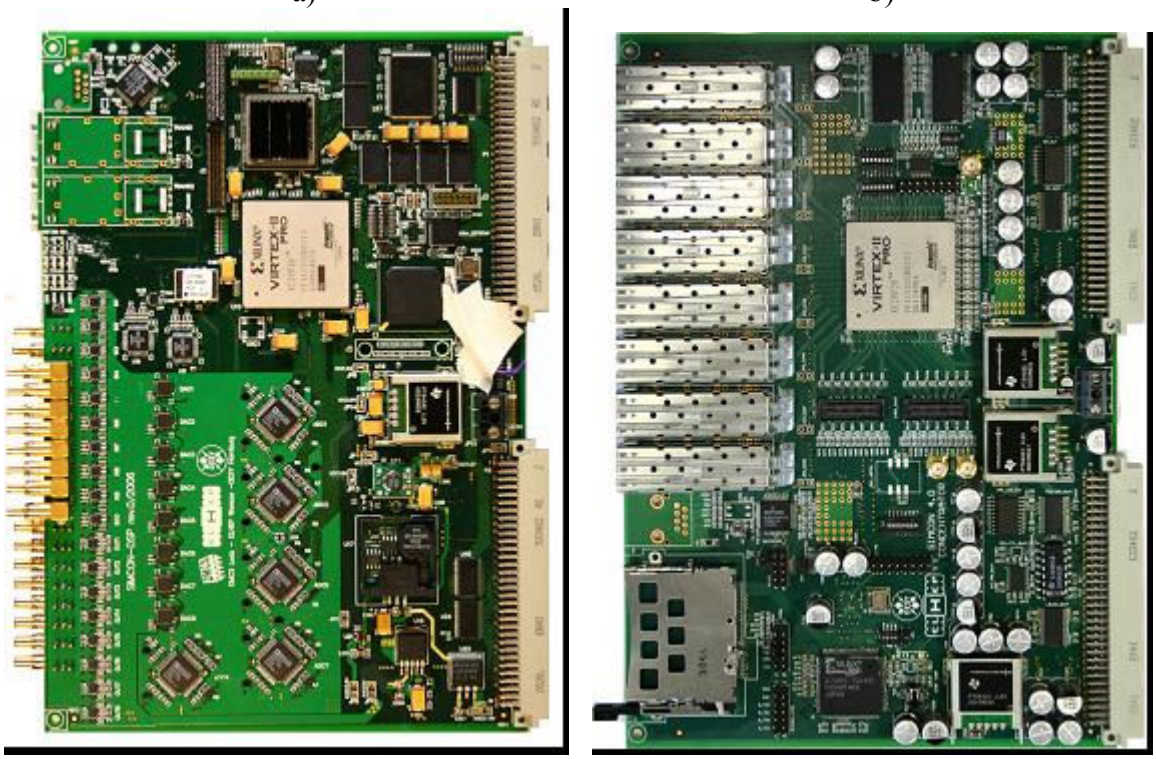

Figure 9.3.2. New control boards (a) SIMCON DSP board, (b) Concentrator board

Milestones and deliverables: None defined in contract for this period
Significant achievements and impact: Development of new controller boards.
Deviations from plan: None

9.3.3 Stable frequency distribution

During the reporting period a new frequency distribution system was designed and partially assembled and tested. The stability requirements of the Master Oscillator were 100 fs and 1 ps for times shorter than 100 ms and longer 1000 s respectively. The frequency distribution system (Fig. 9.3.3) consists of a MO supplying several reference frequencies and power amplifiers for signal distribution. The low-level part of the system is already finished and the stability requirements are fulfilled (Fig.9.3.4). The implementation of the power part of the system is in progress.

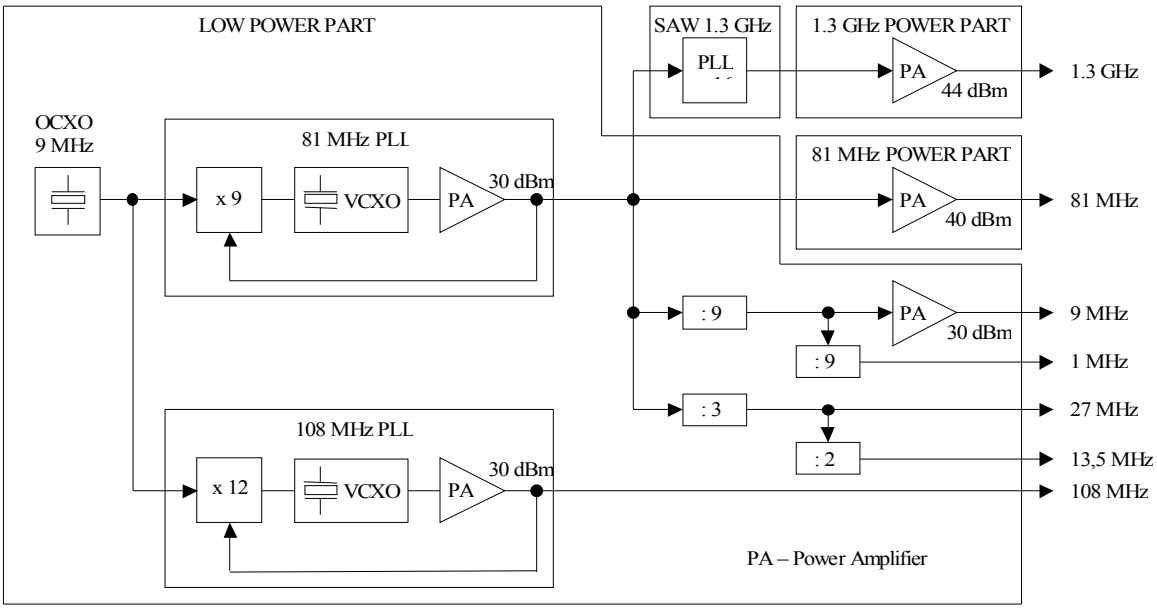

Figure 9.3.3. The block diagram of frequency distribution system

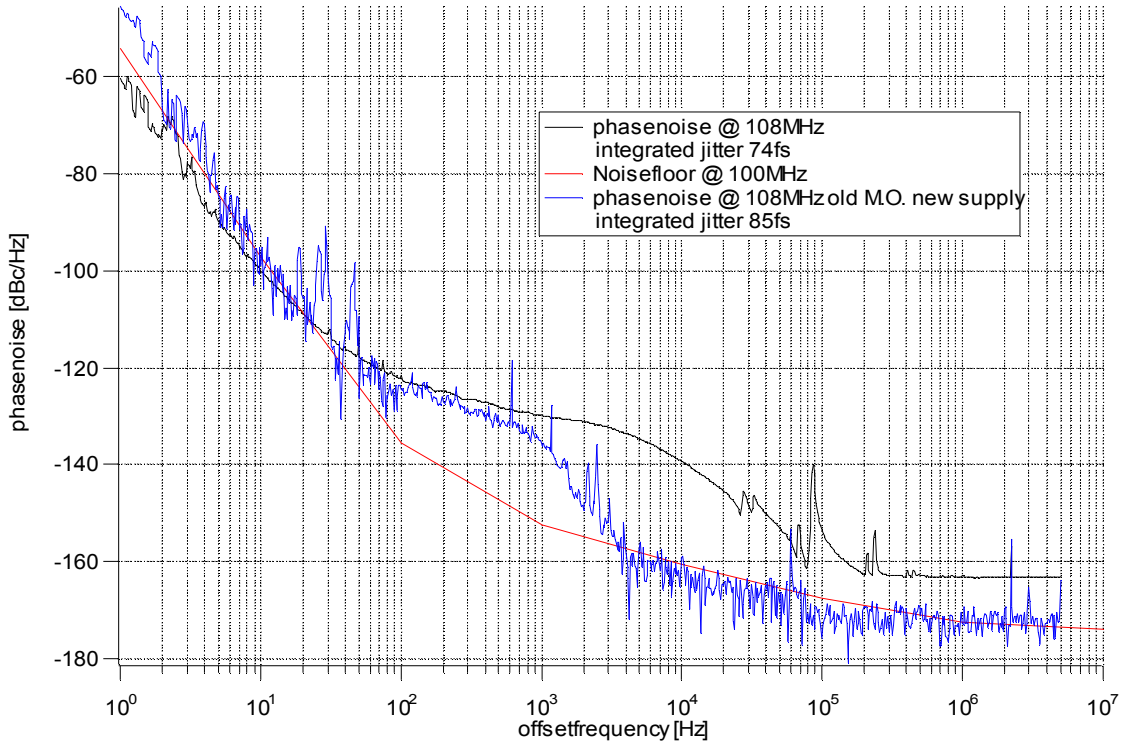

Figure 9.3.4. Stability of 81MHz frequency output of the MO.

Milestones and deliverables: Final report on "New LLRF hardware components"
Significant achievements and impact: Development of a new frequency distribution system.
Deviations from schedule: None

Task 9.4 Software

9.4.1 Data management development

Progress: In line with schedule.
Task completed in 2005 and final report published. The database is currently under tests in DESY – Hamburg.

Milestones and deliverables: None defined in contract for this period
Significant achievements and impact: Database and supporting programs installed and exercised.
Deviations from schedule: None

9.4.2 RF Gun control

During the reporting period the new FPGA based RF gun controller was developed together with control algorithms. The field of the RF gun at FLASH is well stabilized for SASE operation. For RF pulse lengths of the order of 100 μs PI control alone is sufficient. Longer RF pulses and bunch trains require AFF control in addition.

Milestones and deliverables: Final report on "RF Gun Control"
Significant achievements and impact: Development of FPGA based control system for rf gun.
Deviations from schedule: None.

Work Package 10: Cryostat Integration Tests.

Status of activities

At the beginning of 2006 we dedicated our efforts to injecting RF power into a fully equipped 9-cell cavity (C-45 from DESY) installed in the horizontal cryostat CRYHOLAB.

An electronic device has been developed to generate a 200 μs pre-pulse necessary to shorten the cavity filling time and to achieve an RF flat top for 800 μs (Fig. 10.1).

a) 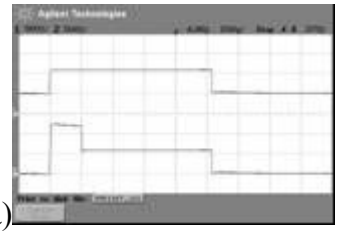 b) 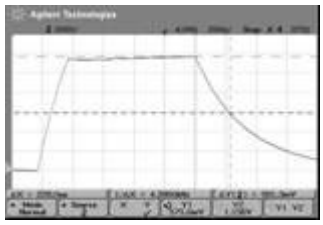

Figure10.1. (a) injected RF power with pre-pulse (total length time: 1 ms),
(b) Flat top (800 μs) on transmitted RF power

After coupler conditioning, the pulsed RF power (P=70 kW to 130 kW, 800 μs, 0.87 Hz) with pre-pulse (4P, 200 μs) was injected into the 9-cell cavity cooled down to 1.7 K. We obtained the Q_0 (E_{acc}) curve using transmitted power (P_t) and cryogenic measurements to determine cavity losses (P_{cav}). The maximum accelerator field (~ 25 MV/m) is limited by field emission with X-rays detected (figure 10.2).

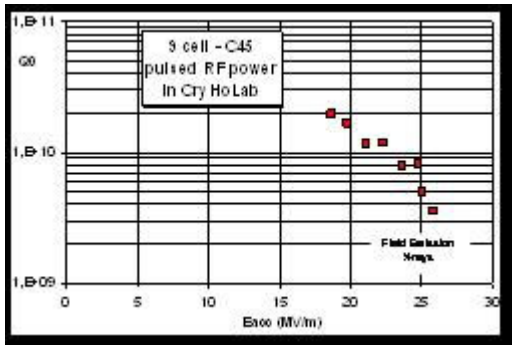

Figure10.2. Quality Factor Q_0 versus Accelerating Field E_{acc} for C45 cavity

Under such conditions, compensation of Lorentz Force detuning has been achieved (Fig. 10.3) using NOLIAC and PICMA piezo-electric devices, characterized by IPN Orsay and assembled on the Cold Tuning System CTS (figure 10.4) developed by CEA Saclay in WP8.

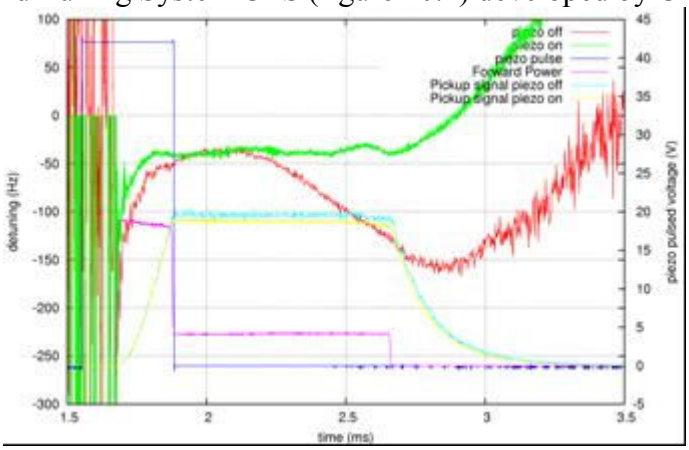

Figure10.3. Lorentz Force Detuning for E_{acc}= 20 MV/m (red curve). Compensation using piezoelectric Cold Tuning System CTS (green curve).

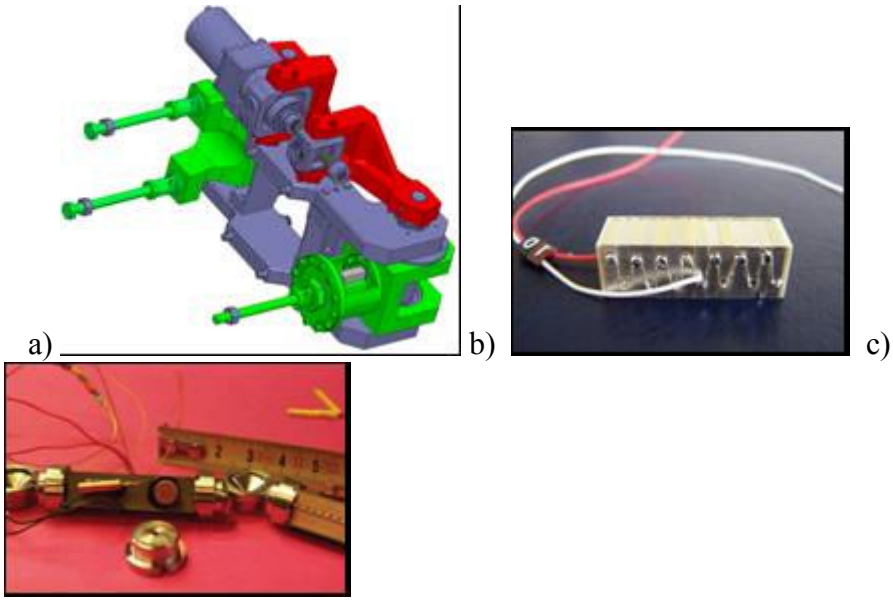

Figure10.4. Cold Tuning System (CTS) equipped with (a) Noliac or (b) PICMA (c) piezo-electric.

A third series of tests is planned using a magneto-strictive tuner. A mechanical adaptation to install it on CTS is under manufacture (Fig. 10.5).

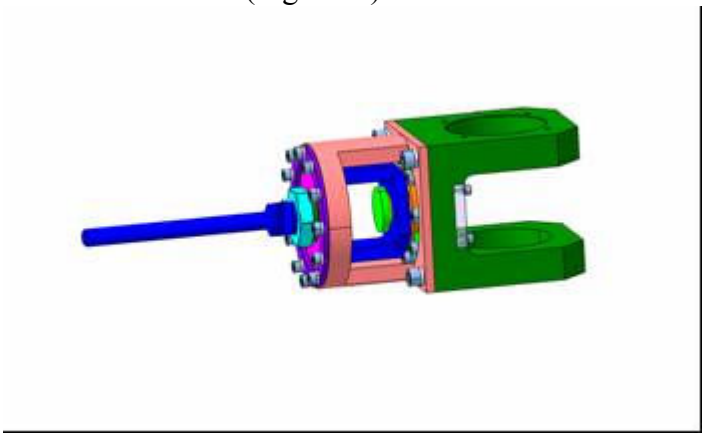

Fig.10.5 CTS Adaptation for Magnetostrictive fast tuner.

Experiments in CryHoLab were stopped at the end of May 2006 due to the transfer of RF Infrastructure transfer from "l'Orme des Merisiers" area to the main Saclay site. They will restart in the beginning of 2007. Re-assembly of the test facility is in progress (Fig. 10.6) with probably one month delay compared to the initial schedule.

Some modifications are being made to improve:

- the diagnostic tool with new high accuracy flow-meters,
- the stability of the Helium bath pressure at 1.7 K using a new regulation valve.

Figure 10.6. Re-installation of the helium compressor and vacuum pumping system (left) and the CryHoLab area (right).

Work Package 11: Beam Diagnostics

Task 11.1: Beam position monitors

Status of activity

1. Development of the re-entrant RF BPM

The activity of this year was dedicated to the simulations, the installation, the calibration and the first beam tests of a new re-entrant beam position monitor (BPM) located in the FLASH tunnel at DESY at room temperature. Moreover, some beam tests were carried out on the re-entrant BPM installed in cryo-module ACC1.

I-1 Beam tests on the BPM installed in cryo-module ACC1

In March 2006, an additional calibration operation was carried out on the BPM installed in ACC1. TTF2 was operated in single bunch mode for these measurements which produced statistics and correlations. Two methods were used to calibrate this BPM, called 9ACC1.

The first method uses steerers to move the beam. The setting and the relative beam position are calculated by using a transfer matrix between the steerers and the BPM (composed of drift spaces and accelerating cavities): $\Delta x = R12*\Delta x'$ where $\Delta x'$ is the angle at the steerer. The HOMs (Higher Order Modes) of cavity 8 installed in the cryomodule ACC1, were minimized by using steerers to move the beam. This minimization permitted adjustment of the BPM center with respect to the beam. The beam tilt was neglected due to the proximity of BPM 9ACC1and cavity 8. An offset was added in the software to have a slope around 1 and to demonstrate the system linearity.

The second method uses 3 BPMs. The relative beam position at the re-entrant BPM (9ACC1) is calculated by extrapolation from the other two BPM readings.

With the first calibration method (transfer matrix), 9ACC1 shows a linear range around 3-4 mm before saturation. We suppose that this saturation comes from the amplifier or ADC saturation.

The second method gives some results which are not very linear in a range of 3-4 mm. The problem may come from long distance between the first and second BPM. In Fig.11.1.1, the plots of the predicted position calculated with the first method vs the position read by 9ACC1, on X and Y channels are presented:

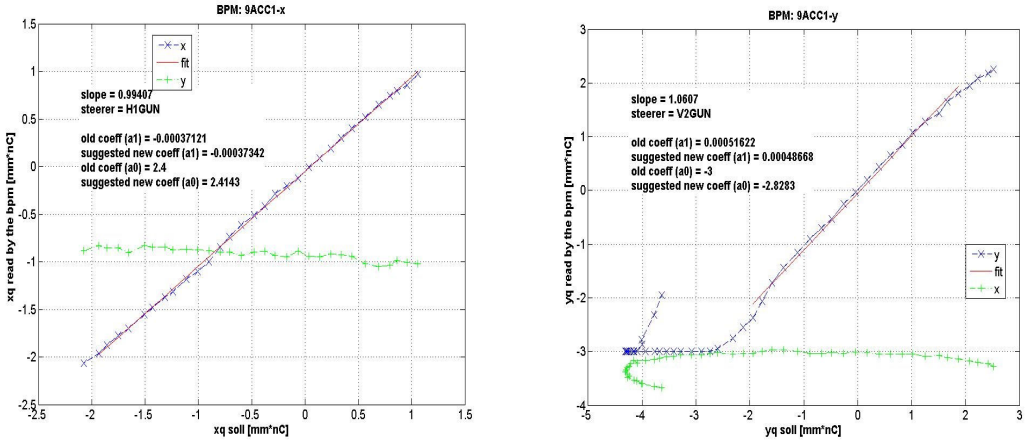

Figure 11.1.1: Position read by 9ACC1 vs. the predicted position.

The raw RMS resolution of the system, measured directly from 9ACC1, is around 50µm on the X channel. By using the correlation between different BPMs, the beam jitter can be cancelled and the real resolution can be estimated to be around 20µm. On the Y channel, the resolution is around 30µm without the beam jitter and around 70µm as a raw measurement.

I-2 Estimation of the prototype absolute resolution.

The resolution is limited by the signal to noise ratio of the system. The signal voltage of the BPM is determined by the beam's energy loss to the "TM110" mode and by the external coupling of the coaxial cable.

The noise comes from the thermal noise from the components used in the signal processing. The thermal noise of a system is given by the following equation

$$P_{th} = k_b * T * BW \qquad (1)$$

where k_b is Boltzmann's constant ($1.38*10^{-23}$J/K), BW is defined by the bandwidth of the band pass filter in Hertz, and T is the room temperature in Kelvin.

The noise level present at the output of the cavity BPMs, is amplified by the signal processing devices. To calculate the noise level, the thermal noise is added to the noise factor and to the gain. The noise level is therefore given by the following equation:

$$P_n = NF * G * P_{th}. \qquad (2)$$

where NF is the total noise figure of the circuit, G is the gain of the signal processing and P_{th} is the thermal noise.

The total noise introduced into the system by the electronics can be evaluated by the noise figure in the cascaded system and is applied using the following formula:

$$NF = F_1 + \frac{F_2 - 1}{G_1} + \frac{F_3 - 1}{G_1 * G_2} + \ldots \qquad (3)$$

where NF is the total noise factor of the signal processing, F_i and G_i are respectively the noise factor and the gain of component i.

To assess the performance of system, a model (cavity+signal processing) was elaborated with Mathcad. The re-entrant cavity model is a resonant RLC circuit. The impulse response of the monopole and dipole modes depends on frequencies and external coupling. The transfer functions of different elements (cables, hybrid couplers, filters, amplifier mixer) which compose the signal processing, are determined by the S parameters measured with a network analyzer. Then those transfer functions are used and combined to simulate the BPM system (RF cavity + signal processing). The transfer function of cables takes the effects of attenuation and dispersion into account.

The results of these simulations show a resolution better that 1 µm for the new re-entrant BPM with a beam offset of +/- 100µm.

I-3 Time Resolution

The damping time can be calculated by using the following formula:

$$\tau_{110} = \frac{1}{\pi * BW}. \qquad (4)$$

where BW is the bandwidth in Hertz .

For bunch to bunch measurements, the time resolution has to be smaller than the interval between bunches of the machine.

Taking an RF cavity, the bandwidth is defined by the relation:

$$BW = \frac{f_{110}}{Q_{l110}}. \qquad (5)$$

where f_{110} is the frequency of the dipole mode and Q_{l110} is the loaded quality factor for the dipole mode. The time resolution is therefore around 9.5 ns for the new re-entrant BPM. It is lower than the separation between bunches on TTF2. The bunch to bunch measurement is therefore possible.

In reality, the rise time of a signal is 3τ. For bunch to bunch measurements, the time resolution has to be smaller than the distance between bunches ΔT. The system has to verify the following equation:

$$6\tau \le \Delta T \qquad (6)$$

To evaluate the time resolution of the BPM system (cavity + electronics), the Mathcad model is used and gives the simulated output signal after synchronous detection. The time resolution is therefore defined by the time interval at 5% of the peak voltage from the baseline.

The time resolution for the new re-entrant BPM was simulated around 40 ns. It confirms the possibility to carry out measurements in multi-bunch mode. Indeed, on TTF2, the time between bunches is 110 ns.

I-4 New monitor installed in beam line and operational

At the beginning of this year, we received the cavity BPM with the feedthroughs (Fig. 11.1.2) designed the last year.

Figure 11.1.2: Cavity BPM

In spring of 2006, during the maintenance time, the re-entrant BPM was installed on a warm part in the FLASH linac (Fig. 11.1.3) at DESY.

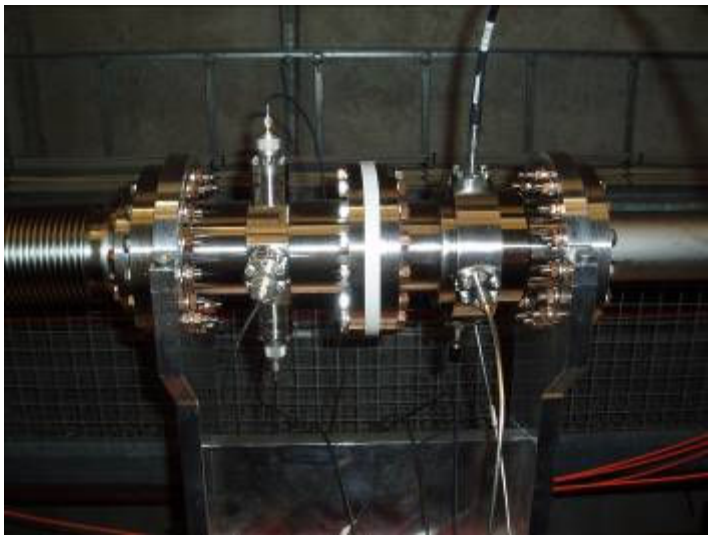

Figure 11.1.3a: Re-entrant cavity BPM (right) and button BPM (left) installed in the FLASH linac

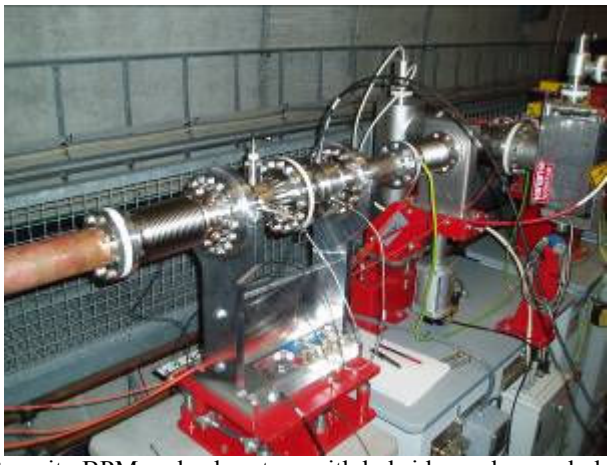

Figure 11.1.3b: Re-entrant cavity BPM and subsystem with hybrid couplers and phase shifters installed in the FLASH linac

After mounting, the first RF measurements were carried out to check that the feed-throughs were properly mounted on the cavity. The resonant cavity was first simulated with the software HFSS (Ansoft) to determine its modes and coupling and then it was measured in the laboratory and finally on the linac. The RF measurements, presented in Table 1, provide a comparison that gives information on the sensitivity of the RF characteristics to the mechanical mounting and operating environments.

TABLE 1. RF characteristics of the new re-entrant BPM.

Eigen modes	**F (MHz)**			**Q_l**		
	Calculated	Measured in lab.	Measured on the linac	Calculated	Measured in lab.	Measured on the linac
Monopole mode	1.250	1.254	1255	22.95	22.74	23.8
Dipole mode	1.719	1.725	1724	50.96	48.13	59

The difference in the Q factors can be explained by the boundary conditions which are not the same during the measurements in laboratory and in the tunnel.

The cross-talk was measured to be around 33 dB instead of 41 dB measured in laboratory. This difference could be explained by the fact that the BPM has a rotation/tilt (11.25 degrees) with respect to a button BPM which is very close.

I-5 Calibration of the electronics of the new re-entrant BPM

In summer of 2006, the two subsystems, composing the signal processing, were installed and calibrated:

- a subsystem composed with hybrid couplers, phase shifters and one combiner was installed in the tunnel during a maintenance day. The spectrum analysis of the "delta" signals from the 180° hybrid coupler output shows good common mode rejection. Tuning of the phase shifters gives a high common mode rejection (30 dB at 1.25 GHz).
- the second subsystem (Figure 11.1.4) was installed in the hall. The synchronous and direct detectors, as well as amplifiers and limiters for protection were adjusted to have a linearity range around +/- 10 mm.

Figure 11.1.4: BPM subsystem located in the hall

I-6 First beam tests of the new re-entrant BPM

After calibration of the electronics, the first beam tests of the re-entrant BPM were carried out. Our objective was to start the calibration of this BPM, for a high precision beam position measurement in single bunch mode.

As the re-entrant BPM is mounted with a tilt angle of 11.25° with respect to the horizontal direction, a frame rotation change, done by software, is necessary. Figure 11.1.5 shows the first results of this calibration with the frame rotation change.

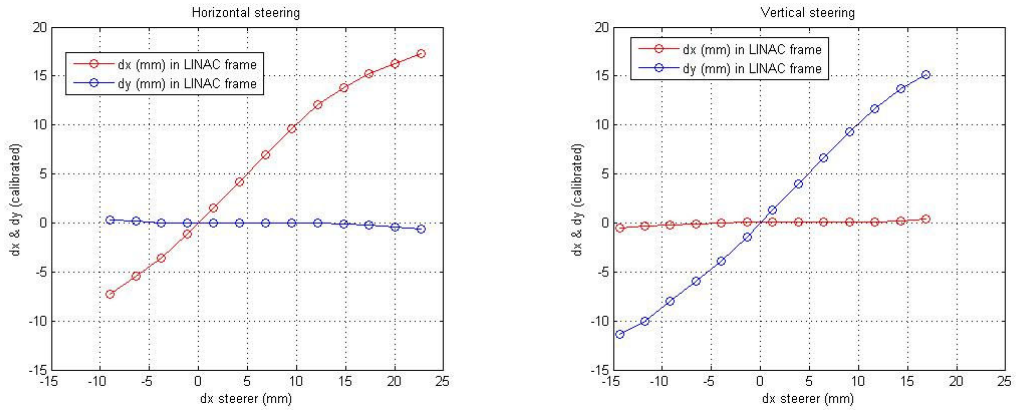

Figure 11.1.5: Calibration results in the LINAC frame from horizontal (left) and vertical (right) steering

The re-entrant BPM has, on the X and Y channels, a good linearity over a range of 15 mm but there is an asymmetry and the linearity is better for a positive deviation. This effect is not yet well understood; it may be related to the steering magnets (residual field or saturation).
The standard deviation of the calibrated position measurement was plotted for the horizontal and vertical steering (Fig. 11.1.6).

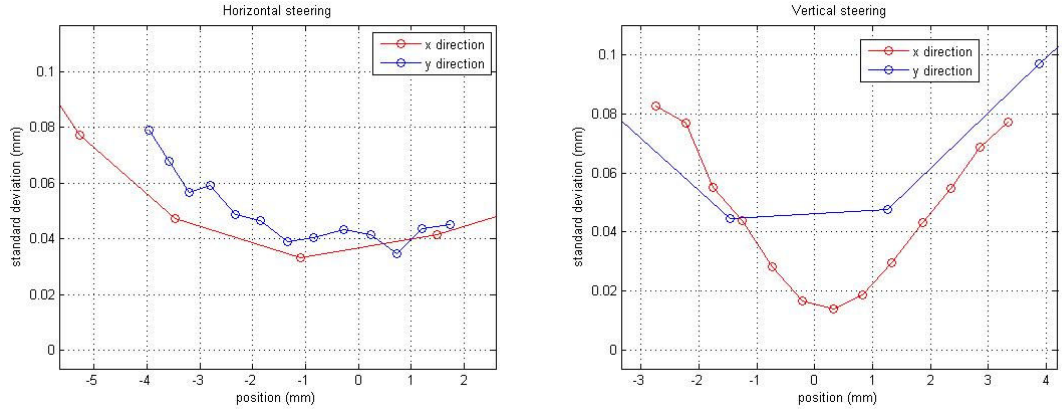

Figure 11.1.6: Standard deviation of the position measurement (calibrated)

The raw RMS resolution of the system directly measured by the standard deviation of the readings from the re-entrant BPM (14ACC7) can reach 20 µm on the X channel and around 40 µm on the Y channel, at the BPM centre. But those results also depend on the beam jitter. With simulations, the resolution of this system was determined to be around 15µm.

A second test period was necessary to validate the first results: the same steerers were used; the deviation range was limited to ±4 mm for a more accurate calibration (Figs. 11.1.7 and 11.1.8).

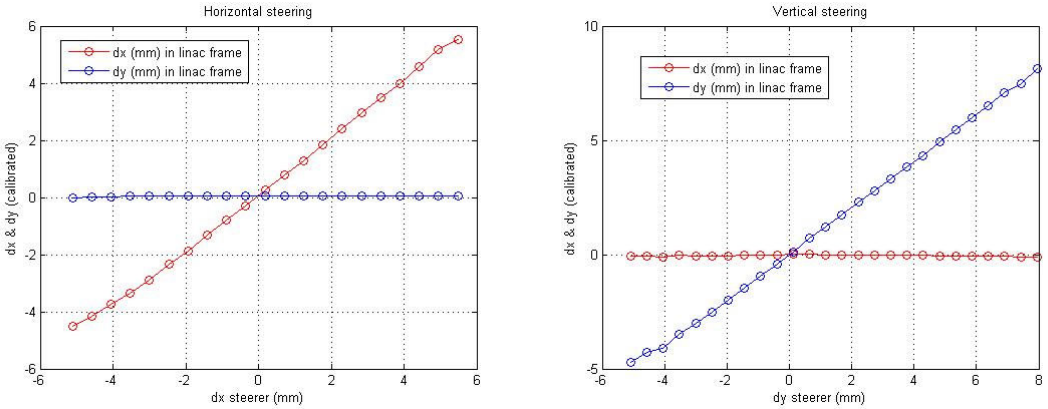

Figure 11.1.7: A more accurate calibration results in the LINAC frame from horizontal (left) and vertical (right) steering

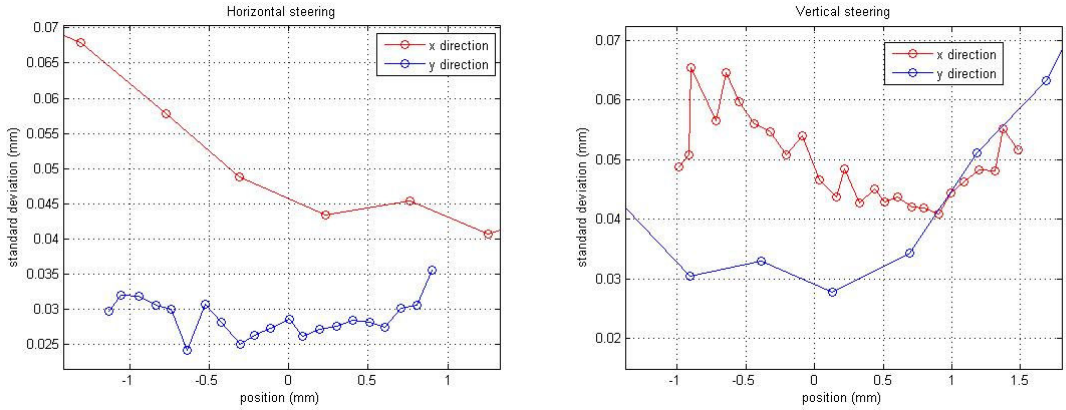

Figure 11.1.8: Standard deviation of the position measurement (calibrated)

This second measurement corroborates the first calibration. The linearity in this calibration range is very good for both channels. The minimum standard deviation of the

measurements at the BPM centre is around 40 μm for the X channel and around 30 μm for the Y channel.

Task 11.2 – Beam Size and Emittance Monitor

In the first period of 2006, two blocks of dedicated shifts were assigned to this experiment. We had the possibility to verify the complete system with the beam. The alignment of the optics has to be improved, but the setting was good enough for the first measurements.
The first shifts were used to optimize the beam transport through the by-pass line and to try to obtain the expected beam size at our screen location. The low energy, 450 MeV, and the larger beam size than expected prevented the observation of Diffraction Radiation, but the shifts were useful for the calibration of the optical system with the much more intense Optical Transition Radiation, showing the presence of a strong background due to synchrotron radiation from the last dipole at more than 50 meters distance, and of the quadrupoles, whose gradient was very high.
This background was not expected, and even if not completely understood, derives from multiple reflections on the pipe surface, showing a much larger angular distribution that what the distance of the magnetic elements would suggest.
In the second set of shifts the energy was higher, about 630 MeV, but still lower than expected. The beam size was still too large, probably due to an imperfectly optimized transport resulting in a higher emittance, so that we were forced to use the largest of the two slits (1 mm width) for which observation of DR was difficult, in particular because the beam was slightly larger than the slit itself. We believe we have found a way to subtract the background by steering the beam out of the screen with the last steerer.
These shifts have taught us that, for the future, hardware shielding of the synchrotron radiation background will be required, a much better transport of the beam will be needed in order to obtain the design beam size and that the ultimate energy of the machine must be reached.

Background Subtraction Procedure
The main limitations during the measurements were given by the background and the large number of hot spots which did not allow us to increase the CCD exposure time.
To separate the background from the beam, the beam needed to be moved out of the screen by using steering magnets upstream of the target. However, since the steered beam hits the beam pipe, this procedure further increases the amount of emitted X-rays. in this regard, an off-line LabView tool, which first eliminates X-rays by selecting a neighbourhood with a 3x3 matrix and then subtracts the background image, has been developed. In order to increase both signal and background intensity, the sum of N images, normalized to the number of images, is analysed.

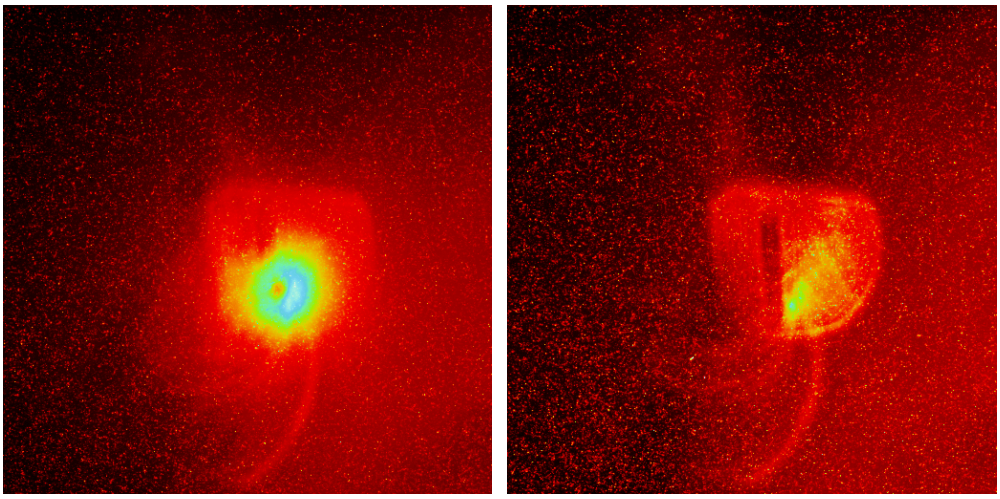

Figure 11.2.1: Signal plus background (left) and background image (right).

Figure 11.2.1 shows the OTR angular distribution and the background image on the focal plane. The beam was steered out of the target by an upstream vertical steerer, and the background image was then isolated and recorded to allow its subtraction. Both images are the result of the sum of 20 images taken with 10 bunches per macro-pulse, 0.3 nC per bunch and 2 s exposure time.
Figure 11.2.2 shows the OTR angular distribution after removing X-rays and subtracting the background. The result is a clean image whose profile is the one we expect.

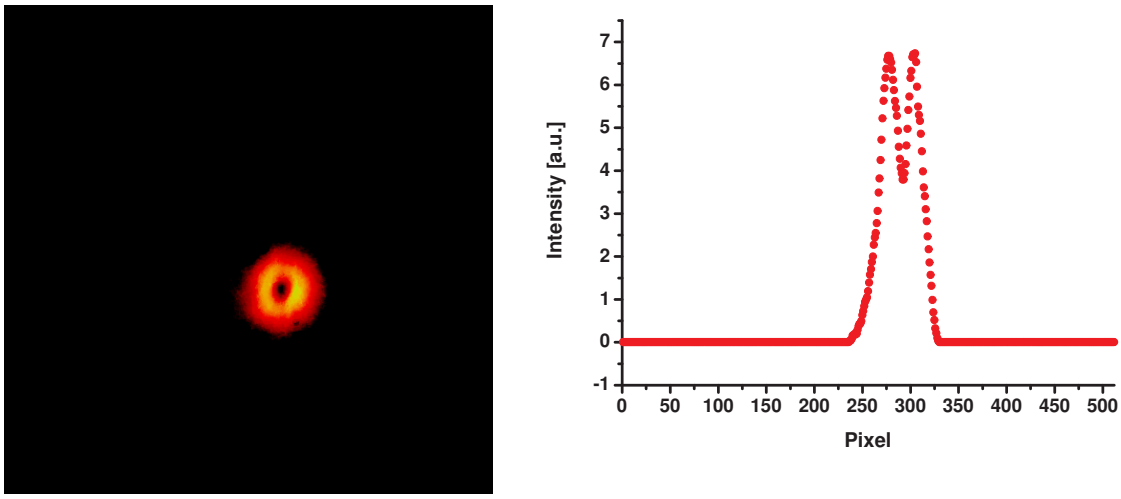

Figure 11.2.2: Subtracted OTR angular distribution (left) and its profile (right).

This tool becomes mandatory for the analysis of ODR signals which, being of the same order of magnitude and even weaker than the background, are covered by it.

From OTR to ODR.
The aim of these first measurements was to demonstrate that we are able to detect a difference between OTR and ODR angular distributions.
To do so we used a vertical steerer to change the position of the beam on the screen in order to smoothly go from OTR to ODR emission. To detect ODR as well as to distinguish OTR and ODR, a high quality electron beam, in terms of small transverse emittance, high beam energy and good stability, is required. Unfortunately, during the whole set of measurements, the transverse beam size was too large even for the 1 mm slit. To reduce the emittance, i.e. the beam size, the charge was reduced down to 0.3 nC per bunch, and to increase the signal

intensity the number of bunches per macro-pulse was increased to 25. The signal was integrated over 1 s. The nominal beam energy was 620 MeV.

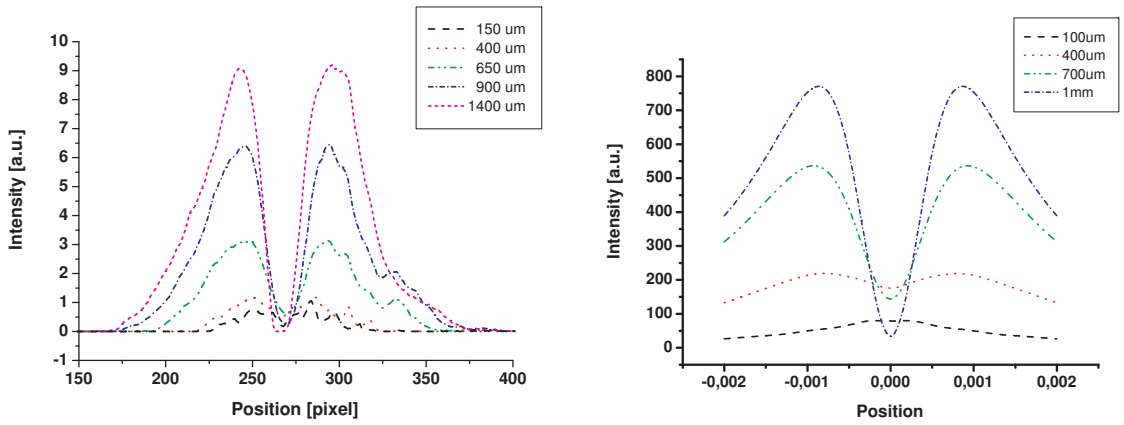

Figure 11.2.3: Angular distributions for different positions of the beam with respect to the center of the slit: experiment (left) and simulations (right).

The plot in Fig. 11.2.3 (left) shows the angular distribution profiles for five steps. The short dashed curve (magenta) corresponds to the beam at 1.4 mm from the centre of the slit, a condition which gives rise to OTR emission. As the distance decreases the OTR contribution gets lower. The dash curve (black) corresponds to the beam at 150 μm from the centre of the slit: ODR emission is now expected, showing a less pronounced minimum in the angular distribution. A simulation (Fig. 11.2.3, right) reproducing the insertion of the slit shows a qualitative agreement with the experimental data.

Signs of ODR.

Only during one of our measurement shifts have we succeeded to have the beam shown in Fig. 11.2.4 with a FWHM of 360 μm, but even in this case, when the beam goes through the slit, the tail hits the edges.

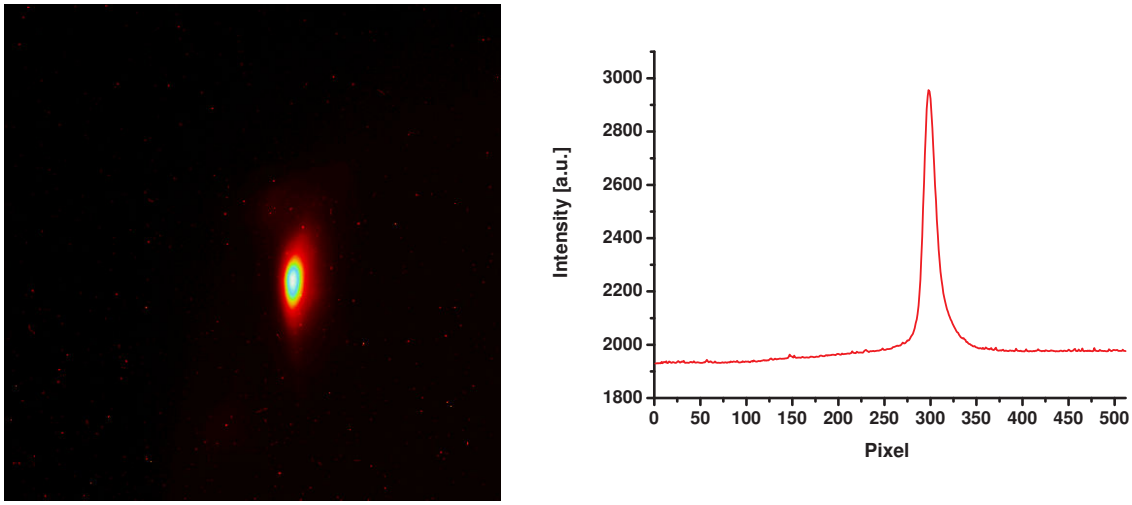

Figure 11.2.4: Image of the beam on the OTR screen (left) and its profile (right).

A measurement dedicated to the ODR detection has been performed with this beam transporting 10 bunches, 0.3 nC per bunch through the centre of the 1 mm slit. Several images of both signal and background have been acquired to allow an easier subtraction procedure. The subtracted ODR angular distribution image is shown in Fig. 11.2.4 (left), the corresponding profile is plotted in Fig.11.2.4 (right: red dots). A simulation which takes into account an rms beam size of 150 μm, compatible with the given beam, and a negligible angular divergence, shows a good qualitative agreement with the measured ODR profile (Fig. 11.2.5, right: straight line).

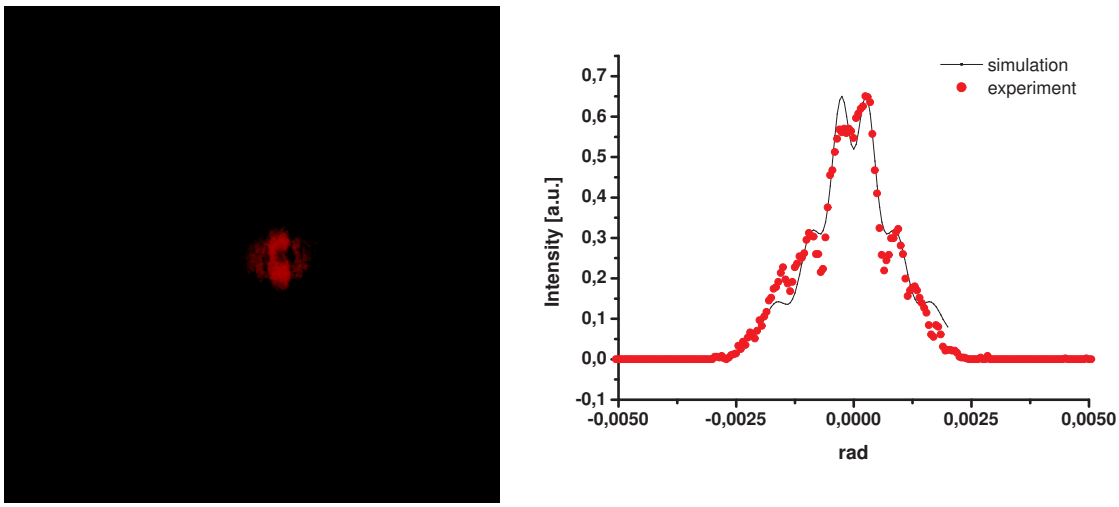

Figure 11.2.5: Subtracted ODR angular distribution (left) and its projection in comparison with a simulation (right).

Although these first preliminary measurements do not yet allow us to quantitatively retrieve beam parameters and showed that effort has still be put on improvement of the experimental set-up and background subtraction, they are encouraging and give us confidence to continue the measurements.

Hardware improvements and plans for the next future.

During a FLASH maintenance period in October 2006, a second target, a replica of the first one, was installed. The second target will be used during preliminary adjustment of the beam to avoid damage to the slit used for measurements. In order to reduce synchrotron light we have installed a diaphragm to cut the background in the OTR station before our experimental station. The whole system has been better aligned using a powerful lamp illuminating the back of a screen in a previous station and simulating a far away source. For the next set of measurements, planned in January 2007, we expect to reduce the contribution from X-rays with better shielding of the camera. In addition, an update of the analysis software is planned.

Task 11.3 - The HOM-BPM Program

The research activity on using the dipolar Higher Order Modes (HOM) of the accelerating superconducting cavities to monitor the beam position along the TTF2-FLASH linac continued with the two main objectives set in 2005:

- to prove the potential of the HOM-BPM instrumentation to monitor the beam orbit through the FLASH cryomodules in order to minimize the bunch emittance growth;

- to measure the cavity centres and relative misalignments within the five TTF cryomodules.

1.1 Emittance tuning

Wakefields are more harmful for the beam emittance in the low energy part of the linac. An emittance tuning experiment has therefore been conducted when the HOM acquisition electronics was operational in the first module ACC1 of the FLASH linac. A feedback algorithm has been implemented in the control system to steer the beam injection in the ACC1 module (Fig. 11.3.1) in such a way that the 16 HOM signals (8 cavities x 2 HOM couplers) are minimized.

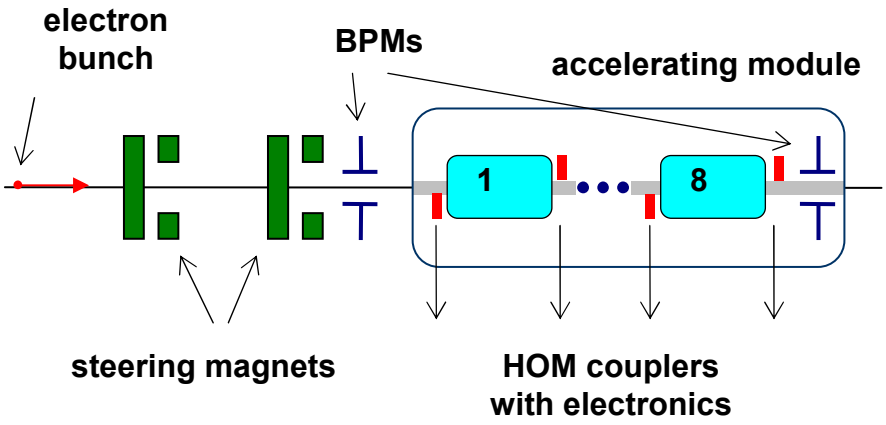

Figure 11.3.1: Layout of the beam injection steering in the FLASH ACC1 cryomodule

The result of the feedback experiment is shown in Fig. 11.3.2. Remarkably, the 16 HOM signals could be minimized with only 4 free injection steerers. This can be explained by the good relative alignment of the 8 ACC1 cavities. The beam emittance was measured before and after the feedback tuning of the injection trajectory in ACC1: a small decrease of the vertical emittance by 10% was observed after the feedback tuning.

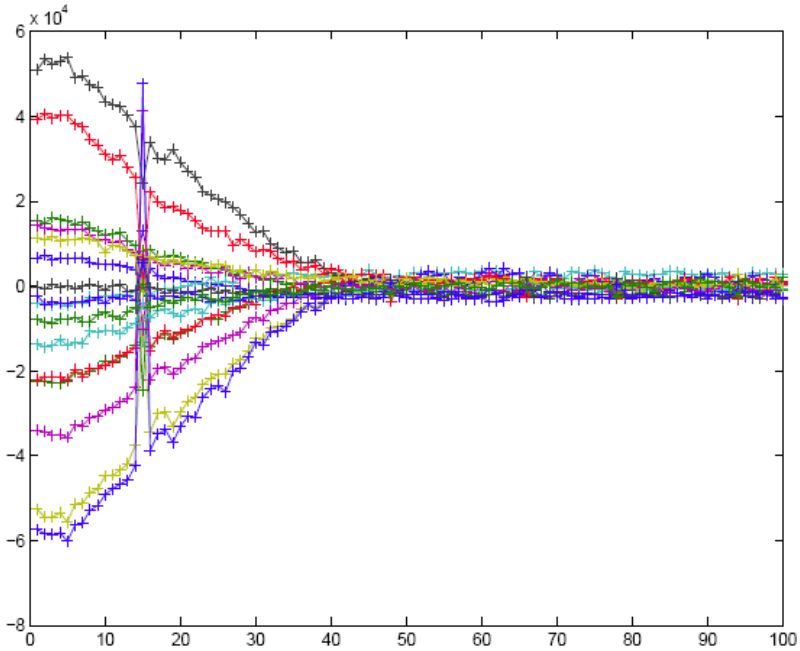

Figure 11.3.2: Minimisation of 16 HOM modes (8 cavities times 2 couplers) component amplitudes in ACC1 module during feedback, vs. machine cycles.

1.2 Cavity relative misalignments

The capability of measuring the cavity centres (actually the electric centres of the dipolar HOM) with a precision better than 50 µm was already demonstrated in 2005. With the dedicated SLAC acquisition electronics installed on the FLASH linac since then, the HOM-BPM resolution was improved and measured to be as low as 5 µm, as shown in Fig.11.3.3. The resolution is estimated from the dispersion around a perfect linear correlation of the measurements of the beam position in cavity 2 either directly or as predicted from the beam position in the neighbouring cavities 1 and 8. These measurements have been performed in the ACC4 cryomodule.

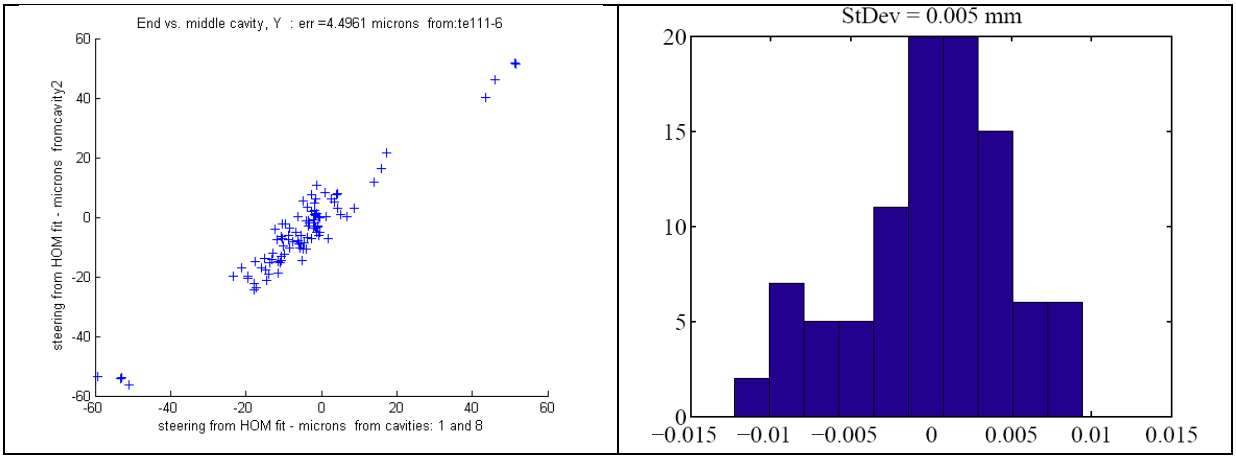

Figure 11.3.3: Correlation plot (left) and histogram (left) of the residual of the beam position (in mm) measured in cavity 2 against the prediction from two adjacent cavities 1 and 8, using the TE111-6 mode

Assuming that the measurement precision on the position of the HOM electric centres is also improved to the 5 µm level of the HOM-BPM resolution, the predicted 300 µm cavity relative alignment in a cryomodule can be verified by measuring the relative alignment of the cavity HOM centres with sufficient precision. To avoid RF steering and focussing effects on low energy bunches, this measurement has been carried out at high energy in the ACC4 and ACC5 cryomodules. The relative horizontal and vertical positions of the eight centres of the TE111-6 dipolar polarizations are plotted in Fig.11.3.4: the rms alignment of the cavities with respect to each other is 105 µm and 215 µm (for *x* and *y*, respectively) for ACC4, and 241 µm and 203 µm for ACC5. It is important to note that measurements using other modes are expected to yield different results. According to theses results, the 300 µm pre-alignment specification is fulfilled.

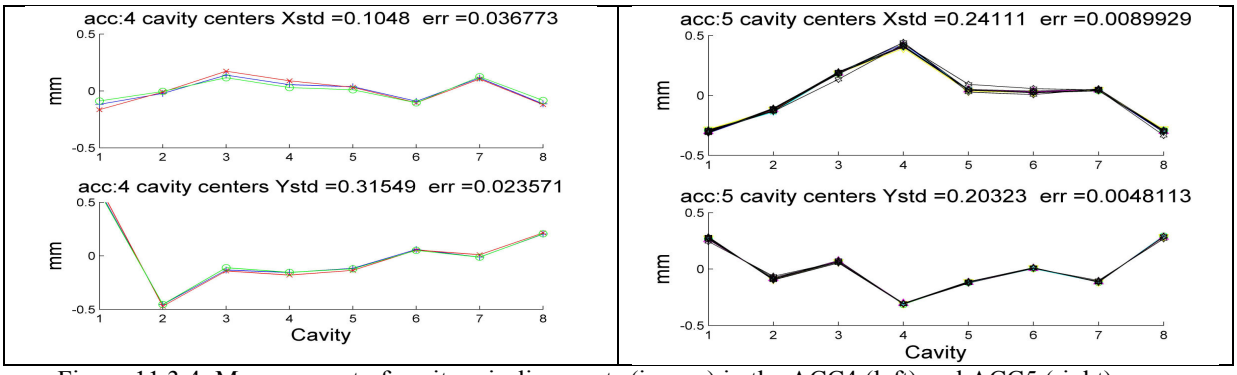

Figure 11.3.4: Measurement of cavity misalignments (in mm) in the ACC4 (left) and ACC5 (right) cryomodules (top, horizontal; bottom, vertical), using the TE111-6 mode in every cavity.